The role of MOR1 in the control of microtubule organization and dynamics in *Arabidopsis thaliana*

by

CAITLIN CHARLOTTE ANNE DONNELLY

BSc, The University of British Columbia Okanagan, 2009

A DISSERTATION SUBMITTED IN PARTIAL FULFILLMENT OF THE REQUIREMENTS FOR THE DEGREE OF

DOCTOR OF PHILOSOPHY

in

THE FACULTY OF GRADUATE AND POSTDOCTORAL STUDIES
(Botany)

THE UNIVERSITY OF BRITISH COLUMBIA
(Vancouver)

April 2017

Abstract

The plant cortical microtubule array plays a role in the control of directional cell expansion, and the organization and dynamics of the array are subject to control by a variety of microtubule-associated proteins, many of which coordinate organization of the cortical array in response to environmental stimuli. Point mutations affecting MOR1, a microtubule polymerase/depolymerase, result in disruption to the organization and dynamic properties of microtubules under specific conditions: mutations in the N-terminal TOG1 (tubulin-binding) domain have temperature-conditional phenotypes, while the phenotype of a mutation in the C-terminal region is induced by treatment with the microtubule-destabilizing drug propyzamide. In this thesis, I used *mor1* mutants with conditional phenotypes to characterize genetic interactions between different domains of the MOR1 protein, microtubules, and components of a microtubule-targeted environmental stress signalling pathway. Analysis of microtubule organization and dynamics in *mor1*-tubulin double mutants demonstrated that the handedness of helical growth phenotypes does not always correlate with microtubule growth and shrinkage rates, and showed that a mutation in β-tubulin promoted recovery of microtubule dynamics in the temperature-sensitive *mor1-1* mutant. I used live-cell imaging to observe interactions between fluorescently tagged MOR1 and microtubules, demonstrating that addition of a fluorescent tag to the MOR1 C-terminus alters MOR1 function and results in phosphorylation of α-tubulin, which is normally a response to environmental stress. Despite this effect, differences in microtubule binding affinity were observed for MOR1 variants with mutations in the TOG1 and C-terminal regions. I determined that mutation of the C-terminal region of MOR1 (*mor1-11*) results in activation of the tubulin kinase PHS1, though this did not appear to be mediated by MPK18, a previously characterized PHS1-interacting MAP kinase. In order to identify other possible components of this signalling pathway, I carried out a modifier mutant screen in the *mor1-11* genetic background, identifying one enhancer and six suppressors of *mor1-11*.

Preface

Part of Chapter 1 (section 1.3, Microtubules and signalling) is in preparation for a review article that I co-authored with Drs. Miki Fujita and Geoffrey Wasteneys.

For Chapter 2, Dr. Geoffrey Wasteneys and I designed the research, with input from Dr. Bettina Lechner regarding tubulin purification. The tubulin-*mor1* double mutant experiments are a continuation of research by Yi Zhang, published in Zhang (2010). Yi Zhang crossed plants expressing *pro35S::GFP-TUB6* to all of the mutants used in Chapter 2, and she and I both genotyped the progeny of these crosses, identifying tubulin/*mor1* mutants that also expressed GFP-TUB6. Dr. Katherine Celler and I acquired the videos used for analysis of microtubule organization and dynamics, and I measured microtubule dynamics and analysed the data. I developed the anion exchange/polymerization cycling method for tubulin purification, and the MOR1^{TOG1234} affinity purification method. The Stu2p^{TOG12} purification method described in this chapter was developed for use with plant tubulin by Dr. Takashi Hotta.

For Chapter 3, Dr. Geoffrey Wasteneys and I designed the research. The MOR1-YPet experiments are a continuation of research by Drs. Bettina Lechner and Ryan Eng, published in Eng (2015). Dr. Bettina Lechner designed the recombineered MOR1 constructs, which were produced in the lab of Dr. José Alonso, and transformed into *Arabidopsis* by Dr. Ryan Eng. Dr. Ryan Eng also identified plants that were homozygous for *proMOR1::MOR1^{WT}-3YPet* and *proMOR1::MOR1$^{1-1}$-YPet*, in the wild-type and *mor1-23* backgrounds, and expressing *p35S::mRFP-TUB6*. I identified plants that were homozygous for *proMOR1::MOR1$^{1-11}$-YPet* in the wild-type and *mor1-23* backgrounds, and expressing *proUBQ10::mCherry-TUA5*. I also identified plants that were homozygous for *proMOR1::MOR1^{WT}-3YPet* in the *mor1-11* background, and crossed plants expressing the MOR1^{X}-YPet constructs into the *mor1-6* putative null background. I carried out all of the experiments, and analyzed the data.

For Chapter 4, Dr. Geoffrey Wasteneys and I designed the research. The *mor1-11* double mutant experiments are a continuation of research by Yi Zhang (Zhang, 2010). Yi Zhang crossed *mor1-11* plants to *mpk18-1*, *phs1-1*, and *phs1-5*. I genotyped and identified the double mutants, carried out all of the experiments, and analyzed the data. I carried out the mutagenesis project, with the help of undergraduate assistants Krysta Wark, Heather Slinn, Guðrún Jónsdóttir, and Arman Brar.

Table of Contents

List of Tables

List of Figures

List of Abbreviations

ATP – adenosine triphosphate

chTOG – human orthologue of MOR1

CLASP – CLIP-ASSOCIATED PROTEIN (a +TIP)

Col – Columbia ecotype of *Arabidopsis*

DMSO – dimethyl sulfoxide

EB1 – END BINDING 1 (a +TIP)

EDTA - ethylenediaminetetraacetic acid, a chelating agent

EMS – ethyl methanesulfonate

EOM – ENHANCER OF MOR1

F1, F2 – filial generation 1 or 2, describing progeny from a genetic cross (F1) and the next generation (F2), resulting from self-pollination of an F1 plant

GFP – green fluorescent protein

GST – glutathione S-transferase (used as a protein affinity tag)

GTP – guanosine triphosphate

HEAT repeat – Huntingtin, Elongation factor 3, pr65/A subunit of protein phosphatase 2A, and TOR (protein-binding domain)

His – histidine (used as a protein affinity tag)

IPTG – isopropyl β-D-1 thiogalactopyranoside

kb – kilobase pairs, or units of 1000 DNA base pairs

kDa – kilodaltons, units used to describe the molecular mass of proteins

L*er* – Landsberg ecotype of *Arabidopsis* with the *erecta* mutation

M1, M2 – mutagenized generation 1 or 2, describing plants that are mutagenized (M1) and their progeny (M2)

MAP – microtubule-associated protein

MAP (kinase) – mitogen-activated protein kinase

mCherry – RFP variant

MKKK – MAP kinase kinase kinase

MKK – MAP kinase kinase

MKP – MAP kinase phosphatase

MOR1 – MICROTUBULE ORGANIZATION 1

MOR1^{X} – denotes variants of the recombineered MOR1 construct (MOR1^{WT} for wild type; MOR1$^{1-1}$ for *mor1-1*; MOR1$^{1-11}$ for *mor1-11*)

MPK (or MAPK) – MAP kinase

MPK18 – MAP KINASE 18

MW – molecular weight

pro35S – Cauliflower Mosaic Virus *35S* promoter

PCR – polymerase chain reaction

PHS1 – PROPYZAMIDE HYPERSENSITIVE 1

proMOR1 – MOR1 promoter

PPM – propyzamide

proUBQ10 – UBIQUITIN 10 promoter

RFP – red fluorescent protein

SDS-PAGE – sodium dodecyl sulphate polyacrylamide gel electrophoresis

SNP – single nucleotide polymorphism

SOM – SUPPRESSOR OF MOR1

SPR1, SPR2 – SPIRAL 1 and *SPIRAL 2* (+TIPs)

Stu2p – *Saccharomyces cerevisiae* orthologue of MOR1

T0, T1, T2, T3 – the T0 plant is transformed with a transgene, using *Agrobacterium tumefaciens*; the next generation (T1) results from self-pollination, and so on with T2 and T3

TAC – transformation-competent bacterial artificial chromosome

TAIR – The *Arabidopsis* Information Resource

T-DNA – transfer DNA

TILLING – Targeting Induced Local Lesions IN Genomes

+TIP – plus end-binding microtubule-associated protein

TOG – tubulin-binding domain containing multiple HEAT repeats (abbreviated from tumor-overexpressed gene)

TUA2/4/5/6 - α-TUBULIN 2/4/5/6

TUB4/6 - β-TUBULIN 4/6

WT – wild type

YFP – yellow fluorescent protein

YPet – YFP variant

XMAP215 – *Xenopus laevis* orthologue of MOR1

Acknowledgments

I consider myself to have been lucky in my choice of co-supervisors, Drs. Geoffrey Wasteneys and Brian Ellis. I am especially grateful for their patience and support, having come across various obstacles in my research projects that seemed insurmountable. (They also throw fantastic dinner parties.) I would also like to thank my committee members, Dr. Leonard Foster and the late Dr. Carl Douglas, for all of their help and advice.

It has been a pleasure working with members of the Wasteneys and Ellis labs, past and present. I would especially like to thank Dr. Bettina Lechner, who taught me about biochemistry and protein purification, and Dr. Miki Fujita, who taught me about spinning disc confocal microscopy. Quite a few hard-working undergraduate assistants were also involved in this project, and it was a privilege to mentor them: Krysta Wark, Heather Slinn, Guðrún Jónsdóttir, and Arman Brar. I would also like to acknowledge the support of the staff in the UBC Bioimaging Facility and Botany Department office (thanks for all the free coffee!).

In addition to the Wasteneys and Ellis labs, I was also a member of the Working on Walls research group. WoW has created a wonderful community in the Botany and Forestry Departments at UBC, and it has been a privilege to be a part of the group. Through WoW, I participated in more professional development activities and conferences than is usually possible for a graduate student, including an exchange trip to the lab of Dr. Takashi Hashimoto at the Nara Institute of Science and Technology (NAIST) in Japan.

I was financially supported in my work by NSERC CGSM and PGSD scholarships, as well as by WoW (itself funded by an NSERC CREATE grant), the UBC Department of Botany, and by the UBC Faculty of Graduate Studies.

During my time in the UBC Botany Department, I became close friends with students and post-docs from various member labs. I'm grateful to have met and worked with so many nice people over the course of my degree. And on that note, I would like to thank my friends and family, for their constant support.

Chapter 1: Introduction

1.1 Introduction to microtubules

1.1.1 Microtubule structure and dynamicity

The plant cytoskeleton is composed of arrays of actin filaments and of microtubules, both of which are polymers of individual protein subunits, and are the subject of precise regulation by networks of associated proteins. Microtubules are dynamic cytoskeletal polymers composed of α- and β-tubulin heterodimers arranged in a hollow tube composed of 13 protofilaments, or rows of tubulin; they are involved in various aspects of plant cell function, including cell division, and the coordination of cellulose synthesis for cell wall formation, which in turn controls the direction of cellular expansion (Hashimoto, 2015; Buschmann and Lloyd, 2008). Their ability to direct these processes is partly a result of their ability to polymerize by the addition of new $\alpha\beta$ heterodimers, and also to depolymerize. One end of the microtubule, which is characterized by higher rates of both polymerization and depolymerization, is termed the plus end; at the minus end, these processes occur at lower rates (Ehrhardt and Shaw, 2006; Wasteneys and Ambrose, 2009). The plus end terminates in a β-tubulin subunit, which can bind to the α-tubulin subunit of an incoming tubulin dimer (Sedbrook and Kaloriti, 2008).

Both α- and β-tubulin bind GTP, although this interaction serves a different purpose for each subunit: the GTP-binding site for α-tubulin is located at the intradimer interface, where the GTP is thought to function in maintaining tubulin structure or stability (Menéndez *et al*., 1998). β-tubulin, however, has a GTP-binding site at the interdimer interface, and the GTP at this site is hydrolysed to GDP after polymerization, affecting the conformation and weakening the bonds between tubulin dimers. As shown in Figure 1.1, below, tubulin is incorporated into microtubules in a GTP-bound form, which allows tubulins to join into a relatively stable, straight orientation (Alushin *et al*., 2014). When the GTP bound to β-tubulin is hydrolyzed after polymerization, a conformational change results in curving of the

protofilaments, which increases the probability of microtubule disassembly (Hyman *et al*., 1992). Assembly or disassembly is made more probable based on the concentration of unbound tubulin dimers: at or above the so-called critical concentration, microtubule growth can occur (Mitchison and Kirschner, 1984). Individual microtubules frequently transition between phases of growth, shrinkage, and pause, a property referred to as dynamic instability (Dixit and Cyr, 2004). It is through this dynamic polymerization and depolymerization that microtubules are able to change their organization or to move and associate with other cellular components.

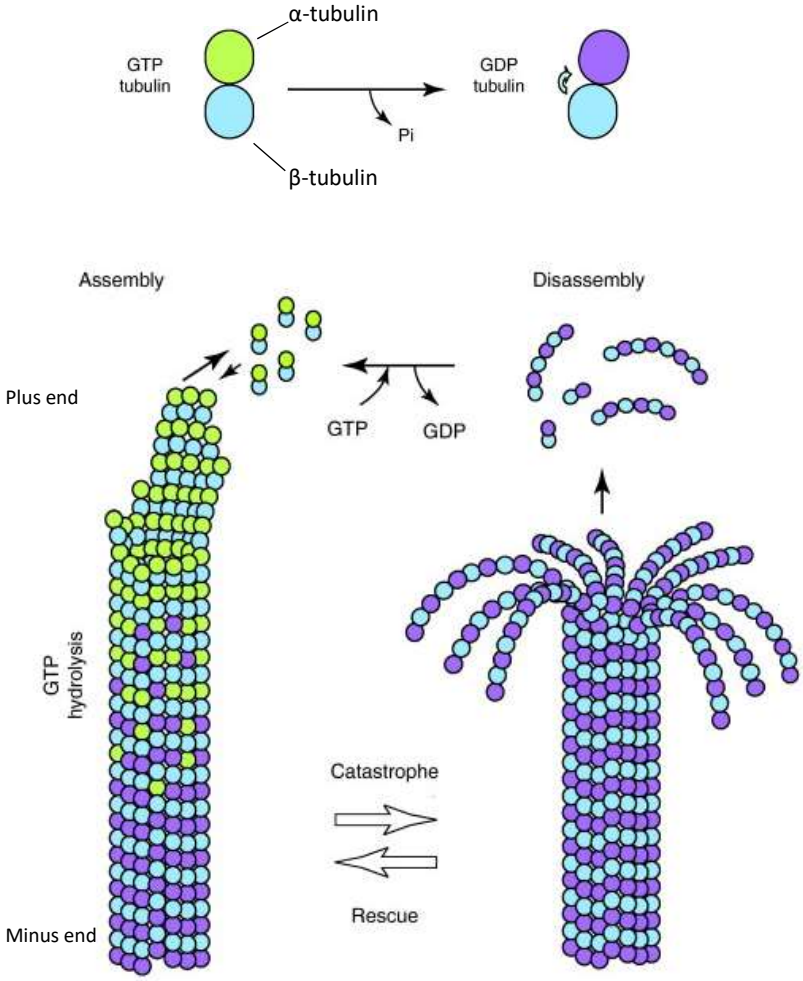

Figure 1.1 Microtubule structure and dynamics

Adapted from Al-Bassam and Chang (2011), with permission from the publisher (© Elsevier/Trends in Cell Biology).

1.1.2 Organization and function of the plant cortical microtubule array

Of particular interest in plant research are the cortical microtubules, which form an array just inside the plasma membrane during interphase. These microtubules associate with cellulose synthase complexes, determining where they insert into the membrane, and guide their motion as they synthesize cellulose microfibrils, allowing for controlled expansion of the cell (Gutierrez *et al*., 2009; Li *et al*., 2012). Specifically, cortical microtubules have been shown to influence the crystallinity of cellulose microfibrils in the cell wall, and thus the ability of the wall to expand and accommodate cellular growth. Disruption of microtubules can result in changes to the velocity of cellulose synthase complex movement, and perhaps consequently, to the crystallinity of their cellulose output (Fujita *et al*., 2011; Fujita *et al*., 2012). The association between microtubules and cellulose synthase complexes is mediated by essential linker proteins such as CELLULOSE SYNTHASE INTERACTIVE 1 and associated proteins that act as part of a linker complex (Li *et al.*, 2012; Lei *et al*., 2013; Endler *et al*., 2016).

To study the effect of the cortical microtubules on growth, it is useful to focus on cells that undergo unidirectional elongation (e.g. hypocotyl or root epidermal cells), in which cortical microtubules are organized into parallel arrays whose orientation changes at different stages of growth. During rapid cell expansion, cortical microtubules are oriented perpendicular to the main axis of growth: this is a requirement for expansion along the main growth axis, which can be prevented by disruption of microtubules (Wasteneys, 2004; Ehrhardt and Shaw, 2006). In axially expanding cells, severe disruptions to microtubule organization (and thus to wall extensibility) manifest as the inability of cells to expand in a controlled direction: cells instead become swollen and spherical (Whittington *et al*., 2001).

Mild disruption of microtubule organization, on the other hand, can lead to slight alterations in directional expansion, e.g. as seen in so-called twisting mutants, characterized by coordinated helical rotation of cell files along the long axis of the organ (Ishida *et al*., 2007a and 2007b; Weizbauer *et al*.,

2011). Similarly, disruption of the association between microtubules and cellulose synthase complexes can also lead to twisting (Landrein *et al*., 2013). Twisting is also seen in natural phenomena where plants bend in response to environmental stimuli such as light or moisture (Bisgrove, 2008), and interestingly, can be induced by exposing plants to stressful conditions: for example, exposure to pathogens, salt, and cold temperatures has been shown to induce microtubule reorganization and, in some cases, twisting (Hardham, 2013; Ban *et al*., 2013; Abdrakhamanova *et al*., 2003).

These observations of microtubule reorganization in response to environmental stress support the hypothesis that microtubules may also function as a plant sensory mechanism. Microtubules have various properties that suit them to such a role: for instance, the ability to direct plant cell expansion and thus growth of a plant toward or away from a stimulus, as well as their dynamicity (Wasteneys, 2003). Their association with the plasma membrane is potentially of use in sensing mechanical stress, as well as effects of cold or osmotic stress on membrane rigidity (Nick, 2013). Moreover, recent studies are uncovering an ever-expanding list of microtubule-associated proteins, including proteins with known signalling functions (e.g. kinases, phosphatases, and calmodulin-binding proteins) as well as proteins of as-yet unknown function (Chuong *et al*., 2004, Hamada *et al*., 2013). Plasma membrane-associated formins and phospholipase D-δ have also been shown to interact with the microtubule cytoskeleton, suggesting the possibility of mechanical or membrane receptor-initiated signal transduction between the plasma membrane and microtubules (Dhonukshe *et al*., 2003; Krtková *et al*., 2016).

1.1.3 Twisting growth and handedness

Twisting has been studied primarily in the root, hypocotyl, and petiole, due to the relative ease of measurement of twisting of these cylindrical organs, which have only one axis of cell expansion. Cortical microtubule arrays in these cell types are organized perpendicular to the axis of expansion, with microtubule bundles in parallel to each other. In twisting mutants, this parallel arrangement of the

cortical array remains largely intact, but slight changes to dynamics and/or organization cause the array to tilt so that it forms a helix; cell expansion still proceeds in a direction that is perpendicular to the orientation of the array, but this direction is now helical, resulting in twisting (Ishida *et al*., 2007a). Cells of all tissue layers twist in phase around the axis of expansion, though the pitch of cell rotation increases with increasing distance from the centre of the organ: thus, twisting is most noticeable in the epidermal layer (Weizbauer *et al*., 2011). Twisting may occur in a right- or left-handed helical pattern, and is in many cases a convenient indicator of disruptions to the microtubule array, as twisting of plant organelles is more easily assessed than microtubule dynamics. For instance, the roots of twisting mutant plants grown on a hard agar surface will skew to the left in left-handed twisting mutants, and to the right in right-handed twisting mutants (Oliva and Dunand, 2007).

In some cases, the handedness of the cortical array has been reported to be the opposite of that of the handedness of cell and organ twisting (Ishida *et al*., 2007b). Left- or right-handedness of twisting is fixed for most twisting mutants, but no explanation for genetic determination of handedness has yet been conclusively proven. Initial observations suggested that mutants with left-handed microtubule arrays (causing right-handed twisting) had increased microtubule stability or reduced microtubule dynamics and vice-versa for right-handed arrays (causing left-handed twisting). For instance, Abe and Hashimoto (2005) demonstrated that blocking GTP hydrolysis by GFP-tagging the N-terminus of α-tubulins results in stable, left-handed microtubule arrays. This seems to apply as a general rule, but is not consistent with observations of less dynamic, disorganized non-helical microtubule arrays causing left-handed twisting in the *mor1-1* mutant (Whittington *et al*., 2001; Sugimoto *et al*., 2003; Kawamura and Wasteneys, 2008). It has also been proposed that twisting may be caused by variable numbers of protofilaments in microtubules, although this does not explain directional twisting and has not been confirmed (Ishida *et al*., 2007b; Sui and Downing, 2010; Hashimoto, 2013).

In cell types that do not expand by simple elongation, organization of the cortical microtubule array is rather more complex: for instance, leaf epidermal pavement cells have a mesh-like array, with microtubules oriented parallel to the multiple axes of cellular expansion that are necessary to form the lobed cell shape (Akita *et al*., 2015). Microtubule dynamics and organization are still disrupted in these cell types, and indeed, microtubule arrays in twisting mutants may be more easily characterized in pavement cells because of better expression of GFP-tagged tubulin (Zhang, 2010); however, since expansion proceeds along multiple axes, the cells cannot grow in a helix.

Cell division in some twisting mutants may be affected, although the microtubule defects are not severe enough to prevent cell division altogether. For instance, in seedlings with the temperature-sensitive *mor1-1* mutation grown at 30 ^{o}C, defects in mitotic microtubule arrays and in cell plate formation were frequently observed in dividing cells (Eleftheriou *et al*., 2005; Kawamura *et al*., 2006).

1.1.4 Tubulin point mutations and their effects on the microtubule array

A large number of tubulin point mutations causing twisting phenotypes were identified by the Hashimoto lab at NAIST (Thitamadee *et al*., 2002; Ishida and Hashimoto, 2007; Ishida *et al*., 2007a). These point mutations are mostly semi-dominant, and affect different domains of α- and β-tubulin, including the intradimer interface, the longitudinal or interdimer interface, and lateral domains, which affect association between protofilaments (Figure 1.2). As tubulins are encoded by multiple, partially redundant genes, recessive or null mutations have not been identified as causing obvious microtubule defective phenotypes (Hashimoto, 2013). Most tubulin point mutants have been characterized only by their twisting phenotypes, although some have been linked to specific effects on microtubule dynamics and organization (Xiong *et al*., 2013). For example, the *tua5*^{D251N} mutation, which affects GTP hydrolysis in β-tubulin, exhibits highly-stabilized arrays of microtubules with reduced dynamicity, confirming that

dynamic instability is dependent on conformational changes related to GTP hydrolysis (Ishida *et al*., 2007a).

Tubulin point mutants are often hypersensitive to disruptions to the microtubule array caused by microtubule-destabilizing or -stabilizing drugs, changes in temperature, *etc*. (Hashimoto, 2013). Interestingly, some such mutants have cryptic phenotypes: for instance, *tua6*^{C213Y} exhibits right-handed root twisting on low doses of propyzamide (PPM), but not in its absence (Ishida and Hashimoto, 2007). PPM is a microtubule-destabilizing drug that binds to plant tubulin, but not animal tubulin, and causes left-handed twisting in roots of wild-type plants (Akashi *et al*., 1988; Nakamura *et al*., 2004). The differential response of the *tua6*^{C213Y} mutant to PPM treatment thus indicates the importance of the cysteine 213 residue for either control of microtubule dynamics or, perhaps, in the putative binding site for PPM in α-tubulin. In addition, the conditional response of *tua6*^{C213Y} and other mutants (discussed subsequently) highlights the usefulness of PPM in chemical genetic approaches to microtubule research (McCourt and Desveaux, 2009).

Studies of other twisting mutants have yielded information about the importance of the affected residue in interactions with particular microtubule-associated proteins, and even linked microtubules to growth responses to environmental stimuli. For instance, studies of the *tua2*^{T349I} and *tua4*^{T349I} mutants have revealed that phosphorylation of the threonine 349 residue by the dual-function tubulin kinase/MAP kinase phosphatase PROPYZAMIDE-HYPERSENSITIVE 1 (PHS1) promotes microtubule depolymerization in response to multiple stressors, including salt and osmotic stress, cold, and heat (Ban *et al*., 2013; Fujita *et al*., 2013). Additionally, Yu *et al*. identified *tub4*^{P287L} as *shade avoidance 2* (2015) and *tub6*^{L246F} as a *suppressor of shade avoidance 2* (2016), suggesting a role for these residues in coordinating microtubule reorientation as a response to light-regulated hormone signalling. Interestingly, *tub6*^{L246F} exhibited hypersensitivity to microtubule-depolymerizing drugs, whereas *tub4*^{P287L} showed reduced sensitivity (Yu *et al*., 2017).

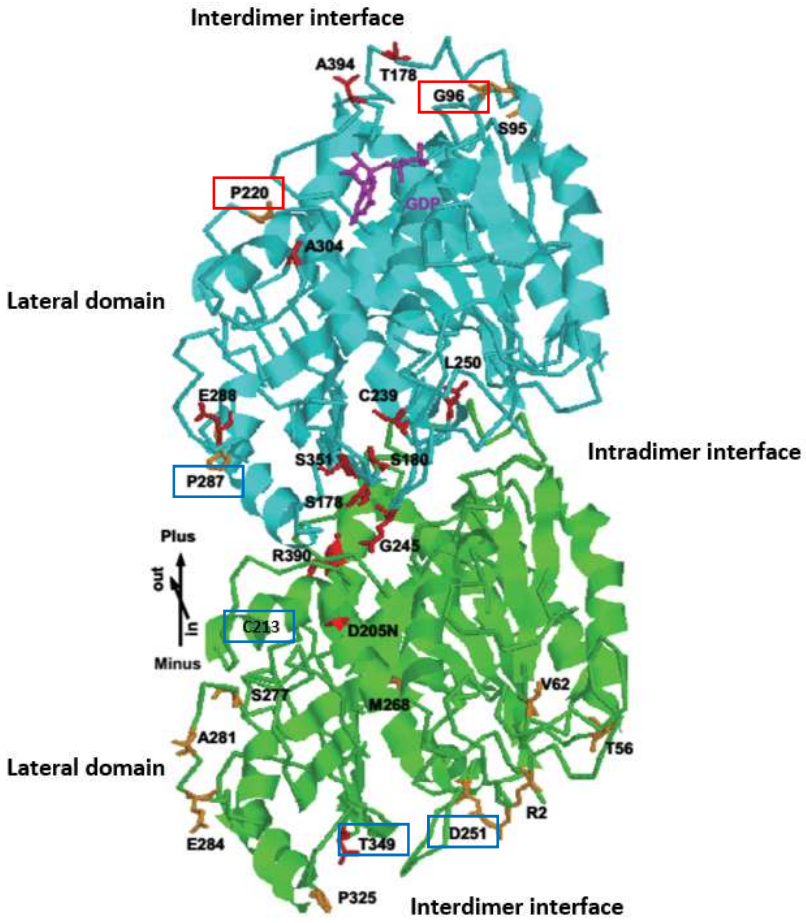

Figure 1.2 Structure of the tubulin dimer, with selected point mutations

Red boxes indicate point mutations under study in this project; blue boxes indicate point mutations mentioned in this chapter. Modified from Ishida *et al*. (2007a), with permission from the publisher. © 2007 National Academy of Sciences, USA.

1.2 Microtubule-associated proteins

The dynamic instability of microtubules is a function not only of tubulin concentration and GTP hydrolysis, but also of microtubule-associated proteins (MAPs). MAPs perform a variety of functions, including catalysis of polymerization and depolymerization, regulation of bundling, severing, and transport of cargo along microtubules (Gardiner, 2013; Hamada, 2014). Sedbrook (2004) notes that the term "MAP" has traditionally been used to describe proteins that can be co-purified with microtubules, and that the term may not include the many proteins that likely interact indirectly or transiently with

microtubules. Even using this conservative definition, hundreds of MAPs have been discovered in *Arabidopsis thaliana* alone, and recent proteomics studies have identified *Arabidopsis* MAPs in a variety of functional classes (Chuong *et al*., 2004; Korolev *et al*., 2005; Hamada *et al*., 2013; Derbyshire *et al*., 2015). Some MAPs identified in these studies have been previously characterised as involved in DNA replication, transcription, translation, RNA-binding, and signalling, while others are metabolic enzymes.

Many (though not all) proteins that regulate microtubule dynamics are plus end-binding proteins, also known as +TIPs. Since the minus end is often stabilized by a microtubule-nucleating complex, and as microtubule stability is dependent upon the presence of GTP-bound β-tubulin at the plus end, the dynamicity of the microtubule is generally a function of plus-end dynamics, and that process is regulated at that end (Hyman *et al*., 1992; Bisgrove *et al*., 2004). +TIPs accumulate at, or "track to", the plus end by various means: transport by motor proteins; binding to other +TIPs; or self-directed movement called treadmilling, which relies on preferential affinity for the conformation of plus-end tubulins (Bisgrove *et al*., 2004; Akhmanova and Steinmetz, 2008; Wong and Hashimoto, 2017). One such group of +TIPs, the EB1 (END-BINDING 1) proteins are frequently expressed ectopically as GFP fusion proteins and used in studies of microtubule dynamics to mark the plus end of the microtubule. Another +TIP is CLASP (CLIP-ASSOCIATED PROTEIN), a protein which can stabilize growing microtubules that encounter cell edges, and which contains helical HEAT (huntingtin, elongation factor 3, pr65/A subunit of protein phosphatase 2A, and TOR) repeat-containing protein-binding domains similar to the TOG (tumor over-expressed gene) domains found in MOR1 (MICROTUBULE ORGANIZATION 1) (Ambrose *et al*., 2011; Akhmanova and Steinmetz, 2008). Several +TIPs have been identified as affecting the orientation of the cortical array, as a result of twisting phenotypes seen in plants with mutated or absent MAPs. For example, mutation of the *SPIRAL1* and *SPIRAL2* genes, which encode proteins that regulate microtubule plus-end dynamics, gives rise to right-handed twisting (Nakajima *et al*., 2006; Galva *et al*., 2014; Yao *et al*., 2008).

1.3 Microtubule-MOR1 interactions

1.3.1 The XMAP215 family and MOR1 protein structure

MOR1 is a member of the XMAP215 family of microtubule polymerase/depolymerase proteins, which are +TIPs that are required for microtubule organization in eukaryotes (Gard *et al*., 2004). Members of this protein family have between 2 and 5 tubulin-binding TOG domains joined by flexible linker domains: each TOG domain contains 6 protein-binding HEAT (α-helix-loop-α-helix) repeats (Cassimeris *et al*., 2001; Al-Bassam *et al*., 2007). MOR1, shown in Figure 1.3, has 5 TOG domains, as do the MOR1 orthologues that have been characterized in humans, *Drosophila melanogaster*, and *Xenopus laevis* (ch-TOG, Msps, and XMAP215, respectively) (Al-Bassam and Chang, 2011). It is less closely related to fungal orthologues Stu2p (*Saccharomyces cerevisiae*), Dis1 and Alp14 (*Schizosaccharomyces pombe*), which have 2 TOG domains; and to Zyg-9 (*Caenorhabditis elegans*), which has 3 TOG domains.

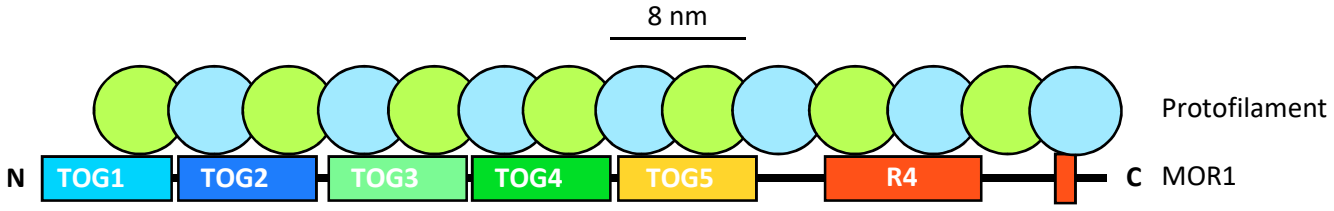

Figure 1.3 MOR1 protein structure and association with the microtubule plus end

MOR1 is a +TIP and microtubule polymerase/depolymerase, shown here interacting with a single protofilament. Adapted from Kawamura and Wasteneys (2008) to update domain nomenclature. Used with permission from the publisher (© Company of Biologists Ltd./Journal of Cell Science).

1.3.2 Functions of the TOG and C-terminal domains

The study of MOR1 described in this thesis uses *mor1* mutants with single nucleotide polymorphisms (SNPs) in TOG domain 1 and at the TOG5/C-terminal domain boundary; characterizing these mutants is of interest for better understanding the role of these domains in the mechanism by which MOR1

functions. The *mor1* point mutant phenotypes will be discussed in greater detail in the introductory sections for Chapters 2, 3, and 4, since the experiments described in those chapters make use of these mutants.

The TOG and C-terminal R4 domains were identified based on sequence homology among XMAP215 orthologues, rather than based on homology to known protein domains (Rashbrooke, 2005). Analysis of XMAP215 constructs with non-functional TOG domains demonstrated that each of the 5 TOG domains has tubulin affinity and contributes to polymerase activity, but that TOG1 and TOG2 make the greatest contribution to polymerization (Widlund *et al*., 2011). Interestingly, the TOG1 and TOG2 domains of XMAP215/MOR1 are homologous to the two TOG domains of *S. cerevisiae* Stu2p, while the other 3 TOG domains in XMAP215/MOR1 may have diverged in function (Al-Bassam and Chang, 2011; Fox *et al*., 2014). TOG domains 3 and 4 of *Drosophila* Msps are structurally divergent from TOG domains 1 and 2, and have only weak affinity for free tubulin, but both still contribute to microtubule binding and polymerization, and TOG3 has conserved tubulin-binding residues that permit binding to curved (free) tubulin dimers in a TOG1/2-like manner (Widlund *et al.*, 2011; Fox *et al.*, 2014; Howard *et al*., 2015). In XMAP215, microtubule lattice-binding domains are found between TOG domains 3 and 4, and 4 and 5; these linker domains are basic, and similar to lattice-binding domains in Stu2p and Dis1 (Currie *et al*., 2011; Widlund *et al*., 2011).

In MOR1, a fragment spanning from the beginning of the TOG5 domain to the C-terminus is sufficient for binding to the microtubule lattice *in vitro*, and antibodies raised against the C-terminal 855 amino acids have been shown to label microtubule lattices in fixed *Arabidopsis* protoplasts at various stages of the cell cycle (Twell *et al*., 2002). The TOG5 domain does not appear to be directly involved in polymerase activity, since Widlund *et al*. (2011) found that mutating tubulin-binding residues in TOG5 caused only a slight reduction in polymerase activity. The C-terminal region also contains the R4 domain, which is not homologous to the TOG domains, but does contain HEAT repeats, implying that it may play a role in

microtubule binding. The R4 domain is conserved among all MOR1 orthologues with 5 TOG domains, although this domain is extended in plant orthologues relative to other taxa (Rashbrooke, 2005).

The C-terminal region of MOR1 may also be involved in interactions with other MAPs: in humans, the C-terminal region of ch-TOG binds to SLAIN2, a linker protein that binds to various +TIPs, including human homologues of EB1 and CLASP (van der Vaart *et al*., 2011). Moreover, human EB1 proteins promote accumulation of ch-TOG at the microtubule plus end, and EB1 and XMAP215 have been observed to promote plus end growth in a synergistic manner (Currie *et al*., 2011; van der Vaart *et al*., 2011; Zanic *et al*., 2013). To date, however, no plant homologue of SLAIN2 has been identified; nor has any physical interaction of the C-terminal domain of MOR1 with other MAPs been confirmed.

1.3.3 Model for microtubule polymerization

The mechanism by which XMAP215 promotes microtubule polymerization has not yet been conclusively determined, but various models have been proposed. While XMAP215 can bind to the length of the microtubule lattice, it targets preferentially to the plus end, which is likely due to two factors: interactions with other +TIPs, and the fact that simultaneous binding of N-terminal TOG domains to curved tubulin dimers and binding of the C-terminal region to the lattice is only possible at the plus end (Ayaz *et al*., 2012, Akhmanova and Steinmetz, 2015). An individual XMAP215 molecule resides at the plus end for long enough to catalyse the addition of multiple tubulin dimers, with approximately 10 XMAP215 molecules binding at once (Kerssemakers *et al*., 2006; Brouhard *et al*., 2008), and preliminary experiments with FRAP (fluorescence recovery after photobleaching) indicate high turnover (A. Walia, personal communication). Brouhard *et al*. (2008) hypothesize that free tubulin dimers may transiently or weakly associate with the microtubule plus end, and that XMAP215 family proteins catalyze microtubule polymerization by stabilizing this association. Conversely, the ability of XMAP215 proteins

to lower the activation energy of the intermediate state between bound and unbound tubulin, may also enable them to catalyse depolymerization of the microtubule at lower concentrations of free tubulin.

As a tubulin dimer is incorporated into the microtubule, its conformation changes from curved to straight; this conformational change weakens the affinity of TOG domains for the dimer, and allows XMAP215 to bind to the next free tubulin dimer, thereby promoting further polymerization (Kawamura and Wasteneys, 2008; Ayaz *et al*., 2012). EB1 proteins are thought to promote the transition of tubulin dimers from a curved orientation to a straight one, thus increasing polymerase activity by XMAP215 (Zanic *et al*., 2013). Processive rounds of binding and detaching are likely facilitated by the flexible inter-TOG linker domains, which allow bending of XMAP215 (Cassimeris *et al*., 2001; Howard *et al*., 2015).

Brouhard *et al*. (2008) used size-exclusion chromatography and electron microscopy to show that XMAP215 binds a single tubulin dimer, and concluded that TOG domains 1 through 4 may be wrapped around the dimer, while TOG5 and the C-terminal end of the protein are associated with the lattice. They did not, however, image XMAP215 in association with the microtubule lattice, so the "wrapped" conformation of XMAP215 may not be the actual conformation of the protein at the plus end. Stoichiometric analysis of tubulin binding by the TOG1 and TOG2 domains of *S. cerevisiae* Stu2p has indicated that in this orthologue, each TOG domain also binds one tubulin dimer (Slep and Vale, 2007; Ayaz *et al*., 2012; Ayaz *et al*., 2014).

1.3.4 Distinct features of MOR1 and other plant members of the XMAP215 family

Because of the homologous domain structure, it is expected that MOR1 functions by a mechanism similar to that of XMAP215. However, some differences in both sequence and function have been noted, which likely reflect the distinct and specialized functions of microtubules in plants. For instance, MOR1 and other plant homologues contain both a putative N-terminal microtubule-binding domain and a conserved region of unknown function between the TOG5 and R4 domains, neither of which is found

in non-plant XMAP215 family members (Lechner *et al*., 2012; Rashbrooke, 2005). Additionally, tobacco MAP200 increases the frequency of both catastrophe and rescue (transition from growth to shrinkage and vice versa, respectively) at concentrations of GTP where XMAP215 increases catastrophe frequency while suppressing rescue (Hamada *et al*., 2009). MOR1 also suppresses the pausing of microtubule growth (Kawamura and Wasteneys, 2008). Because of difficulties with cloning and purifying the full-length protein, work with MOR1 has so far been limited to characterization of defects in microtubule arrays, cell division, and cell walls in *mor1* mutants, and to biochemical assays and transient expression using truncated MOR1 fragments (Kawamura and Wasteneys, 2008; Oh *et al*., 2010; Fujita *et al*., 2011; Lechner *et al*., 2012). More recently, full-length MOR1 has been cloned via recombineering (Zhou *et al*., 2011; Alonso and Stepanova, 2014), allowing more in-depth studies of MOR1 via fluorescence microscopy and biochemical assays (Eng, 2015).

1.4 Microtubules and signalling

1.4.1 Microtubule reorganization in response to environmental stimuli

Certain MOR1 point mutants, described in further detail in the experimental chapters, have conditional phenotypes: the *mor1-1* and *rid5* mutants appear similar to wild type at 21 ^{o}C (the permissive temperature), but exhibit radial swelling and left-handed twisting growth (respectively) at 28 – 31 ^{o}C (the restrictive temperature) (Whittington *et al*., 2001; Konishi and Sugiyama, 2003). The *mor1-11* mutant, on the other hand, has right-handed root twisting when treated with the microtubule-destabilizing drug propyzamide (Zhang, 2010). Characterizing the effects of these mutations on MOR1-microtubule interactions is thus of interest for understanding the role of MOR1, and of the microtubule array, in responses to changes in temperature and in signalling events that cause microtubule depolymerization.

Depolymerization and subsequent reorganization and stabilization of the cortical microtubule array is a common response to a variety of abiotic signals, including cold, salt and osmotic stress, and blue light (Abdrakhamanova *et al*., 2003; C. Wang *et al*., 2007; Sambade *et al*., 2012; Lindeboom *et al*., 2013; Endler *et al.*, 2015; Oda, 2015). Multiple stress-induced signalling pathways converge to promote remodelling of the cortical array, including pathways mediated by ABA, Ca^{2+}, protein degradation, MAP kinase cascades, and activation of phospholipase D (PLD) (Teige *et al*., 2004; C. Wang *et al*., 2011; Nick, 2013; Zhu, 2016). Some of these pathways appear to function in general stress responses, whereas others function only in response to specific stressors.

Blue light, heat, cold, salt, osmotic stress, and ABA treatment all cause an increase in free cytosolic Ca^{2+} concentration (Baum *et al*., 1999; Zhu *et al*., 2016), which promotes dissociation of microtubule-depolymerizing proteins MAP18 and MDP25 from the plasma membrane (X. Wang *et al.*, 2007; Kato *et al*., 2010; Li *et al*., 2011). Various other proteins have been shown to control reorientation of the cortical array in response to blue light, and it is possible that these proteins are also involved in stress-induced array reorientation. For instance, TON2/FASS and AUG8, which promote nucleation and polymerization (respectively) of branching microtubules, allow new microtubules to form at different angles from the dark-formed transverse array (Kirik *et al*., 2012; Cao *et al*., 2013). Katanin severs microtubules at crossover sites, allowing new microtubules to grow from the severed ends, contributing to reorientation in response to blue light and mechanical stress (Uyttewaal *et al*., 2012; Lindeboom *et al*. 2013). WDL3, a microtubule stabilizing/bundling protein, is also degraded via the 26S proteasome upon exposure to light (Liu *et al*., 2013).

Reorganization and stabilization of the microtubule array is mediated by microtubule-stabilizing proteins, some of which have been shown to be involved in the response to multiple stresses. Reorganization in response to chilling stress is mediated by MAP65-1, MAP65-2, and WDL5 (Mao *et al*., 2005; Li *et al*., 2009; Sun *et al*., 2015). MAP65-1 is also involved in the response to salt stress, and both

MAP65-1 and MAP65-2 promote axial expansion in etiolated hypocotyls, independent of their microtubule-bundling function (Zhang *et al*., 2012; Lucas *et al*., 2011).

Post-translational modifications of tubulin may also contribute to changes in microtubule organization and dynamicity during stress responses, likely by modulating interactions with MAPs (Breviario *et al*., 2013; Parrotta *et al*., 2014). For example, treatment of maize suspension culture cells with gibberellic acid caused increased α-tubulin acetylation, which improved microtubule stability during subsequent cold stress treatments (Huang and Lloyd, 1999). Nitration of α-tubulin tyrosine residues also regulates microtubule dynamics and organization (Blume *et al*., 2013). MAPs can also undergo post-translational modifications: e.g. phosphorylation of +TIPs is thought to reduce the affinity of the +TIP for negatively-charged regions of tubulins (Akhmanova and Steinmetz, 2008).

1.4.2 Microtubules and salt stress

As in other stress responses, exposure to NaCl causes the cortical microtubule array to initially depolymerize and then re-organize (C. Wang *et al*., 2007). The initial depolymerization is achieved through 26S proteasome-mediated degradation of SPIRAL1, a +TIP that promotes plus-end stability and that interacts with EB1b (S. Wang *et al*., 2011, Galva *et al*., 2014). This loss of SPR1 is specific to ionic stress rather than osmotic stress; it can be induced by NaCl, but not by mannitol (S. Wang *et al*., 2011). *spr1* null mutants have right-handed twisting phenotypes, and are hypersensitive to microtubule-depolymerizing drugs such as PPM, but less sensitive to NaCl treatment, compared to wild-type plants (Shoji *et al*., 2006; S. Wang *et al*., 2011).

It is thus of interest to screen PPM-sensitive mutants for altered sensitivity to NaCl, as the results may highlight roles for the mutated tubulin residues or MAPs in the response to salt stress. For example, various alleles of *sos1* and *sos2* (SALT OVERLY SENSITIVE 1 and 2) were identified in separate forward-genetics screens looking for modifiers of the root twisting response of the *spiral1* mutant and to

treatment with PPM (Shoji *et al*., 2006; Ishida and Hashimoto, 2007). SOS1 and SOS2 encode a plasma membrane Na^+/H^+ antiporter that removes Na^+ from the cell and a kinase that activates the antiporter, respectively, and have been reported to affect microtubule organization and root twisting (Qiu *et al*., 2002).

The link between PPM- and salt sensitivity is underscored by the function of the tubulin kinase/MAP kinase phosphatase PHS1 (PROPYZAMIDE HYPERSENSITIVE 1), which phosphorylates the T349 residue common to all *Arabidopsis* α-tubulins (Fujita *et al*., 2013; Stecker *et al*., 2014). With its position at the interface between tubulin dimers, phosphorylation of free tubulin dimers at this residue leads to their inability to bind to the β-tubulin exposed at the plus end of the microtubule, and microtubule depolymerization ensues (Ishida *et al*., 2007a; Ban *et al*., 2013). This phosphorylation event was identified as a general response to a variety of stressors, including salt and osmotic stress, heat and cold stress, and treatment with microtubule-depolymerizing drugs (Ban *et al*., 2013; Fujita *et al*., 2013). PHS1 was previously characterized as binding to and dephosphorylating MPK18 (MAP KINASE 18), resulting in destabilization of cortical microtubules (Naoi and Hashimoto, 2004; Walia *et al*., 2009; Pytela *et al*., 2010). It has also been demonstrated that MPK18 transcription was induced with 200 mM NaCl treatment, implying a role for the protein in the response to salt and osmotic stress (Moustafa *et al*., 2008). However, activation of MPK18 via phosphorylation in a MAP kinase signalling pathway has not yet been demonstrated in response to environmental stimuli, though it is known that MPK18 can activate itself through auto-phosphorylation (Walia *et al*., 2009).

As microtubules are associated with cellulose synthase complexes and thus the plant cell wall, regulation of the cortical microtubule array is an important mechanism for regulating changes in plant growth and cell expansion. Indeed, mutants of various genes involved in the formation of the primary cell wall are hypersensitive to salt: for instance, alleles of a cell wall arabinogalactan protein and of *CELLULOSE SYNTHASE-LIKE D5* were identified as *SALT OVERLY SENSITIVE 5* and *6*, respectively (Wang *et*

al, 2016). During microtubule depolymerization in salt- or osmotically stressed plants, cellulose synthase complexes (CSCs) are internalized into intracellular compartments called SmaCCs/MASCs (Small CesA Compartments/Microtubule-Associated CesA compartments) (Crowell *et al*., 2009; Gutierrez *et al*., 2009; Endler *et al*., 2015). Re-establishment of the cortical microtubule array is promoted by the CC1 and CC2 (COMPANION OF CELLULOSE SYNTHASE 1 and 2) proteins, which link microtubules and CSCs and promote microtubule polymerization (Endler *et al*., 2015). It is possible that CC proteins may promote recovery of the array by also facilitating nucleation of microtubules (Endler *et al*., 2015). Whether internalization of CSCs is a response to other stressors remains to be determined, though it may also be induced by treatment with cellulose synthesis inhibitors (Crowell *et al*., 2009; Gutierrez *et al*., 2009).

1.5 Objectives

My primary objective in this study is to characterize domain-specific interactions between MOR1 and microtubules, using chemical genetics, biochemical, and microscopy-based approaches. While focusing on protein-protein interactions, this research raises additional questions about the role of MOR1 and microtubules in responses to environmental stress.

In Chapter 2, I characterize genetic interactions between tubulin and the first TOG domain of MOR1, measuring microtubule dynamics and organization in *mor1*-tubulin double mutants. I also demonstrate that changes in microtubule plus-end dynamics are not the sole determinant of the handedness of twisting growth phenotypes.

In Chapter 3, I use live-cell imaging to observe the effects of *mor1* mutations in the TOG1 domain and C-terminal region on MOR1-microtubule interactions. Using temperature and drug sensitivity assays, I demonstrate that the addition of a fluorescent tag to the C-terminus of MOR1 results in phosphorylation of α-tubulin.

In Chapter 4, I characterize genetic interactions between the C-terminal region of MOR1 and various mutants that are involved in phosphorylation of α-tubulin, using the *mor1-11* allele and a chemical genetics approach. I also measure microtubule dynamics in *mor1-11*, and carry out a modifier mutant screen in the *mor1-11* background.

In Chapter 5, I summarize the main findings of this thesis, and discuss future directions. I also introduce a project to purify tubulin from plant sources, with the aim of using plant tubulin to reconstitute MOR1-microtubule interactions *in vitro*.

Chapter 2: Interactions between microtubules and the TOG1 domain of MOR1

2.1 Introduction

2.1.1 Point mutations in the TOG1 domain of MOR1 have conditional phenotypes

Three point mutations in the N-terminal TOG1 domain of MOR1 have been shown to cause left-handed twisting: *mor1-1* (L174F), *mor1-2* (E195K), and *rid5* (C96Y) (Figure 2.1; see Appendix 1 for images of root skewing phenotypes). Interestingly, the microtubule organization and growth phenotypes of each mutant are conditional: all have mild microtubule defects at 21 °C (the permissive temperature), and more severe microtubule defects when grown at 28 °C or above (the restrictive temperature). These are all partial loss-of-function alleles, altering but not abolishing the ability of MOR1 to interact with microtubules; putative null alleles of MOR1, containing a T-DNA insertion or causing truncation of MOR1, are homozygous-lethal (Twell *et al*., 2002).

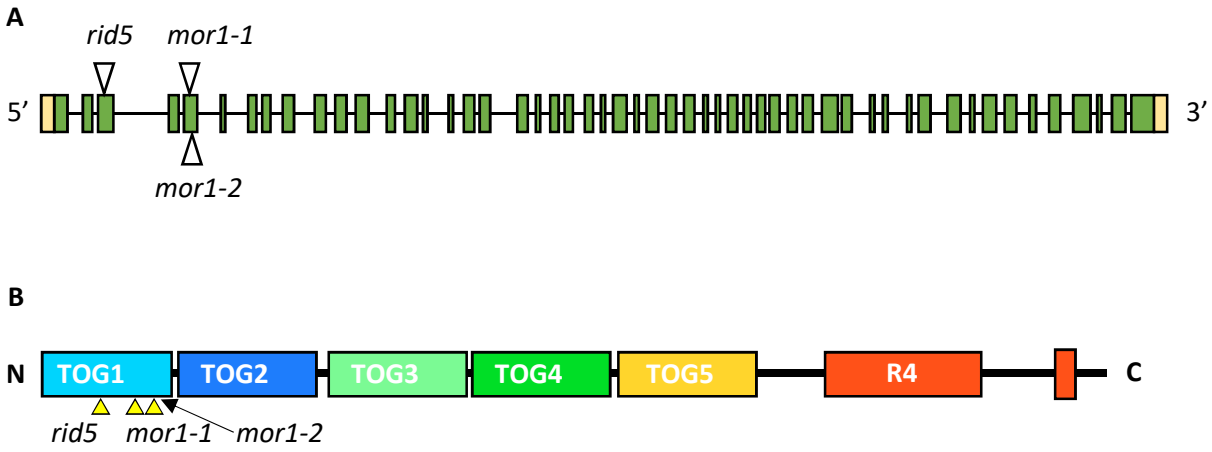

Figure 2.1. Point mutations affecting the TOG1 domain of MOR1

Three mutations causing left-handed twisting are located in the TOG1 domain of MOR1, which associates with the plus end of the microtubule (Kawamura and Wasteneys, 2008). The TOG1 and TOG2 domains make the greatest contribution to polymerase activity (Widlund *et al*., 2011).

(A) MOR1 gene structure, with 5' and 3' untranslated regions indicated in yellow, exons in green, and introns as lines.

(B) MOR1 protein structure, adapted from Kawamura and Wasteneys (2008) to update domain nomenclature and to indicate point mutations. Used with permission from the publisher (© Company of Biologists Ltd./Journal of Cell Science).

The *mor1-1* and *mor1-2* mutations were discovered in a screen for temperature-sensitive disruption of microtubule organization (Whittington *et al*., 2001), while *rid5* (ROOT INITIATION DEFECTIVE 5) was isolated in a screen for temperature-sensitive mutants with defects in the formation of adventitious roots, a process which is mediated by the hormone auxin (Konishi and Sugiyama, 2003). The *rid5* mutation affects a residue in the first α-helix of the 3rd HEAT repeat of TOG1, while both *mor1-1* and *mor1-2* affect conserved residues in the 5th HEAT repeat of the TOG1 domain, located in the first and second α-helices, respectively (Whittington *et al*., 2001; Rashbrooke, 2005; Zhang, 2010). As the intra-HEAT repeat turns mediate tubulin binding (Al-Bassam *et al*., 2007), mutation of nearby residues is likely to alter tubulin binding capacity.

The phenotypes of *mor1-1* and *mor1-2* at restrictive temperature are more severe than that of *rid5*: while *mor1-1* and *mor1-2* seedlings germinated and grown at 31 ^{o}C are extremely stunted and have severe radial swelling (Whittington *et al*., 2001), *rid5* seedlings germinated and grown at 28 ^{o}C exhibit strong left-handed root twisting and a reduction in root length relative to wild type (Konishi and Sugiyama, 2003). Disruption of cortical microtubules in *mor1-1* at restrictive temperature causes radial swelling through changes to the crystallinity of cellulose microfibrils, rather than changes to their orientation (Sugimoto *et al*., 2003; Fujita *et al*., 2011).

Moderately high temperatures (28 – 31 ^{o}C) appear to have little effect on microtubule organization in *Arabidopsis* (Smertenko *et al*., 1997), although microtubule dynamics are increased at 31^{o}C relative to 21 ^{o}C (Kawamura and Wasteneys, 2008). It is possible that this increase in microtubule dynamicity further disrupts already altered interactions between the mutated HEAT repeats of MOR1 and microtubules/tubulin. Indeed, *mor1-1* seedlings exhibit hypersensitivity to the microtubule-destabilizing

drugs oryzalin and propyzamide at both 21 °C and 29 °C, and to the microtubule-stabilizing drug taxol at 29 °C (Collings *et al*., 2006). Temperature-conditional microtubule defects are also observed in other MAP mutants, such as the +TIP mutant *spiral1*, which has a more pronounced twisting phenotype at low temperatures (Furutani *et al*., 2000).

Although *mor1-1* plants grown at 21 °C appear almost phenotypically equivalent to the wild type, microtubule growth and shrinkage both occur more slowly than in wild-type cells; the differences in dynamics appear to be too slight to cause twisting or radial swelling (Kawamura and Wasteneys, 2008). At 31 °C, however, microtubule growth and shrinkage velocities were much lower in *mor1-1* than in wild type (Kawamura and Wasteneys, 2008). Preliminary, non-quantitative analysis of microtubule dynamics in *rid5* suggested that, at 31 °C, microtubules were less dynamic in *rid5* than in *mor1-1* (Zhang, 2010).

Lechner *et al*. (2012) hypothesized that the changes to microtubule organization and dynamics seen in *mor1-1* may reflect altered binding affinity of MOR1 for the microtubule, as MOR1 contains a plant-specific N-terminal motif (KLLK) which may be involved in microtubule binding. Attempts at tagging a MOR1 construct consisting of the first two TOG domains (hereafter, TOG12) with YFP at the N-terminus interfered with microtubule binding, possibly due to the proximity of the tag to the KLLK motif. TOG12 with a C-terminal GFP tag, however, was able to bind to microtubules *in vivo* (Lechner *et al*., 2012). This hypothesis was supported by the finding that TOG12^{mor1-1} bound more strongly to microtubules *in vitro* than did wild-type TOG12: thus, the reduced dynamicity seen in *mor1-1* may be the result of impairing continuous diffusion of MOR1 toward the plus end (Lechner *et al*., 2012).

2.1.2 Tubulin point mutations and genetic interactions with *mor1* point mutations

A large number of tubulin point mutations causing twisting phenotypes were identified by Ishida *et al*. (2007a) (Fig. 1.3). In order to characterize tubulin-MOR1 interactions, and to better understand the genetic basis for twisting handedness, 16 tubulin mutants with right-handed twisting were crossed to 3

mor1 mutants with left-handed twisting (*mor1-1*, *mor1-2*, and *rid5*) by Zhang (2010). The tubulin point mutations affect different domains of α and β tubulin, including the intradimer interface; the longitudinal or interdimer interface; and lateral domains, which affect association between protofilaments (Nogales *et al*., 1999).

Although the exact binding site of MOR1 on tubulin has not been identified, it is known that conserved lysine and tryptophan residues on intra-HEAT repeat turns in the TOG1 domain of Stu2p are required for binding free tubulin dimers (Al-Bassam *et al*., 2007). Basic domains of other MAPs are known to bind to the acidic C-terminal "tail" region of tubulin, which is exposed on the outer surface of the microtubule (Paschal *et al*., 1989; Nogales *et al*., 1999). These (basic) lysine residues in MOR1, as well as the basic putative N-terminal microtubule-binding motif (KLLK) could interact with the C-terminal tails. Additionally, binding of MOR1 to the microtubule may be influenced by other +TIPs, as studies of chTOG have indicated interactions with EB1 and SLAIN2 (Currie *et al*., 2011; van der Vaart *et al*., 2011). The mutated tubulin residues discussed above may therefore not be directly involved in MOR1 binding, but are of interest, nonetheless, for understanding how changes to intradimer, interdimer, and inter-protofilament interactions can ultimately affect microtubule-MOR1 interactions. These mutations may result in changes to microtubule polymerization and depolymerization rates, GTPase activity, and/or interactions between protofilaments, all of which affect curvature of the microtubule plus end, and may thus affect binding of MOR1 and/or MOR1-interacting MAPs.

Zhang (2010) observed that the *tub4*^{G96D}, *tub4*^{P220S}, and *tua5*^{D251N} mutants (of 16 tubulin mutants tested) in combination with *mor1* mutants displayed non-additive phenotypes, with respect to handedness of twisting. Each of the other tubulin-*mor1* combinations resulted in right-handed twisting when grown at 21 ^{o}C, and left-handed twisting with radial swelling at 31 ^{o}C. These three mutations all affect the interdimer interface; in addition, the *tua5*^{D251N} mutation disrupts GTPase activity, as the D251 residue

contacts the GTP-binding site of β-tubulin upon polymerization (Ishida *et al*., 2007a). *tub4*^{G96D} in combination with *mor1-1* or *mor1-2* did not exhibit hypocotyl twisting, *tua5*^{D251N}*mor1-1* was seedling-lethal, and *tub4*^{P220S} in combination with the *mor1* mutants showed both radial swelling and right-handed (*rid5*) or no twisting (*mor1-1*, *mor1-2*) when grown at 31 °C. The right-handed twisting phenotype of *tub4*^{P220S} is thus epistatic to the left-handed twisting phenotypes of the *mor1* mutants, which provides some insight into the genetic basis of handedness. Preliminary, non-quantitative analysis of microtubule dynamics in the *tub4*^{P220S}, *mor1-1*, *rid5*, and *tub4*^{P220S}*mor1-1* and *tub4*^{P220S}*rid5* double mutants indicated that dynamicity was reduced at both 21 °C and 31 °C; additionally, disorganized microtubule arrays with short microtubules were observed in the *mor1-1*, *rid5*, *tub4*^{P220S}*mor1-1*, and *tub4*^{P220S}*rid5* lines at 31 °C (Zhang, 2010).

2.1.3 Objectives

In this chapter, I continued the tubulin-*mor1* double mutant analysis begun by Zhang (2010), characterizing genetic interactions between mutants affecting the interdimer interface of β-tubulin and the TOG1 domain of MOR1. By measuring microtubule dynamics in tubulin mutants (*tub4*^{P220S}, *tub4*^{G96D}), *mor1* mutants (*mor1-1*, *rid5*) and in tubulin-*mor1* double mutants, I aimed to advance the understanding of the functional importance of the affected residues and domains. Additionally, I sought to test previous models of twisting growth, by determining whether twisting handedness is correlated to specific changes in microtubule dynamicity.

2.2 Results

2.2.1 Microtubule dynamics in wild type and *mor1-1* are comparable to previously reported values

Because measurements of microtubule dynamics in the present study used microtubule tracking via ImageJ, rather than the kymograph technique used in previous studies (see section 2.4.4), I first confirmed that this method yielded comparable results. Microtubule dynamics were measured in

tubulin, *mor1*, and tubulin-*mor1* double mutants expressing *pro35S::GFP-TUB6* (β-tubulin 6), at both 21 °C and 31 °C. Average microtubule plus-end growth and shrinkage rates were calculated for each genotype at both temperatures. Mean wild-type and *mor1-1* growth and shrinkage velocities at both temperatures fell within the margins of error of previously-published values (Table 2.1). One exception is that the mean *mor1-1* shrinkage rate was higher at 31 °C than previously reported, although it was decreased relative to the mean *mor1-1* shrinkage rate at 21 °C, as reported by Kawamura and Wasteneys (2008). Because the measurements of microtubule dynamics in wild type and *mor1-1* were similar to previously published values, measurements of dynamics in the tubulin, *rid5*, and tubulin-*mor1* double mutants can be interpreted with reference to these previous studies.

While mean velocities were within previously reported margins of error, I did not observe an increase in wild type plus-end growth rate from 21 °C to 31 °C, though shrinkage velocity did increase from 21 °C to 31 °C, as previously reported (Kawamura and Wasteneys, 2008).

Table 2.1 Comparison of mean microtubule velocity measurements in the present study with previously published results

Standard deviation and number of microtubules measured are indicated, where information is available. Abe and Hashimoto (2005) measured microtubule dynamics in epidermal cells of the upper hypocotyl, whereas Kawamura and Wasteneys (2008) and the present study measured microtubule dynamics in cotyledon epidermal cells.

Genotype		Rates published by Abe and Hashimoto (2005) (μm/min)	Rates published by Kawamura and Wasteneys (2008) (μm/min)	Rates measured in the present study (μm/min)
Wild type (Col)	Growth (21 °C)	4.72 ± 3.02	3.5 ± 1.9 (n = 115)	5.13 ± 1.24 (n = 150)
	Growth (31 °C)		6.5 ± 3.5 (n = 28)	4.77 ± 1.69 (n = 150)
	Shrinkage (21 °C)	9.43 ± 9.12	9.0 ± 5.8 (n = 115)	14.38 ± 5.61 (n = 75)
	Shrinkage (31 °C)		12.4 ± 9.3 (n = 28)	17.35 ± 8.74 (n = 75)
mor1-1	Growth (21 °C)		2.5 ± 1.5 (n = 98)	3.00 ± 0.80 (n = 150)
	Growth (31 °C)		2.0 ± 1.5 (n = 26)	2.67 ± 0.81 (n = 150)
	Shrinkage (21 °C)		6.2 ± 4.3 (n = 98)	11.34 ± 4.34 (n = 75)
	Shrinkage (31 °C)		3.8 ± 3.1 (n = 26)	10.64 ± 4.90 (n = 75)

2.2.2 Microtubule plus-end dynamics are reduced to a similar extent in *mor1-1* and *rid5*

Though microtubule dynamics in *mor1-1* had previously been measured (Kawamura and Wasteneys, 2008), microtubule dynamics in *rid5* and the tubulin mutants had not. At both 21 and 31 °C, plus-end growth and shrinkage velocities of *mor1-1* and *rid5* were significantly lower than wild type (Fig. 2.2 A, B). Plus-end growth velocities of *mor1-1* and *rid5* were statistically equivalent at 21 °C, though growth velocity in *rid5* was significantly lower than in *mor1-1* at 31 °C (Fig. 2.2 A). Plus-end shrinkage velocities of *mor1-1* and *rid5* were statistically equivalent at both temperatures (Fig. 2.2 B). These measurements provide a basis for comparison to the tubulin-*mor1* double mutant dynamics measurements presented in subsequent sections.

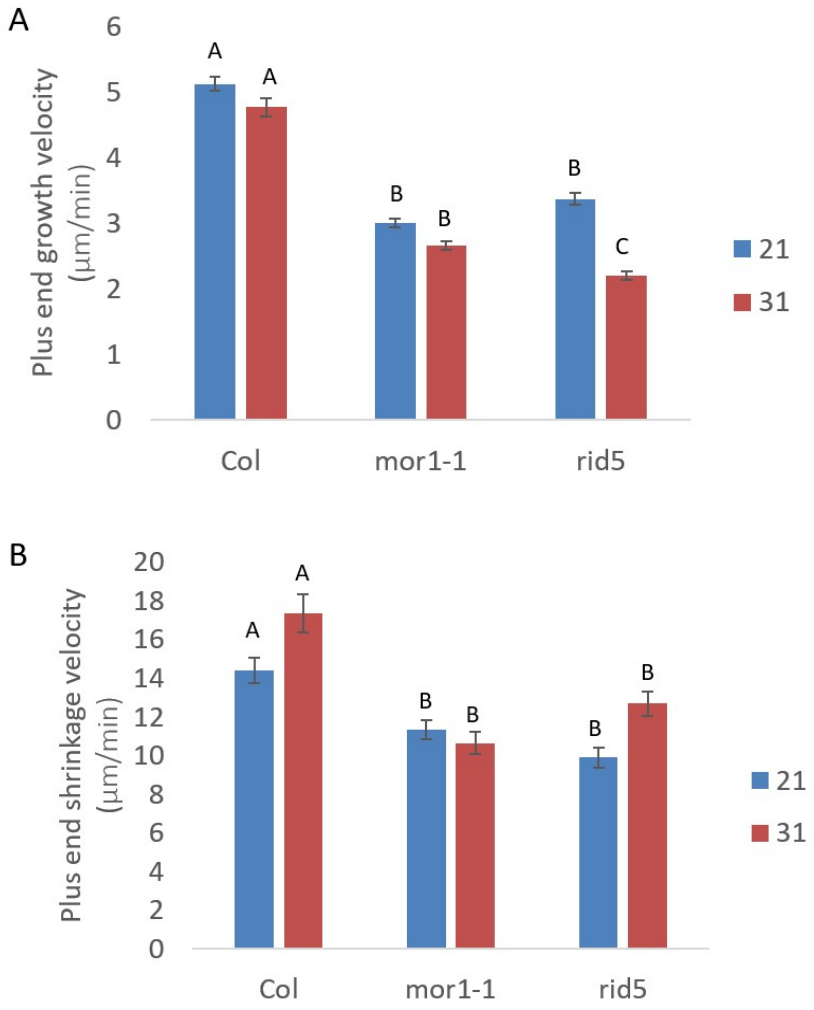

Figure 2.2 Microtubule dynamics in *mor1-1* and *rid5* are reduced relative to wild type at 21 °C and 31 °C

(A) Plus end growth velocity at 21 and 31 °C, n = 150 for each genotype at each temperature.
(B) Plus end shrinkage velocity at 21 and 31 °C, n = 75 for each genotype at each temperature.
Error bars indicate the standard error of the mean. Letters indicate statistically equivalent mean velocities at a given temperature, based on ANOVA with post hoc analysis (Tukey's HSD, $p < 0.01$).

2.2.3 Microtubule dynamics in *tub4^{P220S}mor1-1* double mutants are characteristic of *tub4^{P220S}* at 31 °C

Measurements of microtubule dynamics in the *tub4^{P220S}* and *tub4^{P220S}mor1* double mutants were acquired next, and compared to wild type and the *mor1* single mutants. At 21 °C, plus-end growth and shrinkage velocities of both *mor1-1* and *tub4^{P220S}* were reduced relative to wild type (Col) (Fig. 2.3 A, B). Growth velocity was restored to wild type-like levels in *tub4^{P220S}mor1-1* (Fig. 2.3 A), though shrinkage velocity in *tub4^{P220S}mor1-1* is statistically equivalent to that of the two single mutants (Fig. 2.3 B). At 31 °C, plus-end growth and shrinkage velocities of *mor1-1*, but not *tub4^{P220S}*, are reduced relative to wild type (Fig. 2.3 A, B). Both the growth and shrinkage velocities in *tub4^{P220S}mor1-1* are statistically equivalent to those of wild type and *tub4^{P220S}* (Fig. 2.3 A, B), indicating a recovery from the reduced velocities seen in *mor1-1*. The recovery of microtubule dynamics to wild-type levels in *tub4^{P220S}* and in the *tub4^{P220S}mor1-1* double mutant at 31 °C was unexpected, because of the root twisting and radial swelling phenotypes of these mutants, as well as the disorganized microtubule phenotype of *tub4^{P220S}mor1-1* at 31 °C (Zhang, 2010; Appendix 1). Previous models of anisotropic cell expansion predicted that twisting growth correlated to changes in microtubule dynamicity relative to wild type (Abe and Hashimoto, 2005), though this does not appear to be the case.

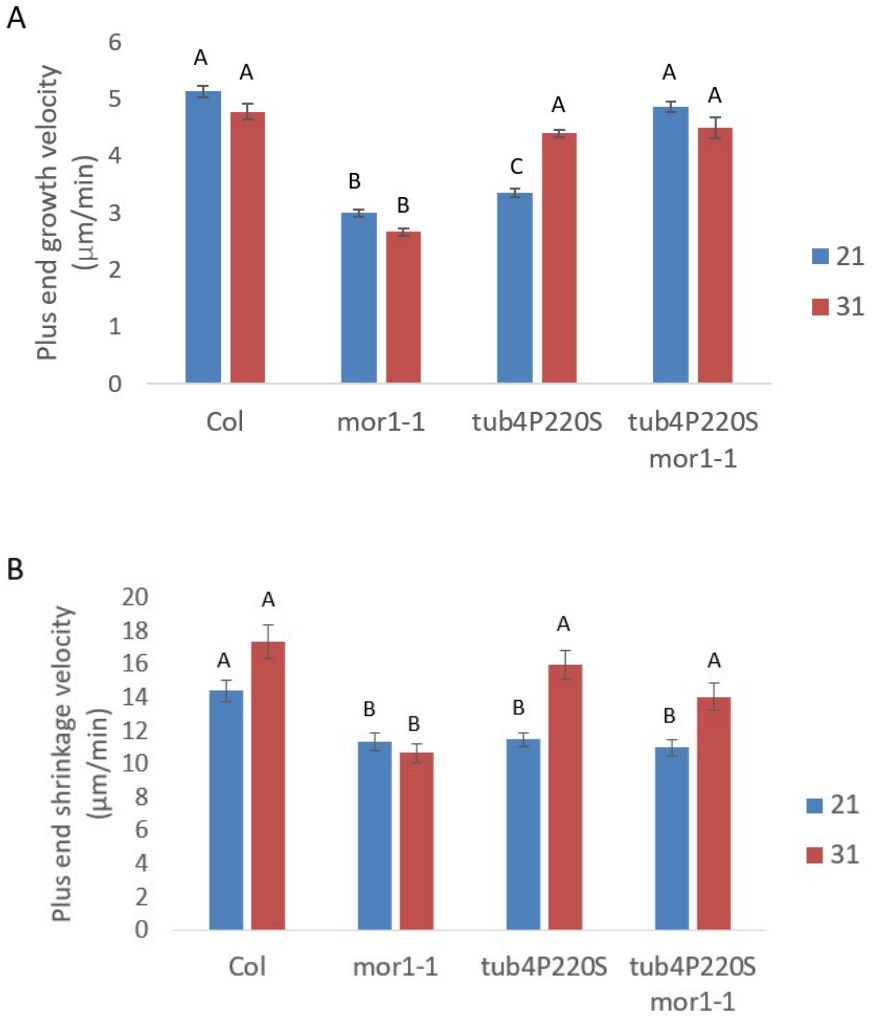

Figure 2.3 Microtubule dynamics in *tub4^{P220S}* and the *tub4^{P220S}mor1-1* double mutant recover to wild type-like levels at 31 °C recover to wild type-like levels at 31 °C

(A) Plus end growth velocity at 21 and 31 °C, n = 150 for each genotype at each temperature.
(B) Plus end shrinkage velocity at 21 and 31 °C, n = 75 for each genotype at each temperature.
Error bars indicate the standard error of the mean. Letters indicate statistically equivalent mean velocities at a given temperature, based on ANOVA with post hoc analysis (Tukey's HSD, $p < 0.05$).

2.2.4 Microtubule dynamics in *tub4^{P220S}rid5* are reduced compared to either single mutant

At 21 °C, plus-end growth and shrinkage velocities of both *rid5* and *tub4^{P220S}* are reduced relative to wild type (Col) (Fig. 2.4 A, B). Growth and shrinkage velocity are further reduced in *tub4^{P220S}rid5*. At 31 °C, plus-end growth and shrinkage velocity are significantly lower in *rid5* than in wild type and *tub4^{P220S}* (Fig.

2.4 A, B). Plus-end growth velocity in *tub4*^{P220S}*rid5* is statistically equivalent to that of *rid5* (Fig. 2.4 A), though shrinkage velocity is further reduced (Fig. 2.4 B). The twisting phenotype of *tub4*^{P220S} is epistatic to that of *rid5* (Zhang, 2010; Appendix 1), though the microtubule dynamics in the double mutant are not equivalent to those of *tub4*^{P220S}. As before, there is no clear correlation between microtubule plus-end dynamics and the root twisting phenotype. Interestingly, though *tub4*^{P220S}*rid5* has wild type-like microtubule organization at 21 °C and short, disorganized microtubules at 31 °C, microtubule dynamics in the double mutant are similar at both temperatures.

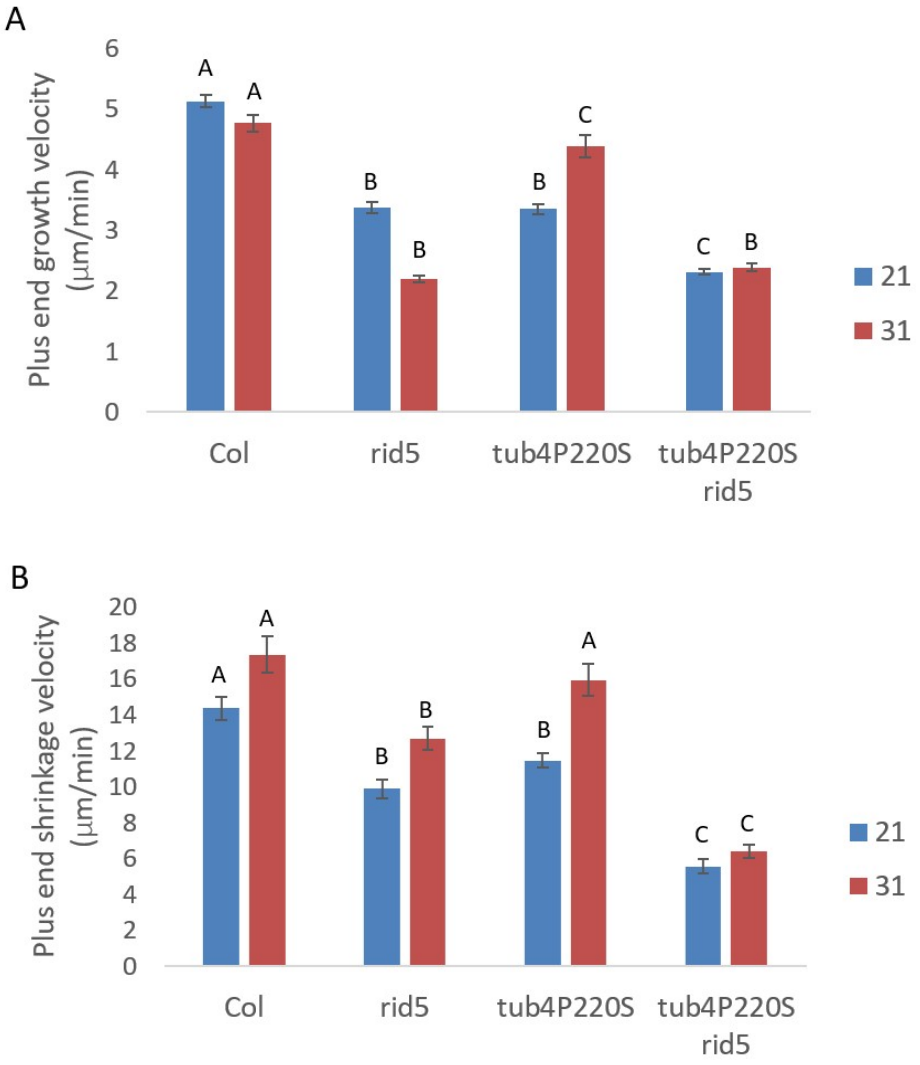

Figure 2.4 Microtubule dynamics in the *tub4*^{P220S}*rid5* double mutant are reduced compared to either single mutant

(A) Plus end growth velocity at 21 and 31 °C, n = 150 for each genotype at each temperature.
(B) Plus end shrinkage velocity at 21 and 31 °C, n = 75 for each genotype at each temperature.
Error bars indicate the standard error of the mean. Letters indicate statistically equivalent mean velocities at a given temperature, based on ANOVA with post hoc analysis (Tukey's HSD, $p < 0.05$).

2.2.5 The *tub4^{G96D}mor1* double mutants have short, disorganized microtubules at 21 °C

Microtubule organization in the *tub4^{P220S}mor1* double mutants was previously characterized (Zhang, 2010; Appendix 1). Here, I characterize microtubule organization in the *tub4^{G96D}mor1* double mutants, for the purpose of comparison. At 21 °C, microtubule organization appears similar to wild type in *mor1-1*, *rid5*, and *tub4^{G96D}* (Fig. 2.5 A, C, E, and G). At 31 °C, no microtubule organization defects are seen in wild type or *tub4^{G96D}* (Fig. 2.5 B, H), but *mor1-1* and *rid5* have short, disorganized microtubules, as reported previously (Fig. 2.5 D, F; Whittington *et al*., 2001; Zhang, 2010). Interestingly, the *tub4^{G96D}mor1-1* double mutant has short, disorganized microtubules at both 21 °C and 31 °C (Fig. 2.5 I, J); whereas *mor1-1* and *tub4^{P220S}mor1-1* only have short, disorganized microtubules at 31 °C (Whittington *et al*., 2001; Zhang, 2010; Appendix 1). The *tub4^{G96D}rid5* double mutant also has short, disorganized microtubules at 21 °C, though microtubules are relatively longer at 31 °C (Fig. 2.5 K, L). This recovery of microtubule length is unexpected, as the double mutant has a radial swelling phenotype at 31 °C (Zhang, 2010; Appendix 1).

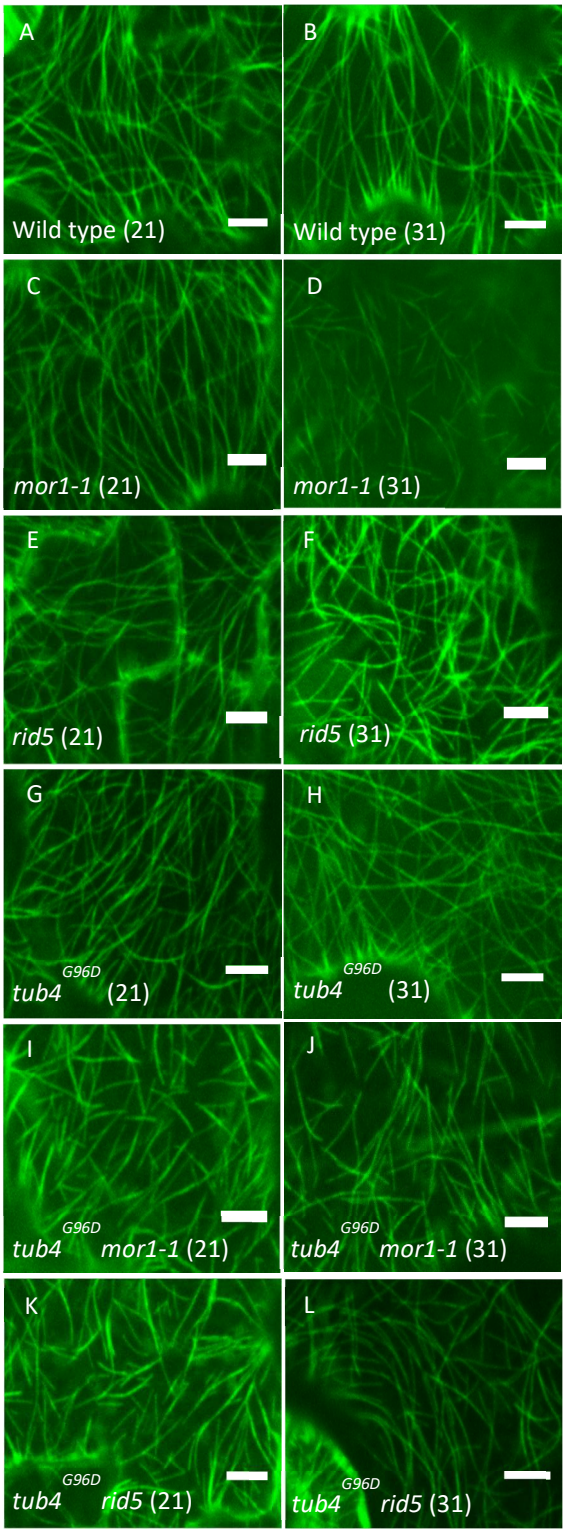

Figure 2.5 Microtubule organization phenotypes in *tub4*^{G96D}*mor1* double mutants

Confocal micrographs of *pro35S::GFP-TUB6* labelling cortical microtubule arrays in cotyledon epidermal cells of 7 day-old seedlings grown and imaged at 21 °C (left column) or 31 °C (right column).

Representative images are shown from a selection of 15-20 images acquired for each genotype at each temperature.
(A, B) Microtubule organization in wild type (Col) is similar at 21 °C and 31 °C.
(C-F) Microtubule organization in *mor1-1* and *rid5* is similar to wild type at 21 °C, but microtubules are short and disorganized at 31 °C.
(G, H) Microtubule organization in *tub4*^{G96D} is similar to wild type at 21 °C and 31 °C.
(I, J) Short, disorganized microtubules are seen in *tub4*^{G96D}*mor1-1* at 21 °C and 31 °C.
(K, L) Short, disorganized microtubules are seen in *tub4*^{G96D}*rid5* at 21 °C, but microtubules are longer at 31 °C.
Scale bars = 5 μm.

2.2.6 Microtubule dynamics in *tub4*^{G96D}*mor1-1* and *tub4*^{G96D}*rid5* are reduced compared to the single mutants

I next measured microtubule dynamics in the *tub4*^{G96D}*mor1* double mutants. At both 21 °C and 31 °C, plus-end growth and shrinkage rates are reduced in *tub4*^{G96D} relative to wild type (Col) (Fig. 2.6 A, B). At both temperatures, both growth and shrinkage velocities of the *tub4*^{G96D}*mor1-1* double mutant are reduced relative to velocities observed in the *mor1-1* and *tub4*^{G96D} single mutants.

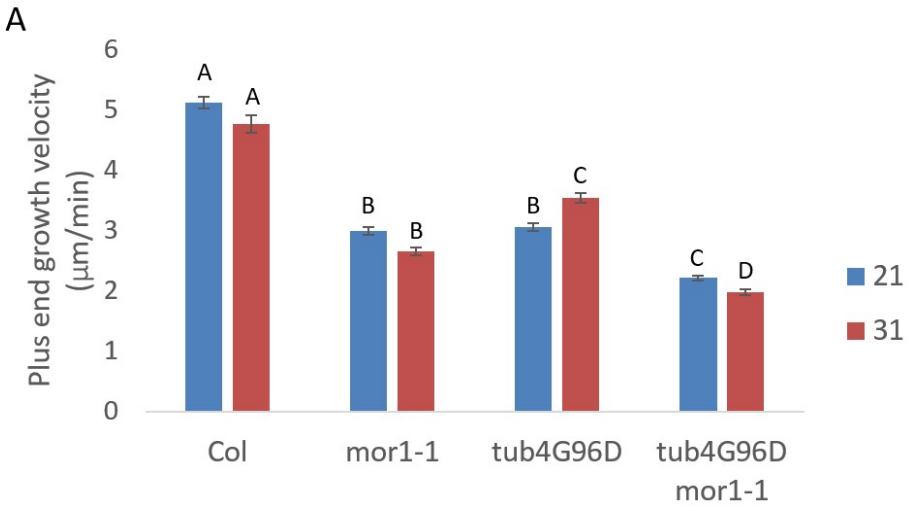

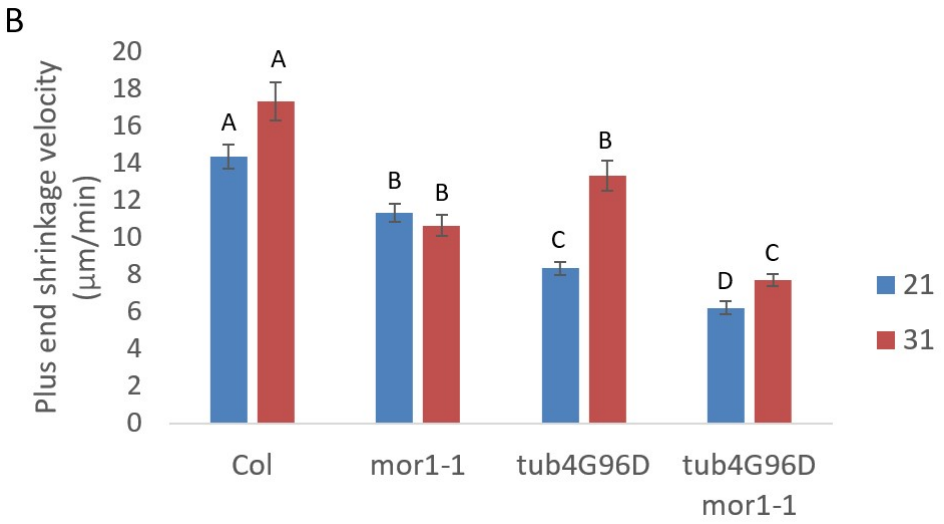

Figure 2.6 Microtubule dynamics in the *tub4^{G96D}mor1-1* double mutant are reduced compared to either single mutant

(A) Plus end growth velocity at 21 and 31 °C, n = 150 for each genotype at each temperature. (B) Plus end shrinkage velocity at 21 and 31 °C, n = 75 for each genotype at each temperature. Error bars indicate the standard error of the mean. Letters indicate statistically equivalent mean velocities at a given temperature, based on ANOVA with post hoc analysis (Tukey's HSD, $p < 0.05$).

A similar trend was observed in the *tub4^{G96D}rid5* double mutant: at both temperatures, growth and shrinkage velocities are reduced relative to velocities observed in the *rid5* and *tub4^{G96D}* single mutants (Fig. 2.7 A, B). One exception is that growth velocity in the double mutant at 31 °C is equivalent to that of *rid5*.

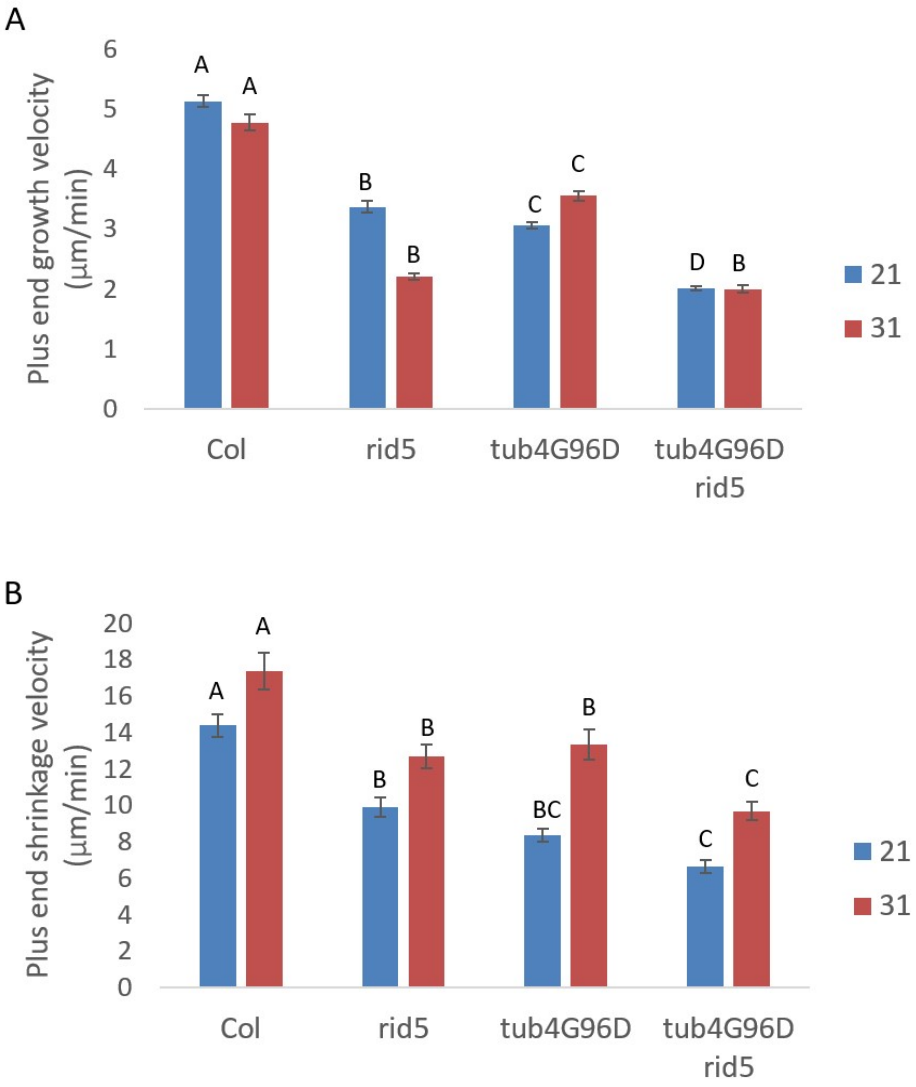

Figure 2.7 Microtubule dynamics in the *tub4^{G96D}rid5* double mutant are reduced compared to either single mutant

(A) Plus end growth velocity at 21 and 31 °C, n = 150 for each genotype at each temperature.
(B) Plus end shrinkage velocity at 21 and 31 °C, n = 75 for each genotype at each temperature.
Error bars indicate the standard error of the mean. Letters indicate statistically equivalent mean velocities at a given temperature, based on ANOVA with post hoc analysis (Tukey's HSD, $p < 0.05$).

2.2.7 No *tua5^{D251N}rid5* line expressing *pro35S::GFP-TUB6* could be isolated

The *tua5^{D251N}mor1-1* double mutant was previously found to be seedling-lethal, though the *tua5^{D251N}rid5* double mutant grew to maturity (Zhang, 2010). Despite genotyping more than 40 plants displaying the

characteristic root twisting phenotype of *tua5*^{D251N}*rid5*, I was unable to isolate any plants that were homozygous for both mutations and that also expressed *pro35S::GFP-TUB6*. Attempts to isolate a *tua5*^{D251N}*rid5* line expressing *proEB1b::EB1b* were also unsuccessful.

2.3 Discussion

2.3.1 Twisting growth does not correlate with microtubule growth or shrinkage velocity

The *tub4*^{P220S} mutant exhibits right-handed twisting at both 21 °C and 31 °C (Ishida *et al*., 2007a; Zhang, 2010; Appendix 1). It has previously been proposed that right-handed twisting was an indication of increased microtubule stability or reduced depolymerization (Abe and Hashimoto, 2005; Ishida *et al*., 2007a). This hypothesis is not supported by the present study: though microtubule dynamics in *tub4*^{P220S} are reduced at 21 °C, they are restored to wild type-like levels at 31 °C (Fig 2.3). *TUB4* gene expression is relatively constant with increased temperature (Kilian *et al*., 2007; Winter *et al*., 2007; *Arabidopsis* eFP browser), so the recovery of microtubule dynamics is unlikely to result from replacement of TUB4^{P220S} with another, wild-type β-tubulin isoform. Unlike *tub4*^{P220S}, wild-type seedling roots do not exhibit any twisting phenotype at 31 °C (Zhang, 2010). This suggests that twisting growth may be determined by some factor(s) other than array stability or dynamicity, or dependent on subtle changes thereto. This finding agrees with a modelling study of microtubule organization, which demonstrated that the dynamic instability parameters of the *tua5*^{D251N} twisting mutant were not sufficient to generate oblique cortical microtubule arrays in a computer simulation, though modelling altered nucleation of microtubules did generate oblique arrays (Eren *et al*., 2010).

Another possibility is that microtubule dynamics may differ in root and cotyledon pavement cells; if so, microtubule dynamics in root cells may differ in wild type and *tub4*^{P220S}. The *pro35S::GFP-TUB6* marker used in this study does not label microtubules in root cells, but observations of petiole twisting in *mor1* and tubulin mutants indicated that microtubules in pavement cells were likely to be affected similarly

(Zhang, 2010). This marker was selected on the basis that it is not known to cause changes in microtubule organization or dynamics, and does not generate a twisting phenotype, as do other fluorescent microtubule markers. Indeed, a previous study of microtubule dynamics in wild type and *mor1-1* yielded significantly different measurements of growth and shrinkage rates using either *pro35S::GFP-TUA6* or *pro35S::GFP-EB1b* as microtubule markers, possibly as the result of an interaction between EB1b and MOR1 (Kawamura and Wasteneys, 2008). Possible promotion of microtubule bundling has also been observed in seedlings expressing *pro35S::GFP-MBD* (Kawamura, 2007), and over-expression of EB1b was shown to alter microtubule dynamics in the *tub4*^{P287L} mutant (Yu *et al*., 2015).

2.3.2 The effects of the *rid5* mutation differ from those of the *mor1-1* mutation

Microtubule plus-end growth and shrinkage rates in *rid5* were seen to be similar to those in *mor1-1* (Figure 2.2), and both mutations affect HEAT repeats in the TOG1 domain. Why, then, does the phenotype of *rid5* seedlings differ from that of *mor1-1* (and *mor1-2*)? *rid5* undergoes left-handed twisting at both the permissive and restrictive temperatures, with mild radial swelling at the restrictive temperature (Konishi and Sugiyama, 2003; Zhang, 2010; Appendix 1). On the other hand, *mor1-1* and *mor1-2* roots appear phenotypically similar to wild type at the permissive temperature, with left-handed twisting and more severe radial swelling when grown at the restrictive temperature (Whittington *et al*., 2001; Appendix 1). Tubulin-*mor1-1* and tubulin-*rid5* double mutants also have different phenotypes with respect to microtubule organization and dynamics (discussed subsequently), and with the twisting phenotypes in combination with certain tubulin mutants (Zhang, 2010; Appendix 1).

The location of the *rid5* mutation in the 3rd HEAT repeat and *mor1-1* and *mor1-2* in the 5th HEAT repeat means that the affected residues interact with different regions of tubulin dimers (free tubulin or the microtubule lattice), with one TOG domain spanning just under the length of a single tubulin dimer (Al-Bassam *et al*., 2007; Kawamura and Wasteneys, 2008). In addition, the location and type of amino acid

substitution may differentially affect protein conformation at other sites that influence interactions with tubulin or the microtubule lattice. MOR1 protein stability and turnover may also differ depending on the site of the mutation, since TOG12$^{mor1\text{-}1}$ was found to be more prone to degradation and aggregation than wild-type TOG12 (Lechner *et al*., 2012). It may be that the phenotypic differences between *mor1-1* and *rid5* reflect altered protein stability.

2.3.3 Microtubule dynamics can be uncoupled from radial swelling

The *tub4*^{P220S}*mor1-1* double mutant exhibits radial swelling and no twisting at 31 °C, and has short, disorganized microtubules (Zhang, 2010; Appendix 1). The lack of twisting likely reflects reduced cell elongation due to radial swelling, as elongation is required for twisting growth (Ishida *et al*., 2007b; Weizbauer *et al*., 2011). Modelling of microtubule dynamics in *mor1-1* showed that reduced dynamicity led to fewer encounters between microtubules, accounting for the disorganization of the cortical array (Allard *et al*., 2010; Eren *et al*., 2010). The short microtubules in *mor1-1* result in higher cellulose crystallinity, and consequently, loss of growth anisotropy (Fujita *et al*., 2011). While the radial swelling phenotype of *tub4*^{P220S}*mor1-1* at 31 °C is accounted for by the short and disorganized microtubules, it is not clear why the microtubules are short and disorganized, when growth and shrinkage velocities recover to wild type-like (*tub4*^{P220S}-like) levels at 31 °C (Fig. 2.3).

The *mor1-1* mutation increases the affinity of MOR1 for the microtubule lattice, and is thought to reduce microtubule dynamicity by impairing diffusion to the plus-end (Lechner *et al*., 2012). The *tub4*^{P220S} mutation is located at the intradimer interface, and results in reduced microtubule dynamicity at 21 °C (Fig. 2.3). This would suggest that the mutation impairs addition of incoming tubulin dimers. However, at 31 °C, this effect is no longer seen in either *tub4*^{P220S} or *tub4*^{P220S}*mor1-1*. This could be attributed to microtubule dynamics changing with temperature, but a recovery in plus-end growth velocity is also observed at 21 °C with the *tub4*^{P220S}*mor1-1* double mutant, so that explanation isn't

satisfactory. It is possible that the *tub4*^{P220S} mutation allows MOR1$^{1-1}$ to track the growing plus end more easily, e.g. due to a change in conformation that reduces the affinity of MOR1$^{1-1}$ for the microtubule lattice. This, in turn, could affect the localization of other +TIPs, such as EB1b, which has reduced plus-end binding in *mor1-1* at 31 °C (Kawamura and Wasteneys, 2008). The *tub4*^{P220S}mutant also has hyperparallel microtubules and increased microtubule bundling at 31 °C (Zhang, 2010; Appendix 1). Though this organization is lost in the *tub4*^{P220S}*mor1-1* mutant, it suggests that the *tub4*^{P220S} mutation may affect various MAP-microtubule interactions, including MAPs that promote bundling, such as MAP65-1 (Jiang and Sonobe, 1993; van Damme *et al*., 2004, Lucas *et al*., 2011).

The right-handed twisting characteristic of *tub4*^{P220S} masks the left-handed twisting of *rid5*, and the *tub4*^{P220S}*rid5* double mutant also has the mild radial swelling characteristic of *rid5* (Zhang, 2010; Appendix 1). Unlike the *tub4*^{P220S}*mor1-1* double mutant, the *tub4*^{P220S}*rid5* double mutant has reduced microtubule dynamicity relative to either single mutant, at both temperatures (Fig. 2.4), highlighting the differences between *mor1-1* and *rid5*, and possibly the functional differences between the different HEAT repeats of TOG1. Although the twisting phenotype of *tub4*^{P220S} is epistatic to that of *rid5*, this is not correlated with the effects of each defect on microtubule dynamicity.

2.3.4 Different types of genetic interactions are observed between *mor1* mutants and those tubulin mutants affecting the interdimer interface

The reduction of microtubule dynamics in *tub4*^{G96D} and in the *mor1-1* and *rid5* mutants has a synergistic effect: at both temperatures, the growth and shrinkage rates of the double mutants are significantly lower than those of the corresponding single mutants (Fig. 2.6, 2.7). In both double mutants at 31 °C, however, the roots exhibit the radial swelling and left-handed twisting characteristic of the *mor1* mutants (Zhang, 2010; Appendix 1). Consistent with this, microtubule organization in the *tub4*^{G96D}*mor1* double mutants is *mor1*-like, with short, disorganized microtubules even at 21 °C (Fig. 2.5 I-L).

Interestingly, although microtubule length recovers at 31 °C in the *tub4^{G96D}rid5* double mutant, radial swelling is still observed.

2.4 Methods

2.4.1 Plant material and growth conditions for tubulin-*mor1* mutant analysis

To remove fungal spores, *Arabidopsis thaliana* (Col ecotype) seeds were treated with a sterilization solution (50% v/v ethanol, 3% v/v hydrogen peroxide) for 60 seconds, then washed twice with autoclaved distilled water. Seeds were grown on plates containing modified Hoagland's growth medium with 1.2% w/v agar (Baskin and Wilson, 1997). Plates were sealed with surgical tape and stored in the dark at 4 °C to promote germination, then placed vertically in a growth chamber (21 °C, continuous light at 80-100 μmol/m^2/second). For imaging experiments, plants grown at the permissive temperature were kept in the 21 °C growth chamber for a further 2 days, whereas plants grown at the restrictive temperature were transferred to a 31 °C growth chamber for 2 days. Plants grown for the purpose of cross-pollinating or genotyping were maintained at the permissive temperature.

2.4.2 Genotyping tubulin-*mor1* mutant plants expressing *pro35S::GFP-TUB6*

Yi Zhang cross-pollinated plants expressing *pro35S::GFP-TUB6* with all of the mutants used in this chapter, and identified F2 plants that were homozygous for *tub4^{P220S}*, *mor1-1*, *rid5*, *tub4^{P220S}mor1-1*, *tub4^{P220S}rid5*, which also expressed the GFP-TUB6 microtubule marker (Zhang, 2010). I genotyped and identified F2 plants that were homozygous for *tub4^{G96D}*, *tub4^{G96D}mor1-1*, *tub4^{G96D}rid5*, which also expressed the GFP-TUB6 marker, and attempted to do the same for *tua5^{D251N}* and *tua5^{D251N}rid5*. Candidate plants for genotyping were identified based on their root twisting/skewing phenotypes when grown on agar plates (at 21 °C and 31 °C) (see Appendix 1). The *mor1-1* mutation was genotyped using PCR primers that detect the presence or absence of the *mor1-1* single nucleotide polymorphism (SNP). Two forward primers were used in conjunction with a single reverse primer: the forward primers differ

at the 3' end, such that the *mor1*^{WT} primer binds only to the wild-type sequence, whereas the *mor1-1* primer binds only to the *mor1-1* sequence (Zhang, 2010). The *rid5* and tubulin mutations were genotyped using PCR primers that amplify the region around the mutation; the purified PCR products were sequenced at the NAPS DNA Sequencing Laboratory (UBC), and sequences were assessed using chromatograms posted to the NAPS website.

Table 2.2 Primers used to genotype *mor1* and tubulin mutant plants

Mutation	Forward primer (5'→3')	Reverse primer (5' →3')
mor1^{WT}	CCTAAAAGGATTTTAAAGATGC	GAGAATAAATAAAAATTCAAGTGT
mor1-1	AAGGATTTTAAAGATGT	As above
rid5	GGGTTCCATTTTGCTTTACTTTT	GCACTTTCATTTCTATGTCAGCTC
tub4^{P220S}	CGTGGAACGAGAATGATTACAA	TGTTCTTTGCATCCCACATC
tub4^{G96D}	TCATATCCAAGGCGGTCAAT	GAGTTCCCATTCCAGATCCA
tua5^{D251N}	CCCTTCTCCTCAGGTACTCTTTC	CTGAACAGTCCTCTTTGTCTTGA

2.4.3 Confocal microscopy

GFP-TUB6 was visualized in epidermal cells of the abaxial side of cotyledons of 7-day-old seedlings, at 630x magnification (using a 63x glycerol lens). Cotyledons were mounted in perfluoroperhydrophenanthrene (Sigma-Aldrich) to improve image quality and gas exchange, as detailed in Littlejohn *et al*. (2014). Videos were taken using Volocity™ software version 6.3, using a PerkinElmer UltraVIEW VoX spinning disc confocal system on a Leica DMI6000B inverted microscope, with a Hamamatsu 9100-02 electron multiplier CCD camera. GFP was excited using a 488 nm laser, and detected through a 525/36 nm emission filter. Z-stacks were acquired using five 0.35 μm slices, so as to follow microtubule plus ends that moved slightly out of the z-plane. Image stacks were acquired every 8 seconds. For each genotype at both 21 °C and 31 °C, three videos were generated for each of five seedlings. A temperature-controlled stage was used (Bionomic Controller BC-110 with a Heat Exchanger

HEC-40; 20-20 Technology Inc.) to maintain the cotyledons at 21 °C or 31 °C during imaging, and a temperature probe (Thermocouple FLUKE 52; John Fluke Manufacturing Co.) was used to measure the temperature of the glycerol on the slide after imaging, confirming that the temperature controls were consistent. Some videos were taken by Dr. Kasia Celler. A sample image of a time series is shown in Appendix 1.

2.4.4 Image processing, microtubule tracking, and statistical analysis

Images were exported to ImageJ (Abràmoff *et al*., 2004), and compressed into a single Z-projection. Representative still images were selected to show microtubule organization in wild type and in each mutant. Microtubule plus-end dynamics were measured using the MTrackJ plugin (Meijering *et al*., 2012). For each video, 10 growing microtubule plus ends and 5 shrinking microtubule plus ends were tracked for at least 16 seconds of continuous growth/shrinkage, yielding 150 measurements of plus-end growth and 75 of plus-end shrinkage velocity for each genotype at both temperatures. Data were exported to Microsoft Excel, and average microtubule growth/shrinkage velocity were calculated, along with the standard error of the mean. Statistical significance was determined using Analysis of Variance (ANOVA; Microsoft Excel) followed by Tukey's Honestly Significant Difference post-hoc test (using a free statistical calculator on astatsa.com, © Navendu Vasavada).

Chapter 3: Live-cell imaging demonstrates altered affinity of MOR1-YPet variants for microtubules

3.1 Introduction

3.1.1 The *mor1-11* mutant has a propyzamide-conditional phenotype

Initial studies of MOR1 used point mutations in the TOG1 domain, generated by EMS mutagenesis (Whittington *et al*., 2001; Konishi and Sugiyama, 2003), as well as the *gem1-1* and *gem1-2* mutants, which both result in truncation of the MOR1 protein such that the TOG5 and C-terminal domains are not translated (Twell *et al*., 2002). In order to study the function of other domains in MOR1, a collection of novel *mor1* point mutants was generated using TILLING (Targeted Induced Local Lesions IN Genomes; T. Shoji, unpublished results; Henikoff *et al*., 2004). One TILLING allele, *mor1-11* (G1399R), was discovered to exhibit strong right-handed root twisting when treated with the microtubule-destabilizing drug propyzamide (PPM) (Zhang, 2010) (Fig. 3.2 B). This phenotype is similar to that of a null mutant (*phs1-5*) of the tubulin kinase/MAP kinase phosphatase PHS1 (Pytela *et al*., 2010). However, microtubule stability is increased in *phs1-5* when challenged with osmotic stress (Fujita *et al*., 2013), whereas stability appears to decrease in *mor1-11*: when treated with PPM, microtubules in *mor1-11* are shorter, and growth rates decrease more than in wild-type plants treated with PPM (Zhang, 2010).

The extent of the TOG5 domain has been defined differently in different bioinformatic studies, so the G1399 residue is described as being either at the end of the TOG5 domain (Rashbrooke, 2005), or at the beginning of the C-terminal domain (Al-Bassam and Chang, 2011) (Fig. 3.1). The TOG5 domain is part of the C-terminal region defined by Twell *et al*. (2002) as being required for binding to the microtubule lattice, though Widlund *et al*. (2011) demonstrated that lattice binding in XMAP215 is mediated by a separate, basic region between TOG4 and TOG5. Interestingly, the R4 domain of the C-terminal region of MOR1 is extended in plant orthologues, and is highly conserved (Rashbrooke, 2005), suggesting specialization of the C-terminal region in plants. The C-terminal region may be involved in interactions

with other MAPs, or with kinases and phosphatases: one phospho-serine site has been identified in the C-terminal domain (Roitinger *et al*., 2015), and Twell *et al*. (2002) report five additional putative phosphorylation sites, though it is not known which kinases or phosphatases might control phosphorylation at these sites, or the functional significance of MOR1 phosphorylation. Interactions between the C-terminal region of ch-TOG and the +TIP-linking protein SLAIN2 have been reported (van der Vaart *et al*., 2011), though no such interactions have been identified for MOR1.

3.1.2 MOR1 recombineering

The *MOR1* gene is exceptionally large, and contains 53 exons (Fig. 3.1 A), which preclude the possibility of cloning *MOR1* using traditional methods. Previous biochemical and microscopy-based studies of MOR1 have therefore relied on the use of partial MOR1 constructs (Rashbrooke, 2005; Kawamura, 2007; Lechner *et al*., 2012), and immunofluorescence (Twell *et al*., 2002; Kawamura *et al*., 2006). Attempts at visualizing MOR1-microtubule interactions using fluorescently-tagged fragments of MOR1 yielded unsatisfactory results: for instance, no microtubule binding was observed when a C-terminal half-fusion protein of YFP-MOR1 was expressed in plant cells (Rashbrooke, 2005), although an equivalent experiment using XMAP215, as well as immunolocalization and microtubule binding assays with MOR1, had demonstrated binding of the C-terminal region to microtubules (Popov *et al*., 2001; Twell *et al*., 2002). Additionally, the expected plus-end localization of MOR1 was not observed using immunofluorescence (Kawamura *et al*., 2006; Walia, 2009): this was later demonstrated to be a consequence of the fixation procedure (Eng, 2015).

In order to clone full-length MOR1 and to add tags for affinity purification and fluorescence microscopy, it was necessary to use a process called recombineering. Briefly, *MOR1* was cloned along with a 6x histidine (His) tag and 1x or 3x YPet (YFP variant) tag at the C-terminus (Fig. 3.1B). 10 kb of upstream sequence and 5 kb of downstream sequence were included, to allow expression under the native

promoter and with any associated regulatory sequences. Along with wild-type *MOR1* (denoted here as MOR1^{WT}), variants with the *mor1-1* and *mor1-11* point mutations were also cloned (denoted as MOR1$^{1-1}$ and MOR1$^{1-11}$; all three constructs will be denoted as MOR1^{X}-YPet). This sequence was integrated into a transformation-competent bacterial artificial chromosome (TAC) binary vector, and transformed into *Arabidopsis* using *Agrobacterium tumefaciens* (Zhou *et al*., 2011; Alonso and Stepanova, 2014).

MOR1^{WT}-3YPet, *MOR1-1-YPet*, and *MOR1-11-YPet* were transformed into wild-type plants (Columbia ecotype), and two *MOR1* putative null mutant backgrounds: *mor1-23*, and *mor1-6* (Fig. 3.1), so that the functionality of the constructs and their associated phenotypes could be assessed in the absence of wild-type *MOR1* (Eng, 2015). Preliminary analysis of plants expressing *MOR1^{X}-YPet* in the *mor1-6* background suggests that phenotypes are similar to those in the *mor1-23* background; as efforts to isolate *MOR1^{X}-YPet*; *mor1-6* plants expressing microtubule markers are ongoing, this chapter will focus on the wild type and *mor1-23* backgrounds.

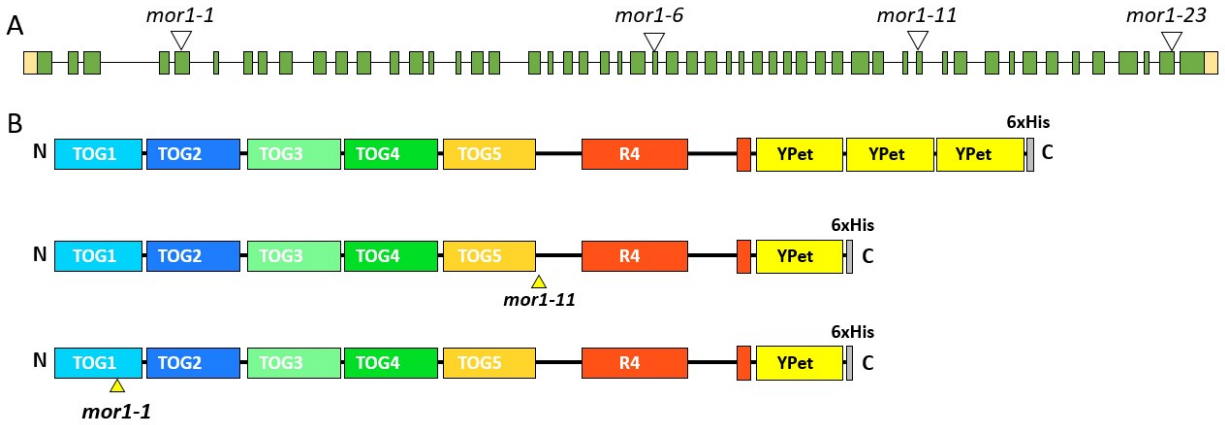

Figure 3.1 Constructs used for live-cell imaging of MOR1-microtubule interactions

(A) *MOR1* gene structure, indicating point mutations (*mor1-1* and *mor1-11*) under study in this chapter, as well as the *mor1-6* (early stop codon) and *mor1-23* (T-DNA; SALK_032056) putative null alleles.
(B) MOR1^{WT}-3YPet-6His (top), MOR1$^{1-1}$-YPet-6His (middle), and MOR1$^{1-11}$-YPet-6His (bottom) constructs.

3.1.3 MOR1^{WT}-3YPet acts as a +TIP

MOR1^{WT}-3YPet rescued the lethal phenotype of *mor1-23*, and localized to microtubule plus ends in mitotic and cytokinetic arrays (Eng, 2015). Localization was observed at both polymerizing and depolymerizing plus ends, including depolymerizing plus ends of recently severed microtubules. MOR1^{WT}-3YPet was not observed at microtubule minus ends, confirming its role as a +TIP. When expressed in the wild-type background, MOR1^{WT}-3YPet was observed to bind to microtubule side-walls, indicating a saturation of plus-end binding sites, and possible competition for binding sites with endogenous MOR1 (Eng, 2015). Competition between wild-type and mutant MOR1 for binding sites was also observed with TOG12 constructs: TOG12 ^{WT}-GFP did not localize to microtubules when expressed in wild-type plants, but did so when expressed in *mor1-1* plants, rescuing microtubule defects (Lechner *et al*., 2012). Determining the relative microtubule binding capacities of recombineered and endogenous MOR1 (with the various mutations) could be useful for understanding the activity of endogenous MOR1, in case the function of recombineered MOR1^{X} is altered by addition of the C-terminal tags.

Additionally, expression of *MOR1^{WT}-3YPet* in the *mor1-1* background was observed to rescue the temperature-sensitive radial swelling phenotype of *mor1-1* (R. Eng, unpublished results). It is of interest to see whether a similar effect is observed with *MOR1^{WT}-3Ypet* in the *mor1-11* background.

3.1.4 Objectives

In this chapter, I investigated whether the various MOR1^{X}-YPet constructs phenocopied wild type, *mor1-1*, and *mor1-11* when expressed in the *mor1-23* background. I also determined whether localization to the microtubule plus end and lattice varies between MOR1^{WT}-3Ypet and the MOR1$^{1-1}$ and MOR1$^{1-11}$ variants, thereby comparing the microtubule binding properties of the TOG1 domain and C-terminal region, which are affected in these mutants (Fig. 3.1 B). These constructs were expressed in the *mor1-*

23 putative null background so as to approximate interactions between endogenous MOR1 and microtubules in wild type, *mor1-1*, and *mor1-11*. I also determined whether localization to the microtubule plus end and lattice varies between $MOR1^{X}$-YPet and endogenous MOR1, by expressing these constructs in the wild-type and *mor1-11* backgrounds; and whether expression of $MOR1^{WT}$-3YPet can rescue the propyzamide (PPM)-conditional phenotype of *mor1-11*. The effects of the *mor1-11* mutation and addition of a C-terminal tag were examined, through analysis of α-tubulin phosphorylation.

3.2 Results

3.2.1 $MOR1^{1-11}$-YPet does not phenocopy *mor1-11*, instead conferring propyzamide hypersensitivity

mor1-11 has a semi-dominant PPM-conditional right-handed root twisting/skewing phenotype (Zhang, 2010; Fig. 3.2A, B). If $MOR1^{1-11}$-YPet functions in the same way as endogenous MOR1-11, expression of *$MOR1^{1-11}$-YPet* in the putative null *mor1-23* background would be expected to phenocopy *mor1-11*. Instead, expression of *$MOR1^{1-11}$-YPet* in the *mor1-23* background resulted in swelling of the root when grown on PPM (Fig. 3.2 C, D), indicative of propyzamide hypersensitivity. A similar effect was seen in plants expressing *$MOR1^{1-11}$-YPet* in the wild-type background (Fig. 3.2 E, F). Plants expressing *$MOR1^{1-11}$-YPet* had significantly shorter roots than *mor1-11* when grown on either DMSO or PPM (Fig. 3.2 G).

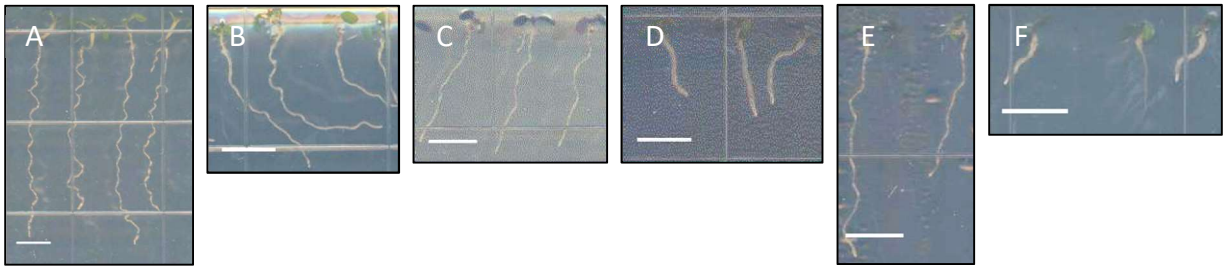

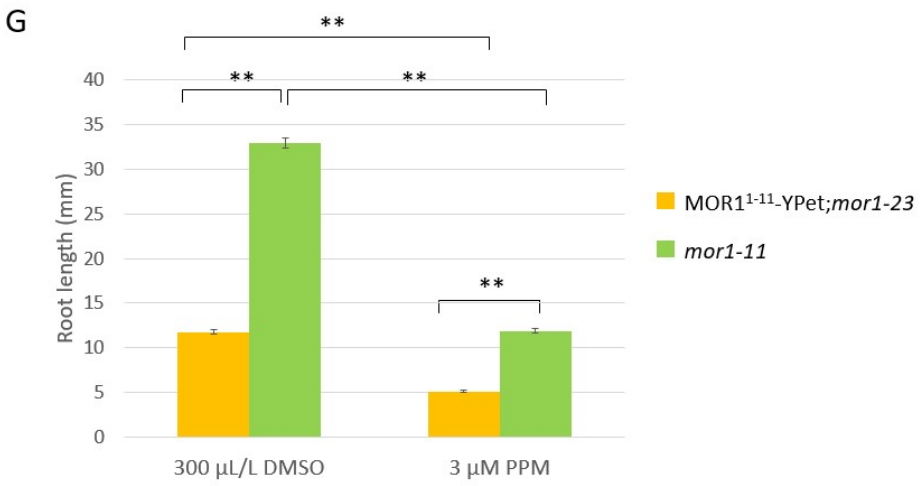

Figure 3.2 MOR1$^{1-11}$-YPet confers a more severe phenotype than is seen in *mor1-11*

Root growth phenotypes of 7-day-old seedlings treated with DMSO or 3 µM PPM. Images were adjusted to enhance brightness and contrast, for greater visibility of roots. Scale bars = 5 mm
(A, B) Root growth response of *mor1-11* to DMSO (A) and PPM (B)
(C, D) Root growth response of *MOR1$^{1-11}$-YPet* in the *mor1-23* background to DMSO (C) and PPM (D)
(E, F) Root growth response of *MOR1$^{1-11}$-YPet* in the wild-type background to DMSO (E) and PPM (F)
(G) Root length is significantly reduced in plants expressing *MOR1$^{1-11}$-YPet* in the *mor1-23* background. Error bars indicate standard error of the mean. n = 48 (*mor1-11*) or 100 (*MOR1$^{1-11}$-YPet*) for each treatment. ** indicates a statistically significant difference in pairwise comparisons; t-test, $p < 0.01$.

3.2.2 MOR1^{WT}-3YPet and MOR1$^{1-1}$-YPet also confer propyzamide hypersensitivity

In order to investigate whether the PPM-hypersensitive phenotype was unique to plants expressing *MOR1$^{1-11}$-YPet*, I conducted a similar experiment with plants expressing the *MOR1^{WT}* and *MOR1$^{1-1}$* variants (Fig. 3.3). Although seedlings appeared wild type-like when grown on DMSO (Fig. 3.3 C, E), expressing *MOR1^{WT}-3YPet* in the *mor1-23* background resulted in strong, right-handed root skewing when grown on PPM, which generates mild left-handed skewing in wild-type seedlings (Fig. 3.3 D). Expressing *MOR1^{WT}-3YPet* in the wild-type background resulted in a more severe phenotype in PPM-treated seedlings, with short, radially swollen roots (Fig. 3.3 F).

A similar effect was seen with the *MOR1$^{1-1}$* variant, again with a more severe phenotype in the wild-type background than in the *mor1-23* background. *mor1-1* exhibits left-handed root skewing on PPM (Fig. 3.3

H), whereas expressing *MOR1$^{1-1}$-YPet* in the *mor1-23* background resulted in short, radially swollen roots with slight left-handed skewing (Fig. 3.3 J). Expressing *MOR1$^{1-1}$-YPet* in the wild-type background resulted in a strong, left-handed root skewing phenotype in combination with radial swelling (Fig. 3.3 L).

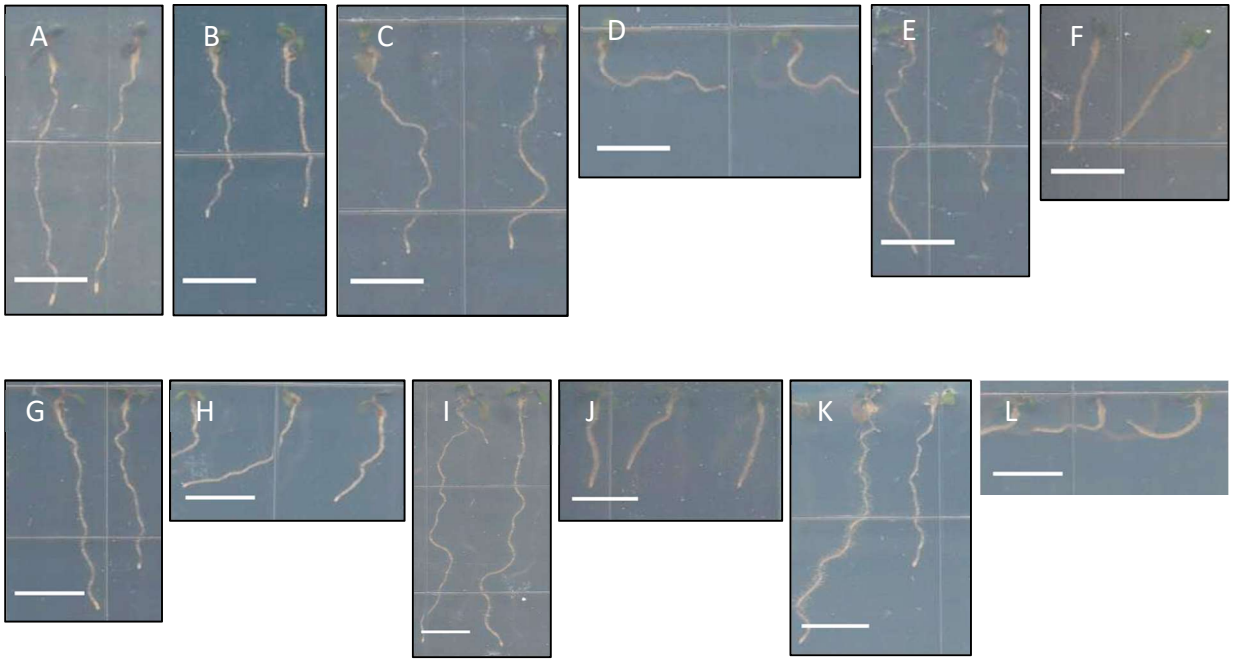

Figure 3.3 MOR1^{WT}-3YPet and MOR1$^{1-1}$-YPet confer propyzamide hypersensitivity

Root growth phenotypes of 7-day-old seedlings treated with DMSO or 3 μM PPM. Images were adjusted to enhance contrast and brightness, for greater visibility of roots. Scale bars = 5 mm.
(A, B) Root growth response of wild type to DMSO (A) and PPM (B)
(C, D) Root growth response of *MOR1^{WT}-3YPet* in the *mor1-23* background to DMSO (C) and PPM (D)
(E, F) Root growth response of *MOR1^{WT}-3YPet* in the wild-type background to DMSO (E) and PPM (F)
(G, H) Root growth response of *mor1-1* to DMSO (G) and PPM (H)
(I, J) Root growth response of *MOR1$^{1-1}$-YPet* in the *mor1-23* background to DMSO (I) and PPM (J)
(K, L) Root growth response of *MOR1$^{1-1}$-YPet* in the wild-type background to DMSO (K) and PPM (L)

3.2.3 Localization of MOR1^{X}-YPet variants changes with mutations and with the level of endogenous MOR1, but not with propyzamide treatment

As it was previously demonstrated that TOG12^{mor1-1} had greater affinity for the microtubule lattice than TOG12^{WT} (Lechner *et al*., 2012), I was interested in determining whether MOR1^{WT}-3YPet, MOR1$^{1-1}$-YPet,

and MOR1$^{1\text{-}11}$-YPet differed in their affinity for the microtubule plus end and/or lattice. Furthermore, as the *mor1-1* and *mor1-11* mutants both have PPM-conditional phenotypes (Collings *et al*., 2006; Zhang, 2010), I hypothesized that PPM treatment might affect the affinity of MOR1 for the microtubule. Plants expressing each MOR1^{X}-YPet variant (in the wild-type and *mor1-23* backgrounds) were crossed to either *pro35S::mRFP-TUB6* (by Ryan Eng), or *proUBQ10::mCherry-TUA5* (by me; chosen as an alternative microtubule marker for improved resolution of microtubules).

When treated with DMSO, MOR1^{WT}-3YPet co-localized with microtubules in the same manner as in untreated seedlings, previously analyzed by Eng (2015): in the *mor1-23* background, MOR1^{WT}-3YPet localized primarily to the microtubule plus end, whereas it bound to both the plus end and lattice in the wild-type background (Fig. 3.4). MOR1$^{1\text{-}1}$-YPet had predominantly plus-end localization (with some lattice binding) in both backgrounds (Fig. 3.5). MOR1$^{1\text{-}11}$-YPet localized to the plus end and lattice in the *mor1-23* background, and to the plus end in the wild-type background (Fig. 3.6). Treatment with PPM did not alter the localization of any of the MOR1^{X}-YPet constructs

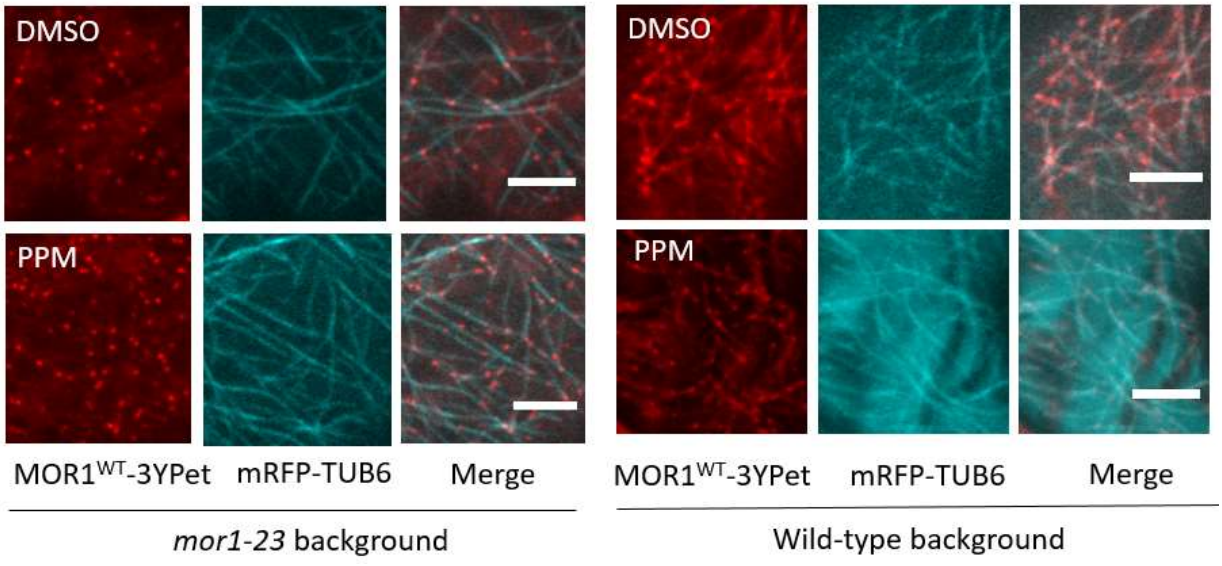

Figure 3.4 MOR1^{WT}-3YPet co-localization with microtubules varies with the level of endogenous MOR1, but not with propyzamide treatment

Confocal micrographs of MOR1^{WT}-3YPet labelling cortical microtubule arrays in cotyledon epidermal cells of 7-day-old seedlings treated with DMSO or 3 μM PPM. Representative still images are shown for each genotype and each treatment, from a selection of 10-25 videos acquired. Microtubule plus ends were identified in each video as the more dynamic microtubule end. Scale bars = 5 μm.

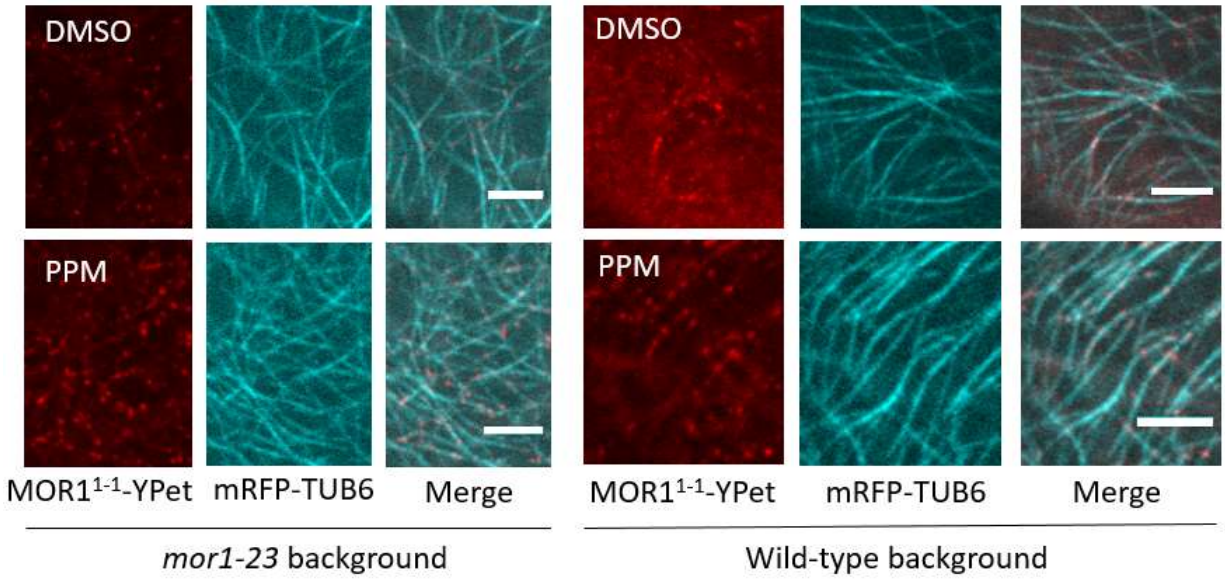

Figure 3.5 MOR1$^{1-1}$-YPet localizes primarily to the microtubule plus end, and localization does not vary with propyzamide treatment

Confocal micrographs of MOR1$^{1-1}$-YPet labelling cortical microtubule arrays in cotyledon epidermal cells of 7-day-old seedlings treated with DMSO or 3 μM PPM. Representative still images are shown for each genotype and each treatment, from a selection of 10-25 videos acquired. Microtubule plus ends were identified in each video as the more dynamic microtubule end. Scale bars = 5 μm.

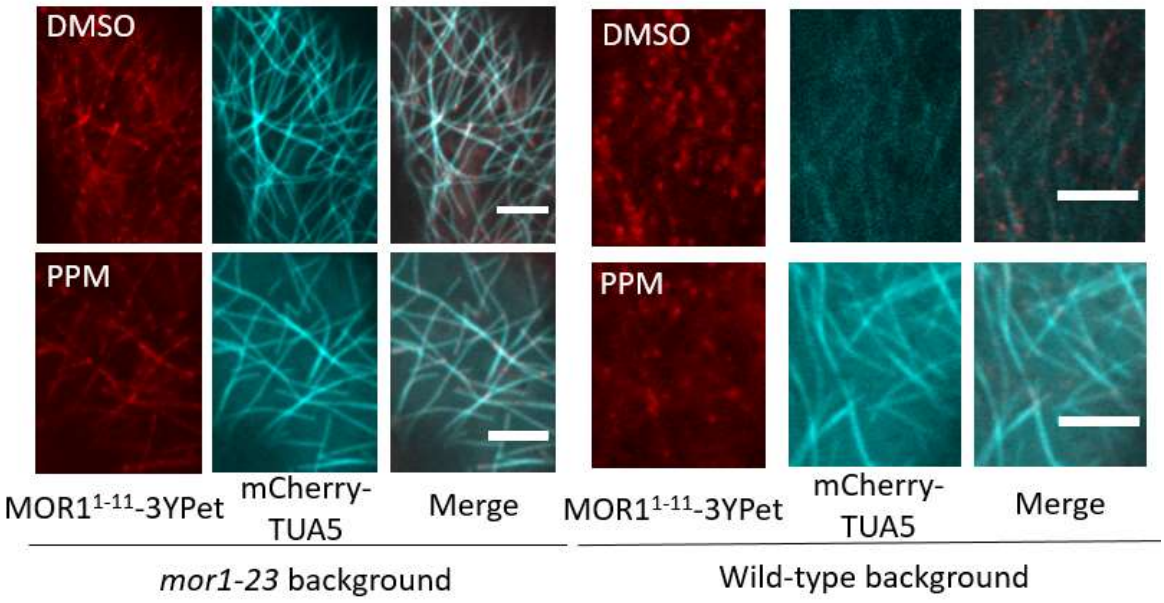

Figure 3.6 MOR1$^{1-11}$-YPet co-localization with microtubules varies with the level of endogenous MOR1, but not with propyzamide treatment

Confocal micrographs of MOR1$^{1-1}$-YPet labelling cortical microtubule arrays in cotyledon epidermal cells of 7-day-old seedlings treated with DMSO or 3 μM PPM. Representative still images are shown for each genotype and each treatment, from a selection of 10-25 videos acquired. Microtubule plus ends were identified in each video as the more dynamic microtubule end. Scale bars = 5 μm.

3.2.4 MOR1$^{1-1}$-YPet localization is not disrupted with temperature

As expressing the various MOR1^{X}-YPet constructs in the *mor1-23* background resulted in greater sensitivity to PPM than the wild-type, *mor1-1*, and *mor1-11* genotypes that they were intended to phenocopy, it was of interest to determine whether they might also confer enhanced temperature sensitivity. As *mor1-1* has a temperature-conditional radial swelling phenotype (Whittington *et al*., 2001), lines expressing MOR1$^{1-1}$-YPet in the wild-type and *mor1-23* backgrounds were assessed for radial swelling at 31 °C, but no radial swelling was observed (R. Eng, unpublished results; similar images given for reference in Fig. 3.7 A). Fig. 3.7 A shows roots that were grown for 5 days at 21 °C, followed by 2 days at 31 °C, as these correspond to the conditions for microtubule imaging. Even in *mor1-1*, radial

swelling is mild under these conditions; but no radial swelling was observed for the lines expressing MOR1$^{1\text{-}1}$-YPet when grown for longer times at 31 ^{o}C (data not shown).

MOR1$^{1\text{-}1}$-YPet localization was not disrupted at the restrictive temperature, with predominantly microtubule plus-end localization and weak lattice binding observed at both 21 ^{o}C and 31 ^{o}C (Fig. 3.7 B). MOR1$^{1\text{-}1}$-YPet was able to track polymerizing and depolymerizing microtubule plus ends at both the permissive and restrictive temperature (Fig. 3.7 C), as is MOR1^{WT}-3YPet (Eng, 2015). Microtubules in plants expressing MOR1$^{1\text{-}1}$-YPet in the *mor1-23* background are of a wild type-like length and organization, unlike the characteristic short, disorganized microtubules found in the *mor1-1* mutant (Fig. 3.7 B).

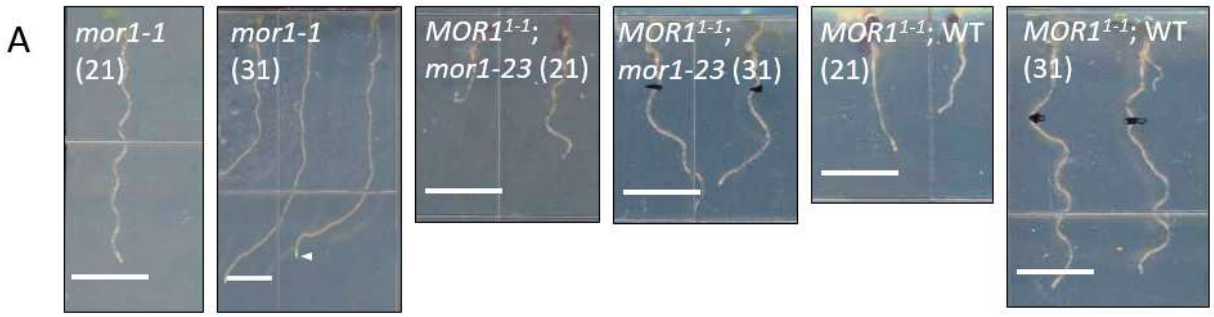

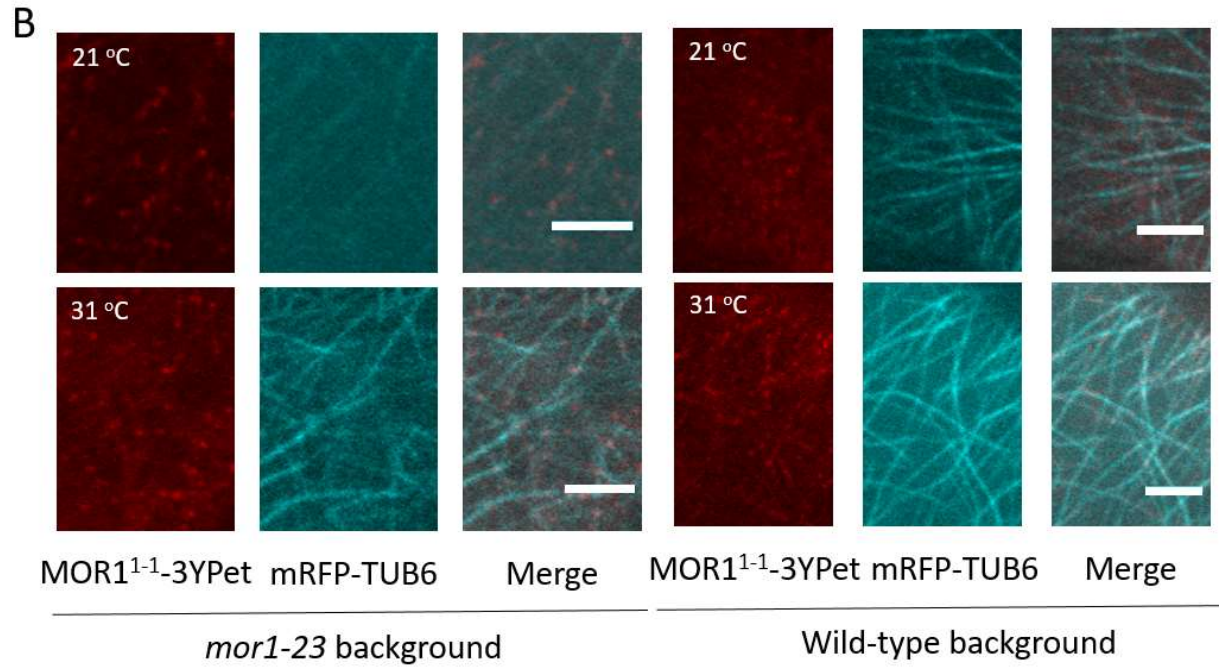

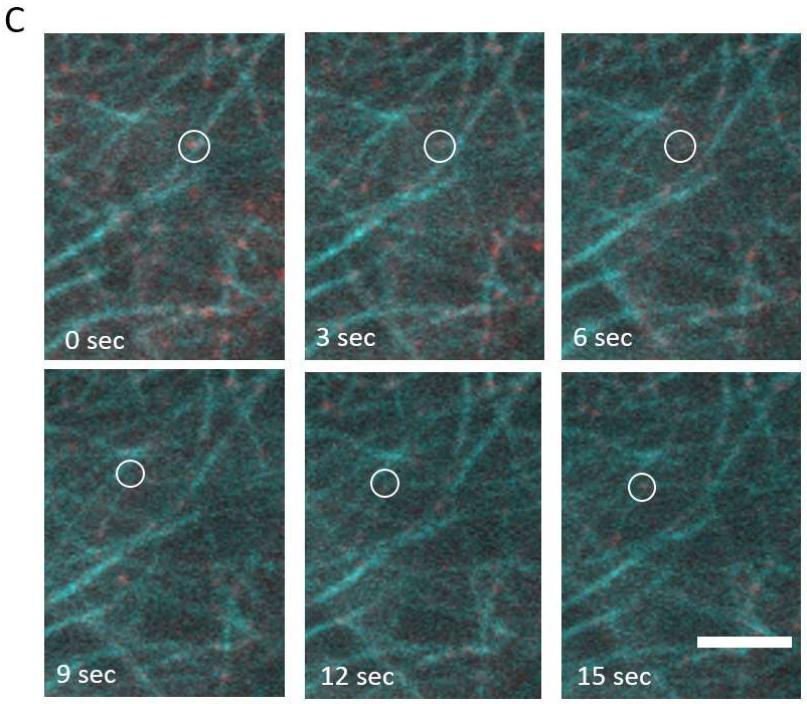

Figure 3.7 MOR1$^{1-1}$-YPet does not phenocopy the radial swelling of *mor1-1* at 31 °C, and is able to track microtubule plus ends at both 21 °C and 31 °C

(A) Root growth phenotypes of seedlings grown for 7 days at 21 °C, or for 5 days at 21 °C followed by 2 days at 31 °C. Black dots indicate the extent of root growth before seedlings were moved to 31 °C.

Images were adjusted to enhance contrast and brightness, for greater visibility of roots. Scale bars = 5 mm. Mild radial swelling in *mor1-1* at 31 °C is indicated with an arrow.
(B) MOR1$^{1-1}$-YPet localizes predominantly to the microtubule plus end in the wild-type and *mor1-23* backgrounds. Localization is unaffected by temperature. Representative still images are shown for each genotype and each treatment, from a selection of 10-25 videos acquired. Microtubule plus ends were identified in each video as the more dynamic microtubule end. Scale bars = 5 μm.
(C) MOR1$^{1-1}$-YPet (circled) is able to track to the plus end of polymerizing microtubules in the *mor1-23* background. Images represent a time series, and were acquired 3 seconds apart. Scale bar = 5 μm.

3.2.5 Endogenous MOR1$^{1-11}$ competes for microtubule binding sites with MOR1^{WT}-3YPet

As the localization pattern of MOR1$^{1-11}$-YPet in the wild-type and *mor1-23* backgrounds was the opposite of that of MOR1^{WT}-3YPet (Fig. 3.4, 3.6), it appears that the *mor1-11* mutation confers altered affinity for the microtubule. Keeping in mind that recombineered MOR1^{X}-YPet constructs might have altered localization relative to endogenous MOR1, I decided to compare the results from expressing *MOR1$^{1-11}$-YPet* in the wild-type background with the opposite combination: MOR1^{WT}-3YPet in the *mor1-11* background. As with plants expressing MOR1^{WT}-3YPet in the wild-type background, these plants were hypersensitive to PPM: roots were very short, and radially swollen (Fig. 3.8 A). Due to time limitations, I was unable to cross a microtubule marker to this line, but localization of MOR1^{WT}-3YPet is suggestive of binding to both the microtubule plus end and lattice (Fig. 3.8 B), as in plants expressing MOR1^{WT}-3YPet in the wild-type background. Thus, endogenous MOR1$^{1-11}$ appears to compete for binding sites at the microtubule plus end, in a similar manner to endogenous MOR1^{WT}. As before, treatment with PPM did not alter localization.

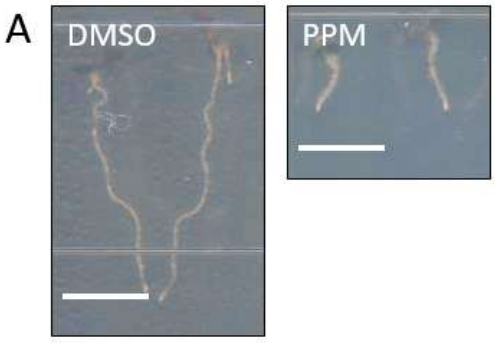

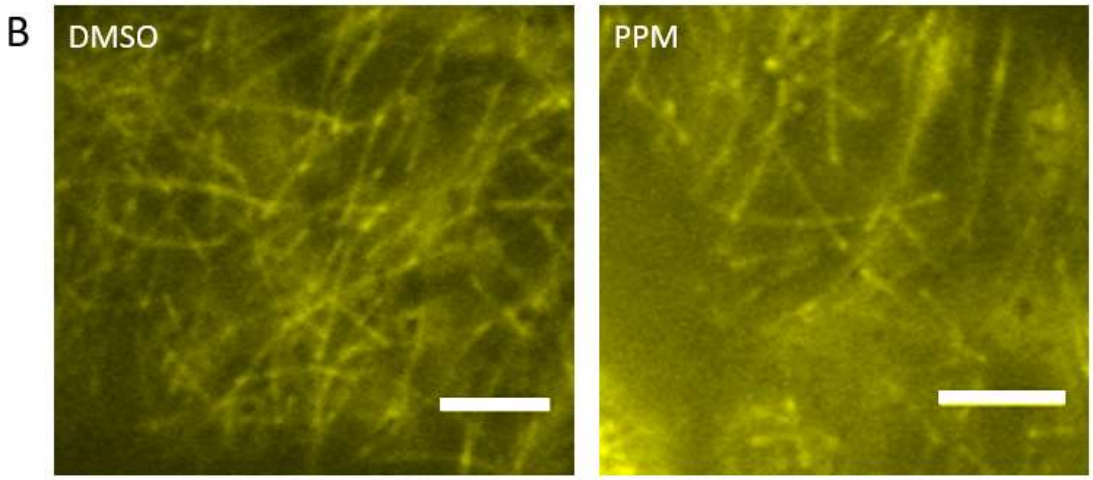

Figure 3.8 MOR1^{WT}-3YPet localization in the *mor1-11* genetic background

(A) Root growth phenotypes of 7-day-old seedlings treated with DMSO or 3 μM PPM. Images were adjusted to enhance contrast and brightness, for greater visibility of roots. Scale bars = 5 mm.
(B) Confocal micrographs of MOR1^{WT}-YPet in cotyledon epidermal cells of 7-day-old seedlings treated with DMSO or 3 μM PPM. Representative still images are shown from a selection of 20 videos (4 videos each of 5 seedlings) acquired per treatment. Scale bars = 5 μm.

3.2.6 Expression of recombineered *MOR1* results in the phosphorylation of α-tubulin

In order to determine whether the root skewing and swelling phenotypes of MOR1^{X}-YPet seedlings resulted from increased phosphorylation of α-tubulin, MOR1^{WT}-3YPet;WT, MOR1-11-YPet;WT, *mpk18-1* (null), and *phs1-1* (*phs1^{R64C}*) seedlings were germinated and grown on Hoagland's growth medium containing either 3 μM PPM (in DMSO), or an equivalent volume of DMSO. The *mpk18-1* and *phs1-1* alleles were chosen as controls, because PHS1^{R64C} promotes phosphorylation of α-tubulin, and MPK18 is thought to activate PHS1 (Fujita *et al*., 2013). Plants expressing MOR1^{X}-YPet in the wild-type background were chosen because the root skewing and radial swelling phenotypes were more severe than in the *mor1-23* background (Fig. 3.2, 3.3); I hypothesized that these more severe phenotypes would correspond to a higher degree of phosphorylation of α-tubulin, and therefore easier detection of phosphorylation.

Protein extracts from 7-day-old whole seedlings were run on an SDS-PAGE gel containing 50 μM Phos-tag™, and a Western blot for α-tubulin was carried out. Phos-tag™ is a molecule that binds to phosphate groups on Ser, Thr, and Tyr residues, slowing the progress of proteins as they migrate through an SDS-PAGE gel (Kinoshita *et al*., 2006). Therefore, a band on a gel or Western blot that contains phosphorylated proteins will appear to have a larger molecular weight than the protein would in a non-phosphorylated state.

Bands representing both non-phosphorylated α-tubulin and phosphorylated α-tubulin were detected for most genotypes and treatment groups. A faint band representing phosphorylated α-tubulin was detected for MOR1^{WT}-3YPet;WT (DMSO) (Fig. 3.9), though most of the α-tubulin in this sample was non-phosphorylated. Phosphorylation of α-tubulin was also detected for MOR1^{WT}-3YPet;WT (PPM), and was increased for MOR1-11-YPet;WT (DMSO and PPM). The level of phosphorylation appears to roughly correspond to the severity of the root growth phenotypes seen in Fig. 3.2 and 3.3.

Extracts from DMSO- and PPM-treated *mpk18-1* (null allele of the PHS1-activating MAP kinase 18) and *phs1-1* (increased activity of PHS1) were included as controls. A mix of non-phosphorylated and phosphorylated α-tubulin was detected in both of the *mpk18-1* samples, and in *phs1-1* (DMSO). The PPM-treated *phs1-1* sample had a strong band for phosphorylated tubulin, similar to a previous experiment using the kinase domain of PHS1 (Fujita *et al*., 2013).

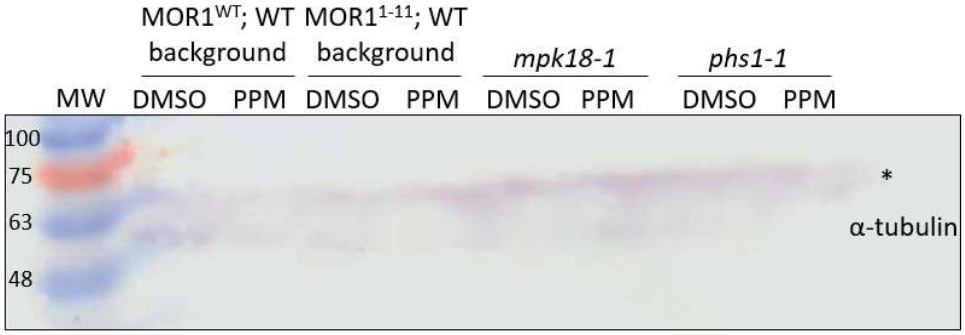

Figure 3.9 Phosphorylation of α-tubulin with expression of recombineered *MOR1*

Western blot analysis following separation of proteins from whole 7-day-old seedlings on a Phos-tag™ SDS-PAGE gel. Seedlings were grown on agarose containing DMSO or 3 μM PPM, and 20 μL of total protein extract was loaded for each sample. (*) indicates phosphorylated α-tubulin, which migrates more slowly than non-phosphorylated α-tubulin on a Phos-tag™ gel. MW, molecular weight standards (in kDa). Phosphorylation of α-tubulin is observed in extracts of MOR1^{WT}-YPet and MOR1$^{1-11}$-YPet, and more so in extracts of plants treated with PPM.

3.3 Discussion

3.3.1 Recombineered MOR1 functions differently than endogenous MOR1

Plants expressing the various MOR1^{X}-YPet constructs exhibit PPM-conditional root growth phenotypes that do not correspond to the phenotypes of wild type, *mor1-1*, or *mor1-11* when grown on PPM (Fig. 3.2, 3.3). Plants expressing MOR1^{WT}-3YPet in the *mor1-23* putative null background have a strong right-handed skewing phenotype, similar to that of *mor1-11* (Fig. 3.2 B, 3.3 D). Plants expressing MOR1$^{1-1}$-YPet and MOR1$^{1-11}$-YPet in the *mor1-23* background have more severe PPM hypersensitivity, with short, radially swollen roots (Fig. 3.2 D, 3.3 J). Root elongation is also inhibited in plants grown on DMSO (Fig. 3.2 G).

Although the recombineered *MOR1* constructs were expressed under the *MOR1* promoter, it is possible that the expression levels of recombineered *MOR1* are different from that of endogenous *MOR1*, as these constructs were inserted randomly in the genome via transformation with *Agrobacterium tumefaciens* (see section 3.4.2). However, expression of all three constructs conferred propyzamide hypersensitivity, and phosphorylated tubulin was detected in plants expressing both the MOR1^{WT} and MOR1$^{1-11}$ constructs. This suggests that the addition of the C-terminal YPet-6His tag, which is common to all three constructs (whereas the site of insertion is not), interferes with MOR1 function. Unlike N-terminal tagging, however, the addition of a C-terminal tag does not prevent MOR1 from localizing to microtubules (Lechner *et al*., 2012). As the fixation procedure for immunolocalization abolishes plus-

end binding of MOR1 (Eng, 2015), live-cell imaging of MOR1^{X}-YPet is currently the best method for visualizing MOR1-microtubule interactions.

Sensitivity to PPM is greater in plants expressing MOR1^{X}-YPet in the wild-type background than in the *mor1-23* background, with increased radial swelling and shorter roots (Fig. 3.2, 3.3). Interestingly, microtubule length and organization do not appear to be affected as in other PPM-sensitive radial swelling mutants, such as *mor1-1* and *phs1-1*, which have short, disorganized microtubules (Whittington *et al*., 2001; Naoi and Hashimoto, 2004). Although the images of MOR1-microtubule co-localization included in this chapter were acquired in cotyledon pavement cells and not in the radially swollen root cells, short microtubules are normally seen in pavement cells of radial swelling mutants, including *mor1-1* at restrictive temperature (Zhang, 2010; Fig. 2.5 D).

Previous studies of the tubulin kinase PHS1, which phosphorylates tubulin dimers and thus promotes microtubule depolymerization, suggested that radial swelling resulted from microtubule destabilization (as in the hyper-active *phs1-1* mutant) and right-handed twisting/skewing from increased microtubule stability (as in the *phs1-5* null mutant) (Naoi and Hashimoto, 2004; Pytela *et al*., 2010). However, right-handed skewing is observed in plants expressing MOR1^{WT}-3YPet in the *mor1-23* (putative null) background, with radial swelling in the wild-type background, which has endogenous MOR1 (Fig. 3.3 D, F): in this case, the root growth phenotypes correspond to different gene dosage of *MOR1*, and are likely not a reliable marker of microtubule stability.

3.3.2 MOR1$^{1\text{-}11}$-YPet has altered affinity for the microtubule

Although the finding that the C-terminal tag can interfere with MOR1 function makes it evident that caution is needed in interpreting the results of this project, it is possible to compare the effects of the different mutations. For instance, radial swelling of PPM-treated plants is more severe in plants expressing MOR1$^{1\text{-}1}$-YPet and MOR1$^{1\text{-}11}$-YPet than in plants expressing MOR1^{WT}-3YPet (Fig. 3.2, 3.3).

MOR1$^{1\text{-}11}$-YPet differs from the other constructs in its affinity for the microtubule plus end and lattice: in the *mor1-23* background, MOR1^{WT}-3YPet and MOR1$^{1\text{-}1}$-YPet localize mainly to the plus end (Fig. 3.4, 3.5), whereas MOR1$^{1\text{-}11}$-YPet localizes to both the plus end and lattice. Microtubule lattice localization was previously observed with MOR1^{WT}-YPet in the wild-type background (Eng, 2015; Fig. 3.4), though this was thought to result from saturation of plus-end binding sites due to binding of both endogenous and recombineered MOR1^{WT}-3YPet. As little or no endogenous MOR1 is present in the *mor1-23* background, this observation would suggest that the *mor1-11* mutation confers increased affinity for the microtubule lattice, suggesting impaired plus-end tracking. However, this localization pattern is observed in both DMSO- and PPM-treated plants (Fig. 3.6), and microtubule growth and shrinkage rates in DMSO-treated *mor1-11* are equivalent to those of wild type (Zhang, 2010). Moreover, expression of MOR1$^{1\text{-}11}$-YPet in the wild-type background resulted in increased plus end localization, and reduced lattice binding (Fig. 3.6), which suggests that MOR1$^{1\text{-}11}$ is able to out-compete endogenous MOR1 for binding sites at the plus end. The opposite combination, with MOR1^{WT}-3YPet expressed in the *mor1-11* background, resulted in MOR1^{WT}-3YPet localizing to both the plus end and lattice (Fig. 3.8), similar to MOR1^{WT}-3YPet expressed in the wild-type background (Eng, 2015; Fig. 3.4). This suggests that endogenous MOR1$^{1\text{-}11}$ is able to compete with MOR1^{WT}-3YPet for binding sites at the plus end, and that plus-end tracking of endogenous MOR1$^{1\text{-}11}$ is not impaired.

3.3.3 MOR1$^{1\text{-}1}$-YPet does not display temperature sensitivity

MOR1$^{1\text{-}1}$-YPet did not phenocopy the temperature-sensitive radial swelling or microtubule organization phenotype of *mor1-1* (Fig. 3.7 A, B), indicating that the addition of a C-terminal tag offsets the effect of the *mor1-1* mutation. Whether this results from the physical bulk of the YPet tag, from phosphorylation of α-tubulin (Fig. 3.9), or from processes downstream of altered interactions with proteins that may bind the C-terminal region of MOR1, is not clear.

Localization of MOR1$^{1\text{-}1}$-YPet was similar at both 21 °C and 31 °C (Fig. 3.8 B), with mainly plus-end localization and some lattice binding (see also Fig. 3.5). While TOG12$^{mor1\text{-}1}$-His bound more strongly to microtubule polymers than did TOG12^{WT}-His (Lechner *et al*., 2012), suggesting that MOR1$^{1\text{-}1}$ might have impaired plus-end tracking, it is likely that this effect is reduced in the full-length protein with a C-terminal tag. Indeed, MOR1$^{1\text{-}1}$-YPet was able to track microtubule plus ends (Fig. 3.7 C). Interactions with other +TIPs, including the EB1 proteins, may be mediated by the C-terminal domain (van der Vaart *et al*., 2011); additionally, inclusion of the TOG345 domains (and the lattice-binding domain between TOG4 and TOG5) is likely to contribute to plus-end tracking (Widlund *et al*., 2011).

Lechner *et al*. (2012) demonstrated competition for microtubule binding sites between TOG12 and endogenous MOR1 or MOR1$^{1\text{-}1}$: TOG12-GFP had greater binding affinity in the *mor1-1* background. The results of the present study show that in the wild-type background, MOR1$^{1\text{-}1}$-YPet is not entirely excluded from microtubule binding, likely due to the inclusion of the lattice-binding domain (Widlund *et al*., 2011), and possibly due to association with other +TIPs via the C-terminal domain.

3.3.4 The addition of a C-terminal tag promotes phosphorylation of α-tubulin

Phosphorylation of α-tubulin was observed in DMSO-treated MOR1^{WT}-3YPet and MOR1$^{1\text{-}11}$-YPet (both in the wild-type background), with increased phosphorylation in PPM-treated samples (Fig. 3.9). Since phosphorylation of α-tubulin is not observed in extracts of non-stressed wild-type seedlings, (Fujita *et al*., 2013), this suggests that the addition of a C-terminal tag to MOR1 promotes phosphorylation of α-tubulin. Phosphorylation was increased in MOR1$^{1\text{-}11}$-YPet relative to MOR1^{WT}-3YPet, corresponding to increased severity of radial swelling (Fig. 3.2, 3.3), and suggesting that the *mor1-11* mutation may cause increased phosphorylation of α-tubulin.

PHS1 is known to phosphorylate α-tubulin at the T349 residue in response to PPM treatment (Fujita *et al*., 2013). While other α-tubulin residues are known to undergo phosphorylation (Durek *et al*., 2010;

Roitinger *et al*., 2015), it is assumed that the α-tubulin phosphorylation detected in this experiment occurs at the T349 residue and is mediated by PHS1. Phos-tag™ analysis of seedlings exposed to osmotic or salt stress previously demonstrated that α-tubulin phosphorylation is not detectable in the *phs1-5* (null) mutant (Fujita *et al*., 2013).

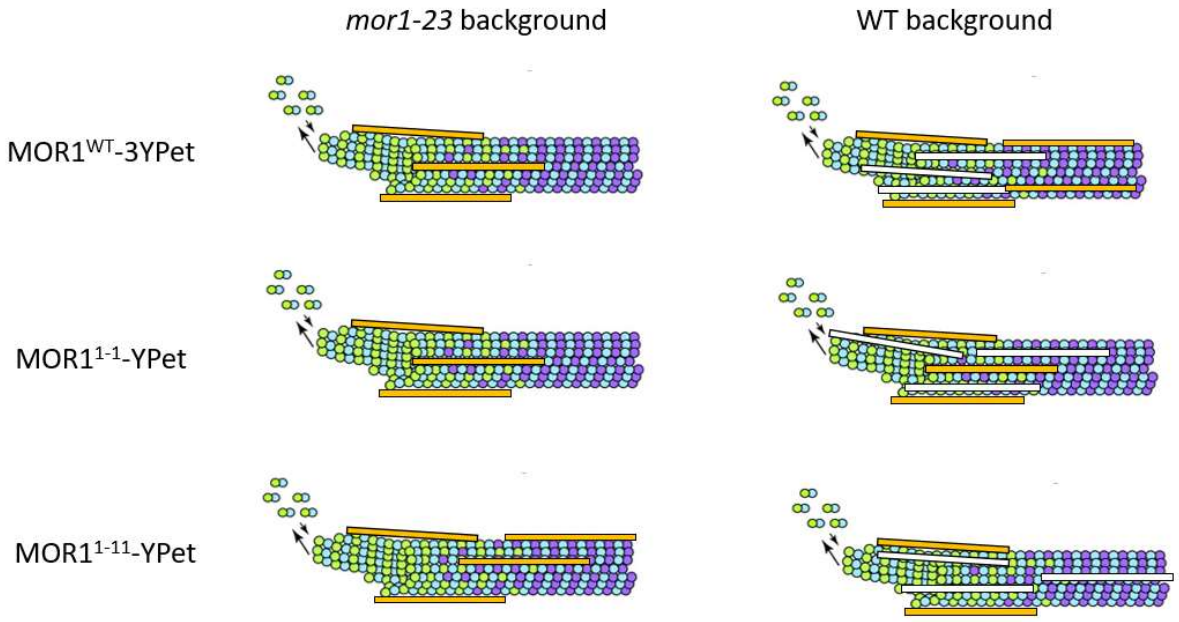

Figure 3.10 Localization of MOR1^{X}-YPet to the microtubule

Localization of MOR1^{X}-YPet (represented in yellow) varies depending on the genetic background in which it is expressed, and on mutations in the *MOR1* gene. Putative localization of endogenous MOR1 (represented in white) is based on analysis of MOR1^{X}-YPet localization in *mor1* putative null and wild-type backgrounds. Microtubule image adapted from Al-Bassam and Chang (2011), with permission from the publisher (© Elsevier/Trends in Cell Biology).

3.4 Methods

3.4.1 Plant material and growth conditions

To remove fungal spores, *Arabidopsis thaliana* (Col ecotype) seeds were treated with a sterilization solution (50% v/v ethanol, 3% v/v hydrogen peroxide) for 60 seconds, then washed twice with autoclaved distilled water. Seeds were grown on plates containing modified Hoagland's growth medium

with 1.2% w/v agar (Baskin and Wilson, 1997). Plates were sealed with surgical tape and stored in the dark at 4 °C to promote germination, then placed vertically in a growth chamber for 7 days (21 °C, continuous light at 80-100 μmol/m_2/second).

For drug treatments, plants were grown on plates containing 3 μM PPM (300 μL of a 10 mM stock solution in DMSO was added per L of medium) (Supelco Analytical), or DMSO (300 μL per L of medium). For temperature treatments, plants were grown at 21 °C for 7 days, or at 21 °C for 5 days followed by transfer to a 31 °C growth chamber for 2 days.

3.4.2 Genotyping plants expressing MOR1^{X}-YPet

Ryan Eng used *Agrobacterium tumefaciens* to transform *Arabidopsis thaliana* with the various MOR1^{X}-YPet constructs, and isolated plants homozygous for *proMOR1:MOR1^{WT}-3YPet* or *proMOR1:MOR1$^{1-1}$-YPet* in the *mor1-23* (SALK_032056) and wild-type backgrounds, with *pro35S:mRFP-TUB6* (provided by Dr. Richard Cyr, Pennsylvania State University). I crossed plants expressing *pMOR1:MOR1$^{1-11}$-YPet* to a *mor1-23* heterozygote, and to plants expressing *proUBQ10:mCherry-TUA5* (provided by Dr. David Ehrhardt, Stanford University), and isolated plants homozygous for *proMOR1:MOR1$^{1-11}$-YPet* in the *mor1-23* and wild-type backgrounds, with *proUBQ10:mCherry-TUA5*. I isolated T3 plants expressing *proMOR1:MOR1^{WT}-3YPet* in the *mor1-11* background, which were initially transformed by Ryan Eng. I also crossed plants expressing the various *proMOR1:MOR1^{X}-YPet* constructs to *mor1-6* heterozygotes.

Plants were screened for resistance to BASTA (glufosinate), indicating expression of *proMOR1:MOR1^{X}-YPet*, and to kanamycin, indicating presence of the *mor1-23* T-DNA insertion (SALK_032056). Presence of the *mor1-23* T-DNA insertion, or of the *mor1-1*, *mor1-11*, and *mor1-6* point mutations was confirmed by PCR (Table 3.1). Plants were screened for *pro35S:mRFP-TUB6* or *proUBQ10:mCherry-TUA5* by checking for microtubule labelling using confocal microscopy (see section 4.4.3). As each plant had four copies of the *MOR1* gene (two transgenic and two endogenous), homozygosity was confirmed by

assessing the segregation ratio of a plant's progeny: e.g. 100% of the progeny of a plant that was homozygous for *mor1-23* would be resistant to kanamycin, and test positive for the T-DNA insertion using PCR. The *mor1-6* mutation was genotyped using PCR primers that amplify the region around the mutation; purified PCR product was sequenced at the NAPS DNA Sequencing Laboratory (UBC), and sequences were assessed using chromatograms posted to the NAPS website.

Table 3.1 Primers used to genotype *mor1* mutations

Mutation	Forward primer (5'→3')	Reverse primer (5' →3')
mor1^{WT} (for *mor1-1* SNP)	CCTAAAAGGATTTTAAAGATGC	GAGAATAAATAAAAATTCAAGTGT
mor1-1	AAGGATTTTAAAGATGT	As above
mor1^{WT} (for *mor1-11* SNP)	AGGATATGGAGAAAAGAAGAGAAG	TTCCAGTCTGTAGGGCCATT
mor1-11	AAGGATATGGAGAAAAGAAGAGAGA	As above
mor1-23 (T-DNA)	TTCAACAGCCAACAATCCTTC	GAATCTGGCACACTCACCATC
LBa1 primer for T-DNA	TGGTTCACGTAGTGGGCCATCG	For use with *mor1-23* primers
mor1-6	AACATCTTCTGGAGGGTTGG	GCAACACCTCCAATAGTAGTCA

3.4.3 Confocal microscopy

MOR1^{X}-YPet and mRFP-TUB6 (or mCherry-TUA5) were visualized in epidermal cells of the abaxial side of cotyledons of 7-day-old seedlings, at 1000x magnification (using a 100x oil lens). Cotyledons were mounted in perfluoroperhydrophenanthrene (Sigma-Aldrich) to improve image quality and gas exchange, as detailed in Littlejohn *et al*. (2014). Videos were taken using Volocity^{TM} software version 6.3, using a PerkinElmer UltraVIEW VoX spinning disc confocal system on a Leica DMI6000B inverted microscope, with a Hamamatsu 9100-02 electron multiplier CCD camera. YPet was excited using a 516 nm laser, and detected through a 540/30 nm emission filter. mRFP and mCherry were excited using a 561 nm laser, and detected through a 595/50 nm emission filter. For each genotype and each treatment, 3 time-lapse series were generated for each of 5 seedlings, using images acquired every 3

seconds in a single z-plane. A temperature-controlled stage was used (Bionomic Controller BC-110 with a Heat Exchanger HEC-40; 20-20 Technology Inc.) to maintain the cotyledons at 21 °C or 31 °C during imaging, and a temperature probe (Thermocouple FLUKE 52; John Fluke Manufacturing Co.) was used to measure the temperature of the oil on the slide after imaging, confirming that the temperature controls were consistent. Because the different recombineered MOR1^{X} constructs used different numbers of YPet tags, microscope settings were kept consistent when imaging all three constructs, so as not to misrepresent fluorescence intensity. Laser intensity was set at 57% for RFP and mCherry, and 79% for YPet, with an exposure time of 1 sec, and sensitivity set at 200.

3.4.4 Image processing, microtubule tracking, and statistical analysis

Images were exported to ImageJ (Abràmoff *et al*., 2004). Representative still images were selected from each time series, to show microtubule organization in each genotype and with each treatment.

3.4.5 Phos-Tag™ and Western blotting

For each genotype and treatment, approximately 50 whole 7-day-old seedlings were homogenized in 300 μL protein extraction buffer, using a micropestle in a 1.5 mL Eppendorf tube (buffer recipe from Ban *et al*., 2013: 15 mM Na_2HPO_4, 5 mM NaH_2PO_4, pH 7.4; 1% Tween-20; 50 mM β-glycerophosphate; 100 μM Na_3VO_4; 0.5 mM phenylmethylsulfonyl fluoride; with 1 Complete™ EDTA-free protease inhibitor tablet (Roche) added per 25 mL aliquot of buffer). Protein extract was centrifuged at 14,000 RPM, and the protein-containing supernatant transferred to a fresh tube. Protein concentration was determined using a spectrophotometer, by measuring absorbance at λ = 280 nm.

In order to remove impurities that might interfere with the Phos-tag™ gel, approximately 50 μg of total protein was precipitated from each sample by mixing with cold acetone (1 part protein extract: 4 parts acetone), and incubating at -20 °C for 1 hour. Samples were then centrifuged at 14,000 RPM, yielding a pellet containing purified protein. Pellets were then washed 3 times in a cold solution of 80% acetone,

centrifuging 2 minutes for each wash. The precipitates were then dissolved in 20 μL SDS-PAGE sample buffer (125 mM Tris-HCl, pH 6.8; 12% w/v SDS; 10% v/v glycerol; 22% v/v β-mercaptoethanol; 0.001% w/v bromophenol blue), and boiled for 10 minutes.

Proteins were separated on a pre-cast SuperSep Phos-tag™ gel containing 50 μM Phos-tag™ and 12.5% acrylamide (Wako Pure Chemical Industries, Ltd.), according to the method described by Kinoshita *et al*. (2006). After electrophoresis, the gel was incubated for 10 minutes with Towbin buffer with added EDTA (192 mM Tris-HCl, pH 8.3; 25 mM glycine; 10% v/v methanol; 10 mM EDTA), then for a further 15 minutes with regular Towbin buffer. The proteins were transferred to a PVDF membrane (Bio-Rad) using the Trans-Blot® SD Semi-Dry Transfer Cell (Bio-Rad), running at 15 V for 35 minutes. α-tubulin was detected using a mouse anti-tubulin primary antibody (1:1000) (B-5-1-2, Sigma-Aldrich) and an anti-mouse horseradish peroxidase-conjugated secondary antibody (1:5000). α-tubulin bands were detected using the colourimetric 3,3',5,5'-tetramethylbenzidine liquid substrate for horseradish peroxidase (Sigma-Aldrich). This experiment was repeated once.

Chapter 4: Genetic interactions involving the *mor1-11* mutation

4.1 Introduction

4.1.1 Genetic interactions between *MOR1* and *PHS1*

The *mor1* mutants show interesting parallels with mutants of the tubulin kinase/MAP kinase phosphatase *PHS1* (PROPYZAMIDE HYPERSENSITIVE 1). PHS1 phosphorylates α-tubulin at the T349 residue in response to various environmental stressors, preventing incorporation of phosphorylated tubulin dimers into microtubules, and resulting in microtubule depolymerization (Ban *et al.*, 2013; Fujita *et al*., 2013). The *phs1-1* (R64C) mutant, which affects a putative MAP kinase docking motif and in which PHS1 has increased activity (Fujita *et al*., 2013), exhibits radial swelling of root cells when grown on PPM, similar to *mor1-1* grown at the restrictive temperature (Naoi and Hashimoto, 2004). Furthermore, *mor1-1phs1-1* double mutant roots had radial swelling and reduced cell elongation, even when grown at the permissive temperature and without PPM (Naoi and Hashimoto, 2004). And like *mor1-11*, the null *phs1-5* mutant exhibits strong right-handed root skewing when grown on PPM (Pytela *et al*., 2010). The handedness of skewing does not appear to reflect microtubule stability, as microtubules in *phs1-5* are reported to be hyper-stable (Fujita *et al*., 2013), whereas those in *mor1-11* are less stable (Zhang, 2010). Nonetheless, the similarity of these PPM-conditional phenotypes suggests a connection between MOR1 and PHS1.

No direct interaction between MOR1 and PHS1 has been demonstrated, and no phosphorylation of MOR1 was observed in the *phs1-1* mutant background; nor is MOR1 co-localization with microtubules disrupted in *phs1-1* (Walia, 2009). However, *PHS1* transcript is up-regulated in *mor1-1* at 30 ^{o}C, and not in wild type at 30 ^{o}C or in oryzalin-treated plants (Walia, 2009). In addition, modification of the C-terminal region of MOR1 may result in activation of PHS1, as α-tubulin phosphorylation was increased with C-terminal tagging of MOR1, and more so with tagged MOR1$^{1\text{-}11}$ (Chapter 3). It is possible that the

PPM-conditional phenotype of *mor1-11* results from increased PHS1 activity, either due to destabilization of microtubules through α-tubulin phosphorylation, or perhaps through the activity of another substrate of PHS1. For instance, PHS1 dephosphorylates MPK18 (Walia *et al*., 2009), and is also a negative regulator of ABA signalling (Quettier *et al*., 2006) and a positive regulator of flowering (Tang *et al*., 2016) though the pathways by which these processes occur have not yet been elucidated.

While the C-terminal domain of human ch-TOG is known to interact with other +TIPs (van der Vaart *et al*., 2011), no such interactions have been demonstrated for MOR1. If modification of the C-terminal domain of MOR1 (through tagging or the *mor1-11* mutation) results in activation of PHS1, it is possible that the C-terminal region interacts with a component of the PHS1-activating MAP kinase cascade. Alternatively, MOR1 may affect the activity of another +TIP that interacts with components of this signalling cascade. MAP kinase cascades include a MAP kinase kinase kinase (MAPKKK), which phosphorylates and activates a MAP kinase kinase, (MAPKK), which in turn phosphorylates and activates a MAP kinase (MAPK or MPK), which phosphorylates and regulates the activity of effector proteins (Hamel *et al*., 2006; Fiil *et al*., 2009; Suarez Rodriguez *et al*., 2010). In the case of PHS1, these components may include MAPKK proteins MKK3 and MKK6, which activate MPK18 *in vitro* (Hua *et al*., 2006). MPK18 is thought to activate PHS1, which in turn inactivates MPK18 by dephosphorylation (Walia *et al*., 2009). If the C-terminal domain of MOR1 negatively regulates activity of MPK18, loss of this negative regulation in the *mor1-11* mutant could result in increased activity of PHS1.

Association of components of MAP kinase signalling cascades with microtubules or MAPs has previously been demonstrated for the MAPKKK NPK1, which binds the NACK1/HINKEL kinesin (Soyano *et al*., 2003), for MPK6, which associates with γ-tubulin and phosphorylates EB1c (Müller *et al*., 2010; Kohoutová *et al*., 2015), and for MPK4, which co-localizes with mitotic microtubule arrays (Beck *et al*., 2011). MAP kinases also phosphorylate and regulate multiple members of the MAP65 family (Sasabe *et al*., 2006;

Beck *et al*., 2010; Sasabe *et al*., 2011). Association of MAP kinases with microtubules and MAPs is also seen in animal cells: for instance, MAP kinases ERK1 and ERK2 bind to and phosphorylate MAP2 (Ahn *et al*., 1990; Boulton *et al*., 1990; Morishima-Kawashima and Kosik, 1996). It has been suggested that the polymerization/depolymerization status of microtubules may regulate the activity of MAP kinase cascades, as depolymerization of phragmoplast microtubules resulted in deactivation of *Medicago sativa* MAP kinase 3 (Bögre *et al*., 1999), and of components of the MAP kinase cascade downstream of NACK1/HINKEL (Soyano *et al*., 2003; Sasabe and Machida, 2012). Thus, MAP kinase signalling and microtubule organization and dynamics may be regulated in a reciprocal manner, perhaps allowing fine-tuning of the microtubule array in response to environmental stimuli.

4.1.2 A *mor1-11* modifier mutant screen

A modifier mutant screen in the *mor1-11* background is an ideal approach for identifying potential components of a MOR1-associated signalling pathway, as genetic interactions between *mor1-11* and other mutants may indicate that the proteins encoded by the affected genes interact physically with MOR1, or act in the same pathway (Page and Grossniklaus, 2002). Therefore, MOR1-interacting proteins that interact indirectly or transiently with MOR1 may be identified through forward genetic screening more successfully than by co-precipitation. Recently, a biotin ligase-based method for identifying transient interactions between proteins has been developed (Roux *et al*., 2012), though optimization of this method for use with *Arabidopsis thaliana* is ongoing (A. Walia, personal communication).

A modifier screen may yield suppressor mutants, which alleviate or reverse the phenotype of the primary mutant, or enhancer mutants, which worsen the phenotype (Page and Grossniklaus, 2002). In the case of *mor1-11*, which has strong right-handed root skewing when grown on PPM (Zhang, 2010), a suppressor mutant would have left-handed or no root skewing, whereas an enhancer mutant would

have stronger disruptions to microtubules than *mor1-11*, likely resulting in constitutive right-handed skewing or radial swelling. The root skewing phenotype of *mor1-11*, and of modifier mutants, may be used as a proxy for disruption of microtubule organization and dynamics, e.g. with suppressor mutants counteracting the mild microtubule destabilization seen in *mor1-11* (Zhang, 2010). Use of PPM in a *mor1-11* modifier screen increases the likelihood that modifier mutants are not simply MOR1-interactors (e.g. tubulins), but that they may have some role in the signalling pathway involved in responses to PPM; thus, such an approach is a combination of forward genetics and genotypic chemical screening (McCourt and Desveaux, 2009).

4.1.3 Objectives

In this chapter, I characterized genetic interactions between *mor1-11* and alleles of *MPK18* and *PHS1*, in order to determine whether MPK18 is involved in signalling events downstream of modification of the C-terminal region of MOR1. I also aimed to build upon previous studies of genetic interactions between the *mor1-1* (L174F) allele and *mpk18*/*phs1* mutants, in order to better understand whether genetic interactions between MOR1 and PHS1 were domain-specific with respect to MOR1.

In order to complete analysis of *mor1-11* microtubule dynamics begun by Zhang (2010), I analyzed properties of the dynamic instability of wild-type and *mor1-11* microtubules in response to PPM treatment.

I also conducted a modifier mutant screen in the *mor1-11* background, with the aim of identifying proteins that might interact with the C-terminal region of MOR1, or that are part of signalling pathways affected by the *mor1-11* mutation.

4.2 Results

4.2.1 The *mpk18-1* mutation does not modify the propyzamide-conditional phenotype of *mor1-11*

MPK18 is thought to activate PHS1, since microtubule stability is increased in the *mpk18-1* null mutant compared to the wild type, and since absence of *MPK18* partially rescues the *phs1-1* phenotype in the *mpk18-1phs1-1* double mutant (Walia *et al*., 2009). Root growth, skewing, and radial swelling phenotypes of a *mor1-1mpk18-1* double mutant were neither enhanced nor suppressed relative to *mor1-1*, suggesting no genetic interaction between *MOR1* and *MPK18* (Walia, 2009). However, as the *mor1-11* mutant has a distinct, PPM-conditional phenotype similar to that of *phs1-5* (Zhang, 2010; Pytela *et al*., 2010), and as modification of the C-terminal region of MOR1 leads to increased phosphorylation of α-tubulin (Chapter 3), I hypothesized that a genetic interaction might be detected using the *mor1-11* allele and in response to treatment with PPM. However, root length and skewing of *mor1-11* and of the *mor1-11mpk18-1* double mutant were statistically equivalent (Fig. 4.1), indicating that the *mor1-11* phenotype does not depend on functional MPK18.

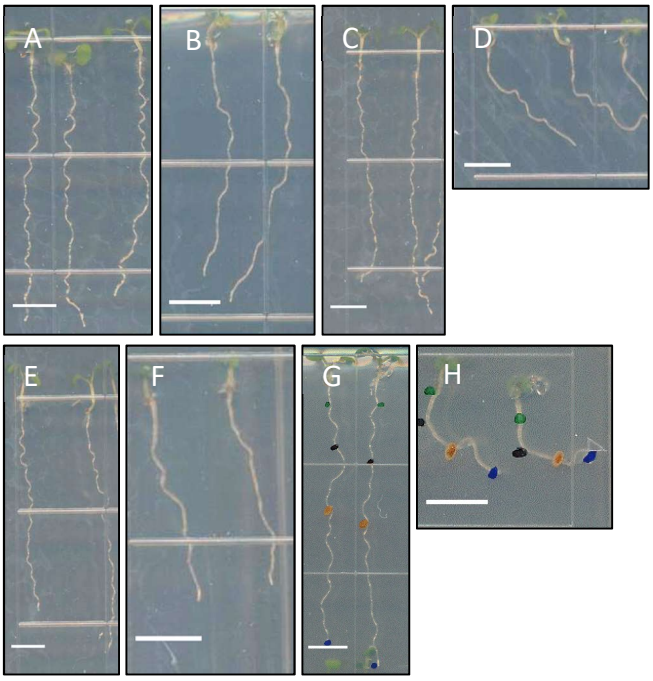

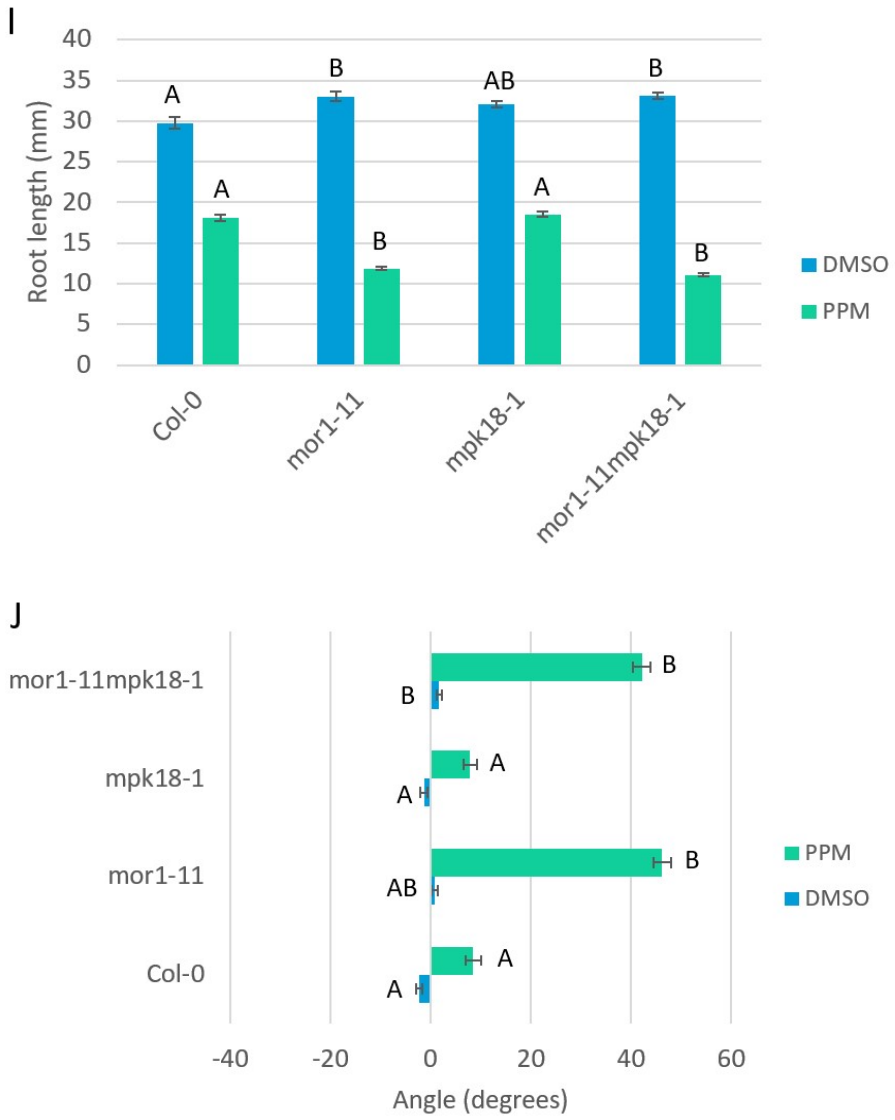

Figure 4.1 The root growth phenotype of the *mor1-11mpk18-1* double mutant in response to treatment with DMSO or 3 μM PPM is equivalent to that of *mor1-11*

Root growth phenotypes of wild type (Col-0) grown on (A) DMSO and (B) PPM, *mor1-11* on (C) DMSO and (D) PPM, *mpk18-1* on (E) DMSO and (F) PPM, and *mor1-11mpk18-1* on (G) DMSO and (H) PPM. Scale bars = 5 mm.
(I) Root length and (J) root skewing for each genotype and treatment (n = 40 – 60). Error bars indicate the standard error of the mean. Letters indicate statistically equivalent mean root skewing for a given treatment, based on ANOVA with post hoc analysis (Scheffé's test, $p < 0.01$).

4.2.2 The root growth phenotype of *mor1-11phs1-1* is equivalent to that of *phs1-1*

It was previously demonstrated that root elongation defects and radial swelling were enhanced in the *mor1-1phs1-1* double mutant, relative to either single mutant (Naoi and Hashimoto, 2004). This suggests that the radial swelling of *mor1-1* and *phs1-1* may originate from distinct effects on microtubule disorganization. As MOR1$^{1\text{-}1}$-YPet did not phenocopy *mor1-1* (Chapter 3), it is difficult to say exactly what the effect of the *mor1-1* mutation is on the activity of full-length MOR1, though analysis of MOR1 fragments suggests that the mutation interferes with plus-end targeting (Lechner *et al*., 2012). The enhanced double mutant phenotype is consistent with the separate activity of PHS1 as a tubulin kinase (Fujita *et al*., 2013).

However, no synergistic phenotype was observed in the *mor1-11phs1-1* double mutant (Fig. 4.2). Instead, root length of both DMSO- and PPM-treated plants was statistically equivalent to that of *phs1-1* (Fig. 4.2 I). The root skewing phenotype on DMSO was also equivalent to that of *phs1-1*; and root skewing was abolished on PPM, since severe radial swelling inhibited cell elongation to the extent necessary for skewing (Fig. 4.2 J).

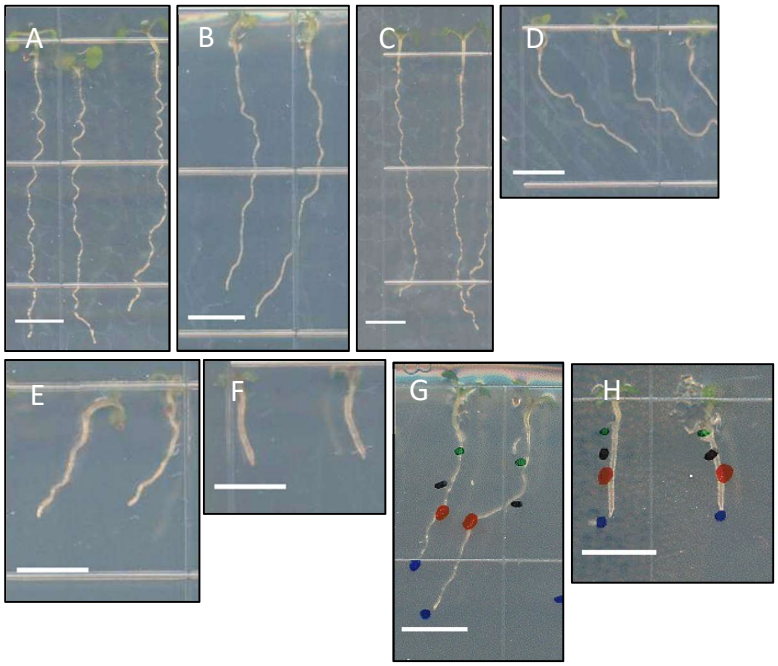

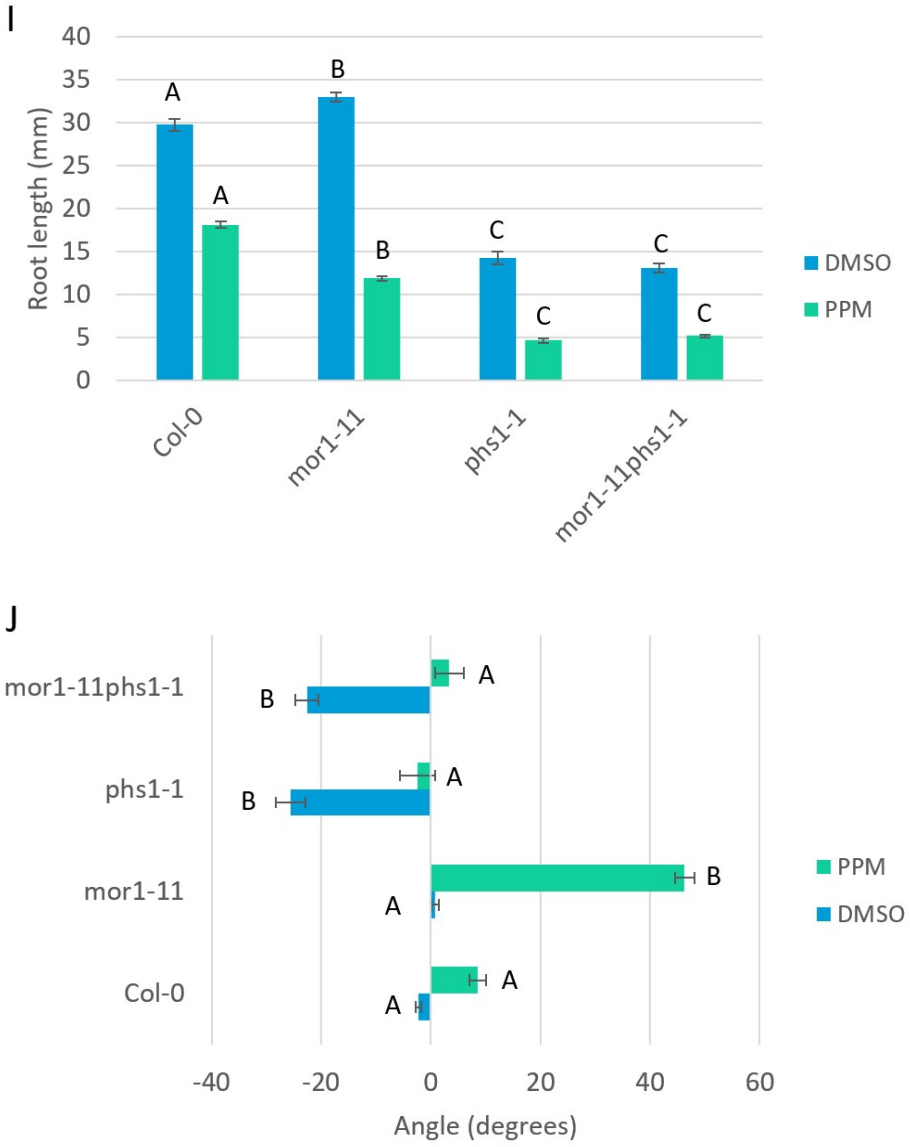

Figure 4.2 The root growth phenotype of the *mor1-11phs1-1* double mutant in response to treatment with DMSO or 3 μM PPM is equivalent to that of *phs1-1*

Root growth phenotypes of wild type (Col-0) grown on (A) DMSO and (B) PPM, *mor1-11* on (C) DMSO and (D) PPM, *phs1-1* on (E) DMSO and (F) PPM, and *mor1-11phs1-1* on (G) DMSO and (H) PPM. Scale bars = 5 mm.
(I) Root length and (J) root skewing for each genotype and treatment (n = 40 – 60). Error bars indicate the standard error of the mean. Letters indicate statistically equivalent mean root skewing for a given treatment, based on ANOVA with post hoc analysis (Scheffé's test, $p < 0.01$).

4.2.3 Root elongation in *mor1-11phs1-5* is reduced relative to either single mutant, with mild radial swelling on propyzamide

Although *mor1-11* and *phs1-5* have similar PPM-conditional root skewing phenotypes (Fig. 4.3 D, F), the *mor1-11phs1-5* double mutant has an additive phenotype, with shorter roots than either single mutant when treated with either DMSO or PPM (Fig. 4.3 I). Root skewing in response to PPM is reduced in the double mutant, presumably as a result of reduced cell elongation (Fig. 4.3 J). Because *phs1-5* is a null mutant (Pytela *et al*., 2010), this suggests that PPM-treated *mor1-11* seedlings have microtubule defects besides those caused by α-tubulin phosphorylation by PHS1.

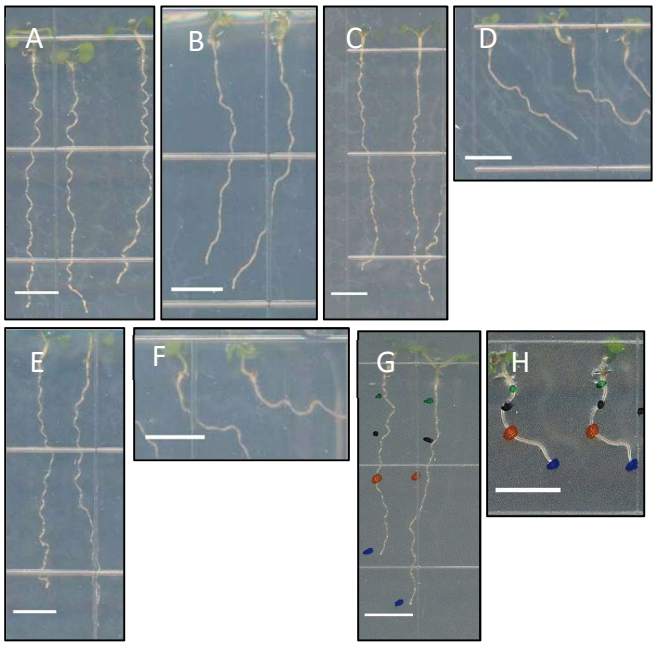

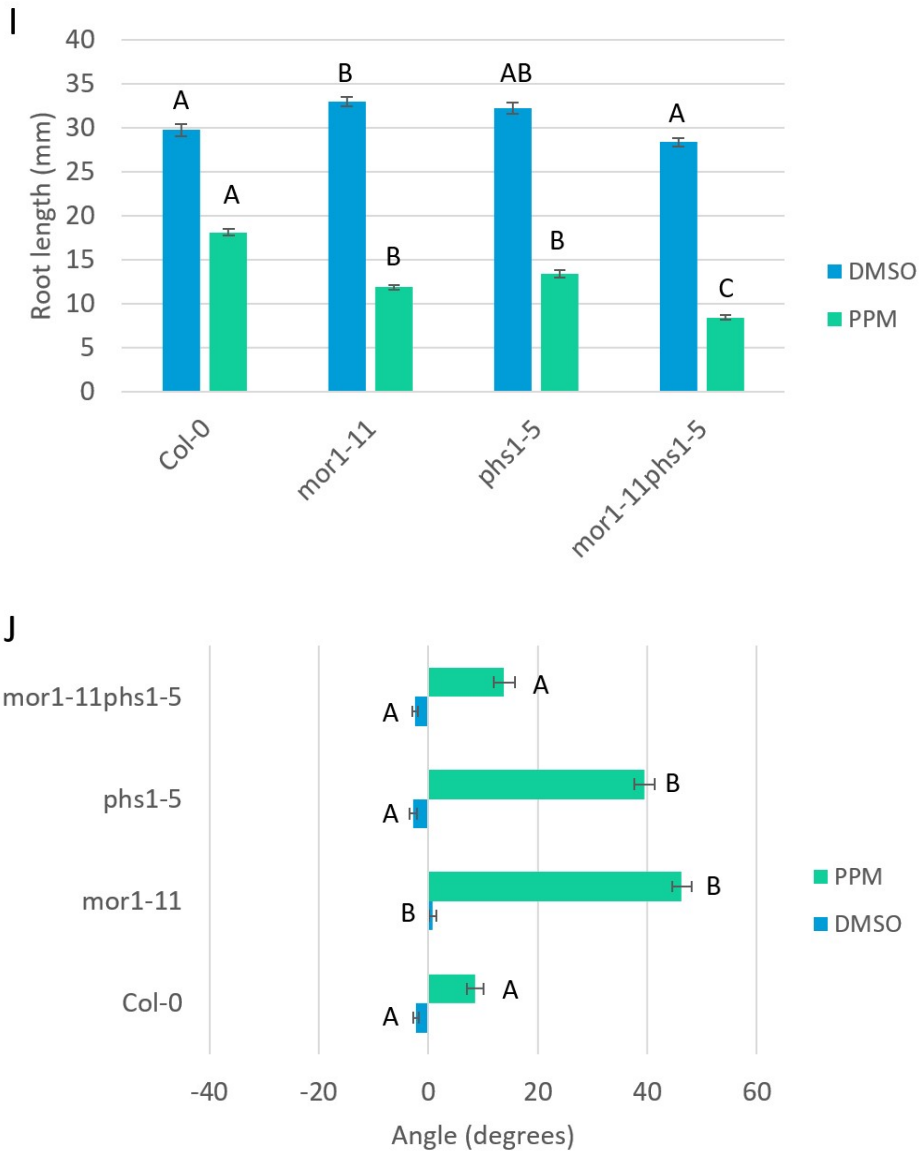

Figure 4.3 Root length and skewing are reduced in the *mor1-11phs1-5* double mutant on 3 μM PPM, relative to either single mutant

Root growth phenotypes of wild type (Col-0) grown on (A) DMSO and (B) PPM, *mor1-11* on (C) DMSO and (D) PPM, *phs1-5* on (E) DMSO and (F) PPM, and *mor1-11phs1-5* on (G) DMSO and (H) PPM. Scale bars = 5 mm.

(I) Root length and (J) root skewing for each genotype and treatment (n = 40 – 60). Error bars indicate the standard error of the mean. Letters indicate statistically equivalent mean root skewing for a given treatment, based on ANOVA with post hoc analysis (Scheffé's test, $p < 0.01$).

4.2.4 Microtubule dynamic instability is altered in the *mor1-11* mutant

Because analysis of the *mor1-11phs1-5* double mutant indicates that the *mor1-11* mutation does not only cause altered PHS1 activity, I analyzed *mor1-11* microtubule dynamics, with the aim of determining what other effects the mutation might cause. Analysis of $MOR1^{X}$-YPet co-localization with microtubules suggests that $MOR1^{1-11}$ has increased affinity for the microtubule lattice relative to $MOR1^{WT}$, and that treatment with PPM does not alter localization of MOR1 (Chapter 3). However, since addition of a C-terminal fluorescent tag appears to alter MOR1 activity, analysis of *mor1-11* microtubule dynamics might give a more realistic indication of the effect of the mutation on endogenous MOR1.

Microtubule plus-end dynamics in the *mor1-11* mutant are similar to those of wild-type plants, with equivalent growth and shrinkage rates. However, treatment with PPM reduces the plus-end growth rate in *mor1-11* more than in wild type (Zhang, 2010). For reference, images showing microtubule organization in *mor1-11* are provided in Appendix 1.

Microtubules in DMSO-treated *mor1-11* seedlings spend less time in pause phase than wild type, indicating that they are more dynamic than those in wild type (Fig. 4.4 A). Differences in these parameters were not detected between microtubules in PPM-treated *mor1-11* and wild-type seedlings (Fig. 4.4 B), likely due to overall suppression of microtubule dynamicity by PPM (Zhang, 2010). As indicated by the previous analysis of plus-end growth and shrinkage rates in *mor1-11* (Zhang, 2010), microtubules in PPM-treated *mor1-11* seedlings spent less time growing than wild type, though the difference was not statistically significant.

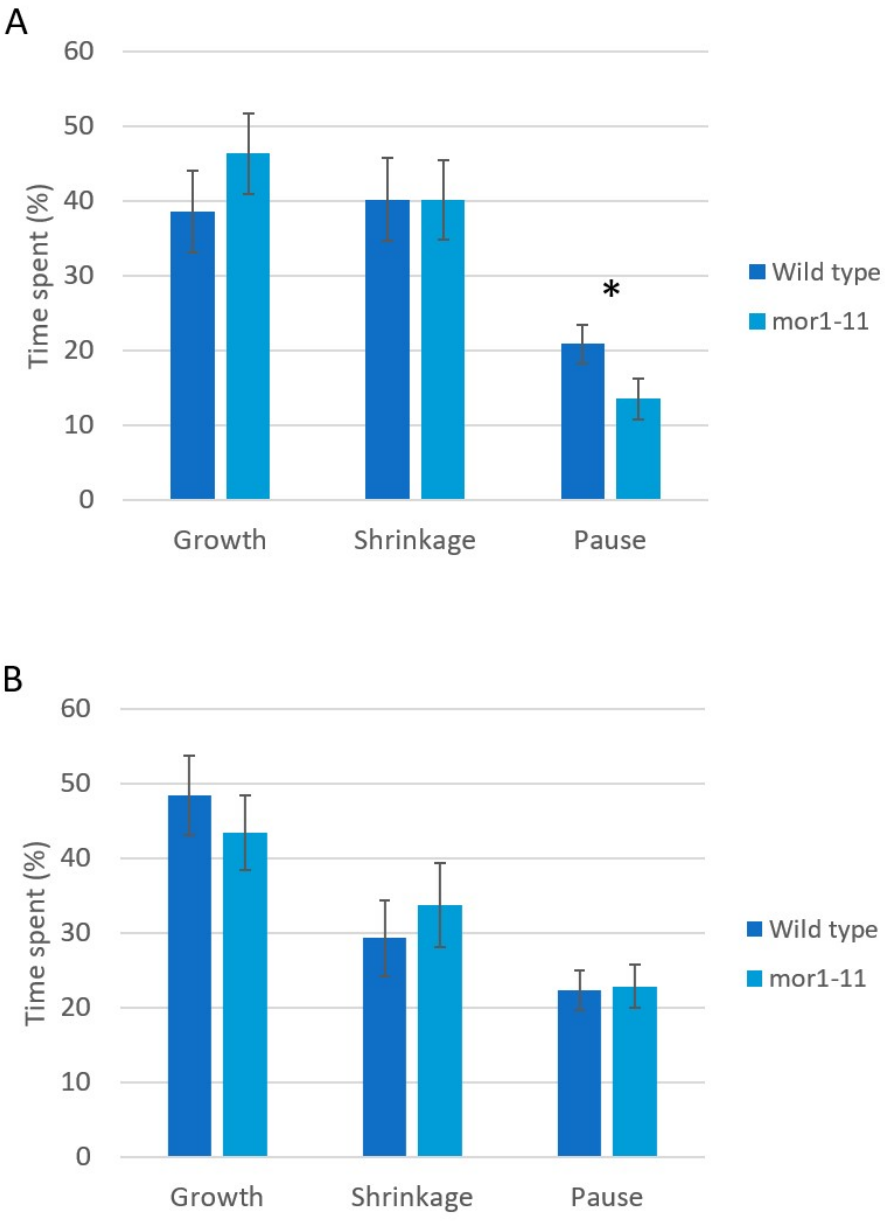

Figure 4.4 Microtubule plus-end dynamic instability is altered in DMSO-treated *mor1-11* and wild-type plants

Time spent in different phases of dynamicity by microtubules in cotyledon epidermal cells of 7-day-old seedlings treated with (A) DMSO or (B) 3 μM PPM. n = 46-50 for each genotype and treatment. Error bars indicate the standard error of the mean. (*) Significantly different from wild type (t-test, $p < 0.05$).

4.2.5 A modifier mutant screen in the *mor1-11* background

In order to identify mutants that have a genetic interaction with *mor1-11*, possibly indicating a physical interaction with the MOR1 C-terminal region, I used EMS (ethyl methanesulfonate) to generate point mutations in the *mor1-11* genetic background. One enhancer mutant and six suppressor mutants were identified in this screen (Table 4.1): these were designated *eom* (enhancer of *mor1-11*) or *som* (suppressor of *mor1-11*). As *mor1-11* root skewing is right-handed at 21 °C, but left-handed at 31 °C (Zhang, 2010), M2 seedlings were screened at both temperatures. However, all identified modifier mutants modified the *mor1-11* phenotype at 21 °C, and no modifier mutants that only suppressed the left-handed skewing at 31 °C were identified. Therefore, subsequent analysis of putative modifier mutants did not take temperature into account, and the results presented in the present study focus on phenotypes at 21 °C.

The *som1* and *som2* mutants are semi-dominant, whereas the other four *som* mutants are recessive. Complementation testing of the recessive *som* mutants demonstrated that two additional *som* mutants were allelic to *som5* and *som6*, respectively; so only one allele for each (*som5* 58-3 and *som6* 61-3) was chosen for map-based cloning. Analysis of two other *som* alleles was abandoned, due to a lack of germination of progeny from *mor1-11* back-crossing, which was attempted repeatedly without success.

Table 4.1 Analysis of *eom* and *som* modifier mutants

Allele	Screening name	Root phenotype (with PPM)	Dominant/recessive	Progress
eom1	36-1	Short, swollen roots	Semi-dominant	Identified
som1	6-2	Left-handed skewing	Semi-dominant	Rough mapping
som2	8-1	Left-handed skewing	Semi-dominant	Rough mapping
som3	36-2	Left-handed skewing	Recessive	Ready to map
som4	56-2	No skewing	Recessive	Ready to map
som5	58-3	No skewing	Recessive	Ready to map
som6	61-3	No skewing	Recessive	Ready to map

Screening names were assigned based on the M2 screening pool from which the modifier mutant was identified, and the number of mutants identified in each pool. E.g. *som1* is 6-2, as it was the 2nd putative mutant identified in the 6th pool of M2 seedlings that were screened.

F2 mapping populations were established for each of the remaining *som* mutants. Map-based cloning of the semi-dominant *som1* and *som2* mutations is in progress; these mutants were prioritized, as they have stronger left-handed skewing phenotypes than the other *som* mutants (Fig. 4.5).

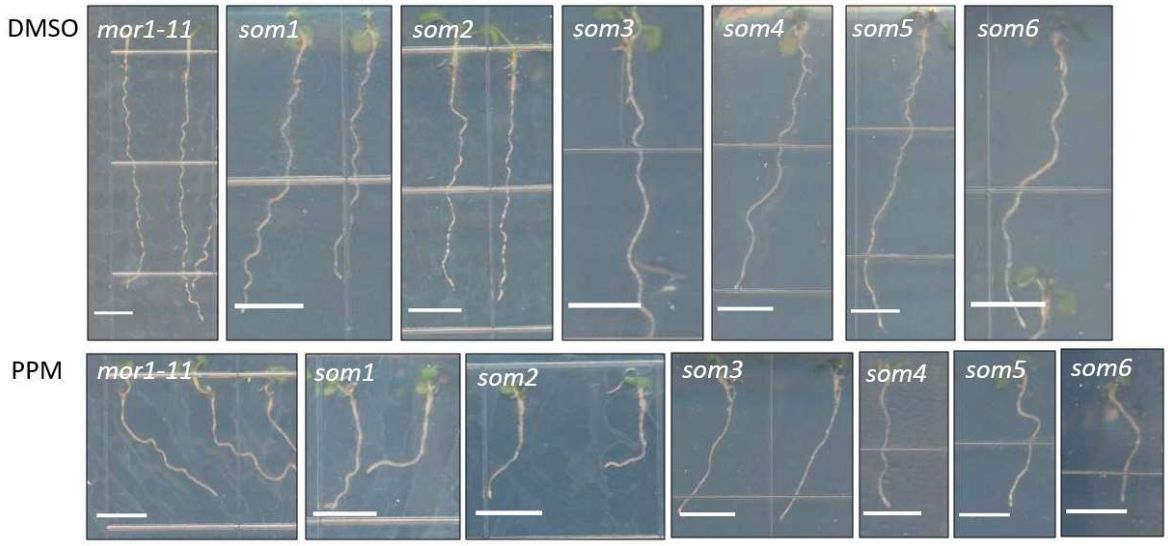

Figure 4.5 Root growth phenotypes of *suppressor of mor1-11* mutants

Seedlings were grown for 7 days at 21 °C on DMSO (top) or 3 μM PPM (bottom). Images were adjusted to enhance contrast and brightness, for greater visibility of roots. Scale bar = 5 mm.

4.2.6 The *eom1* enhancer mutant is *phs1-1*

The *eom* enhancer mutant was identified as a *phs1* allele, based on the similarity of its phenotype to that of *mor1-11phs1-1* (Fig. 4.6). Treatment with 3 μM PPM results in short, radially swollen roots in both *eom1* and *mor1-11phs1-1*. However, treatment with DMSO produces different phenotypes: *eom1* roots do not skew, whereas those of *mor1-11phs1-1* do (Fig. 4.6). Analysis of the *PHS1* sequence determined that there was only one mutation in the *PHS1* gene (CGT → TGT, causing the R64C amino acid substitution); this is identical to the mutation in the original *phs1-1* mutant, which was also discovered using EMS mutagenesis (Naoi and Hashimoto, 2004).

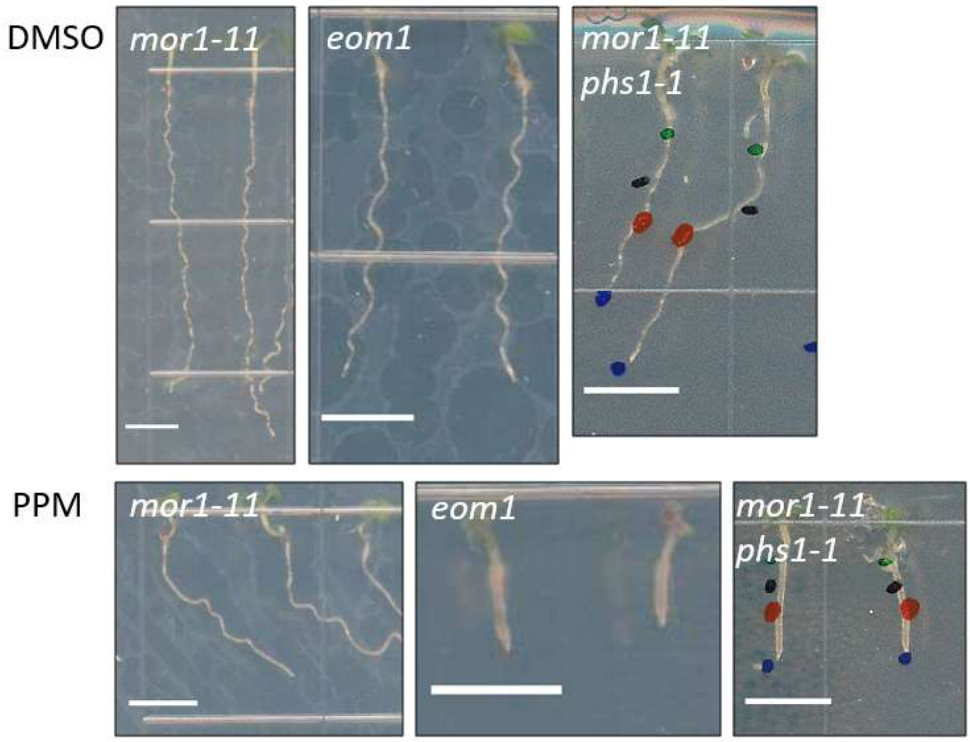

Figure 4.6 The *eom1* modifier mutant has a similar phenotype to *mor1-11phs1-1* on PPM, but not on DMSO

Seedlings were grown for 7 days at 21 °C on DMSO (top) or 3 μM PPM (bottom). Images were adjusted to enhance contrast and brightness, for greater visibility of roots. Scale bar = 5 mm.

4.3 Discussion

4.3.1 Genetic interactions between *MOR1* and *PHS1*

No genetic interaction between *MOR1* and *MPK18* was detected in *mor1-1mpk18-1* (Walia, 2009), nor in *mor1-11mpk18-1*, in the current study. As the *mpk18-1* (null) mutation neither enhanced nor suppressed the PPM-conditional phenotype of *mor1-11* (Fig. 4.1), this suggests that signalling with MPK18 does not contribute to the microtubule defects seen in *mor1-11*. Phosphorylation of α-tubulin was seen in the *mpk18-1* mutant (Chapter 3), and *mpk18-1* has only moderately stabilized MTs relative to wild type (Walia *et al*., 2009). If modifications of the C-terminus of MOR1 result in activation of PHS1, this may be mediated by another MAP kinase or by some other PHS1-interacting protein. MPK12 is a

potential PHS1-interacting MAP kinase, and was shown to interact with PHS1 in a yeast two-hybrid assay, although the interaction could not be confirmed with bimolecular fluorescence complementation (Walia *et al*., 2009). Expression of *MPK12* is tissue-specific, with highest expression in guard cells; lower expression is observed in other tissues, including the root and hypocotyl (Winter *et al*., 2007; *Arabidopsis* eFP browser). It might be informative to test for a genetic interaction between *MOR1* and *MPK12*, though efforts to identify other potential MOR1-interacting proteins (e.g. through the *mor1-11* modifier screen described in this chapter) are likely to be more fruitful.

The similarity of the *mor1-11phs1-1* mutant phenotype to that of *phs1-1* (Fig. 4.2) is consistent with the hypothesis that modification of the MOR1 C-terminal region in *mor1-11* results in activation of PHS1 and phosphorylation of α-tubulin (Chapter 3). Because α-tubulin in PPM-treated *phs1-1* seedlings is highly phosphorylated (Chapter 3), any further cell elongation or radial swelling defects would result from microtubule organization defects unrelated to α-tubulin phosphorylation, as in *mor1-1phs1-1* (Naoi and Hashimoto, 2004). No additional defects were observed in the *mor1-11phs1-1* double mutant, suggesting that the effect of the *mor1-11* mutation is primarily mediated through increased activity of PHS1.

The PPM-treated *mor1-11phs1-5* double mutant, on the other hand, has reduced cell elongation relative to either single mutant, as well as slight radial swelling (Fig. 4.3). *phs1-5* is a null allele (Pytela *et al*., 2010), which means that the PPM-conditional phenotype of *mor1-11* is enhanced in the absence of PHS1. It is possible that moderate PHS1 activity (i.e. phosphorylation of some α-tubulin) might offset the effect of the *mor1-11* mutation. Whether the effect of *mor1-11* in the absence of *PHS1* is the result of altered microtubule polymerase/depolymerase activity by MOR1, or perhaps by changes to signalling pathways affecting microtubules, is not clear. A model of the relationship between MOR1 and PHS1 is proposed below (Fig. 4.7).

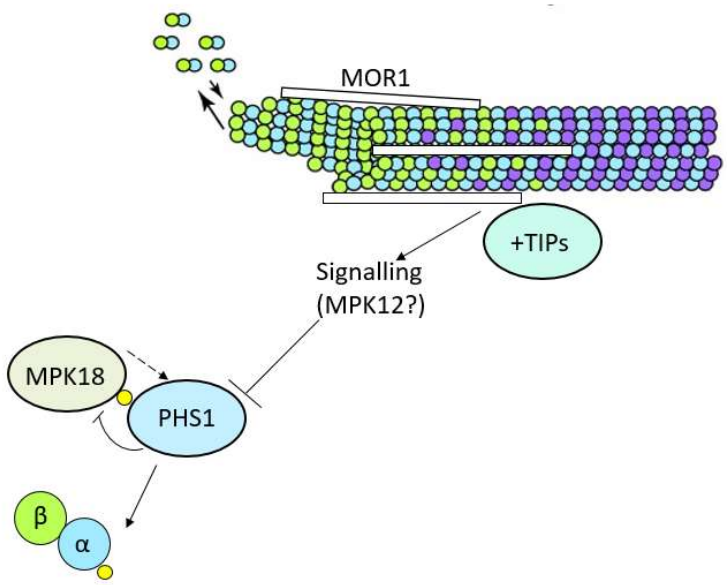

Figure 4.7 Model for MOR1 control of PHS1 tubulin kinase activity

The C-terminal region of MOR1 is a negative regulator of PHS1 α-tubulin kinase activity. MOR1 and PHS1 are unlikely to interact directly (Walia, 2009), and regulation of PHS1 activity may therefore be mediated by MOR1-interacting +TIPs or signalling proteins (e.g. components of a MAP kinase signalling cascade). Phosphorylation is represented by a yellow circle, e.g. on the MPK18-PHS1 module and on α-tubulin. MPK18 is thought to phosphorylate and activate PHS1 (dotted arrow), which dephosphorylates and deactivates MPK18 (Walia *et al*., 2009). Activated PHS1 phosphorylates α-tubulin, blocking incorporation of tubulin dimers at the microtubule plus-end (Fujita *et al*., 2013). Modification of the C-terminal region of MOR1 (e.g. in the *mor1-11* mutant, or with the addition of a C-terminal tag) interferes with the ability of MOR1 to inhibit PHS1 activity.

Analysis of microtubule dynamics in the *mor1-11* mutant demonstrated that microtubules in PPM-treated *mor1-11* seedlings grow more slowly than in wild type (Zhang, 2010), and that *mor1-11* dynamicity is altered relative to wild type (Fig. 4.4). A similar analysis of microtubule dynamics in *mor1-11phs1-1* and *mor1-11phs1-5* could determine whether MOR1 polymerase/depolymerase activity is changed in the absence of *PHS1*, and *mor1-11phs1-1* and *mor1-11phs1-5* double mutants expressing *pro35S::GFP-TUB6* have been generated, in order to address this question.

4.3.2 *mor1-11* modifier mutants

I initially considered that *eom1* might be a *phs1-1* or *mor1-11phs1-1* double mutant seed that was accidentally introduced into the M2 screening pool, but the mutagenesis project was carried out a year after completing the *mor1-11 phs1*/*mpk18* double mutant analysis project (section 4.2.2), seeds for each project were stored in separate boxes, and the laboratory bench was thoroughly cleaned with ethanol before and after harvesting each pool of M2 seeds. The probability of contamination was therefore judged to be low. In addition, unlike *mor1-11phs1-1*, *eom1* does not display constitutive left-handed skewing (Fig. 4.5). This is likely because the *eom1* M3 seedlings were not back-crossed to *mor1-11* in order to segregate the *eom1* mutation from background mutations. A similar effect was seen in the original *mor1-11* TILLING allele, which had constitutive right-handed skewing in the M3 generation; this constitutive phenotype disappeared after back-crossing to wild-type (Col) plants, leaving only the PPM-conditional skewing phenotype (Zhang, 2010). Because no other mutations were detected in the *PHS1* gene in *eom1*, any background mutations that affect the constitutive skewing phenotype of *mor1-11phs1-1* would affect other genes.

Map-based cloning of the *som* mutants is ongoing, and will be discussed in greater detail in Chapter 5.

4.4 Methods

4.4.1 Plant material and growth conditions for *mor1-11-mpk18-1* and *mor1-11-phs1* mutant analysis

The *mor1-11* mutant was identified through a TILLING forward genetics screen (T. Shoji, unpublished results; Zhang, 2010). *phs1-1* mutant seeds were a kind gift from Dr. Takashi Hashimoto (NAIST), and *phs1*-5 (SALK_070121) and *mpk18-1* (SALK_069399) mutant seeds were acquired from the Arabidopsis Biological Resource Center (Ohio State University).

To remove fungal spores, *Arabidopsis thaliana* seeds were treated with a sterilization solution (50% v/v ethanol, 3% v/v hydrogen peroxide) for 60 seconds, then washed twice with autoclaved distilled water. Seeds were grown on plates containing modified Hoagland's growth medium with 1.2% w/v agar (Baskin and Wilson, 1997). Plates were sealed with surgical tape and stored in the dark at 4 ^{o}C to promote germination, then placed vertically in a growth chamber (21 ^{o}C, continuous light at 80-100 μmol/m^2/second).

For drug treatments, plants were grown on plates containing 3 μM PPM (300 μL of a 10 mM stock solution in DMSO was added per L of medium) (Supelco Analytical), or DMSO (300 μL per L of medium). For temperature treatments, plants were grown at 21 ^{o}C for 7 days, or at 21 ^{o}C for 5 days followed by transfer to a 31 ^{o}C growth chamber for 2 days.

4.4.2 Genotyping *mor1-11mpk18-1* and *mor1-11phs1* mutant plants

Candidate plants for genotyping were identified based on their root skewing phenotypes when grown on agar plates containing 3 μM PPM. All primers used for genotyping are listed in Table 4.2.

Table 4.2 Primers used to genotype *mor1*, *phs1*, and *mpk18* mutations

Mutation	Forward primer (5'→3')	Reverse primer (5' →3')
mor1^{WT} (for *mor1-11* SNP)	AGGATATGGAGAAAAGAAGAGAAG	TTCCAGTCTGTAGGGCCATT
mor1-11	AAGGATATGGAGAAAAGAAGAGAGA	As above
phs1^{WT} (for *phs1-1* SNP)	TTTACTCAATGGTTGGATTTAGGTC	TTAATAACTGCTGCTTCTTCCTTAC
phs1-1	TTTACTCAATGGTTGGATTTAGGTT	As above
phs1-5 (T-DNA)	CTCCACCTTTACCGGATCTTC	AGAGAGCTGCTGCAGCTCTAG
mpk18-1 (T-DNA)	TTTTGGTGTGCCAAGAAGATC	GATCAAAAGCATTATGCTGCC
LBa1 primer for T-DNA	TGGTTCACGTAGTGGGCCATCG	For use with *phs1-5* and *mpk18-1* primers

4.4.3 Image processing and statistical analysis for root growth phenotypes

Images were exported to ImageJ (Abràmoff *et al*., 2004). Root length and skewing were quantified by measuring roots using the NeuronJ plugin for ImageJ (Meijering *et al*., 2004; Abràmoff *et al*., 2004).

4.4.4 Confocal microscopy

Yi Zhang crossed the *mor1-11* mutant to a microtubule marker line (*pro35S::GFP-TUB6*), and measured microtubule growth and shrinkage rates. For analysis of microtubule dynamicity (phase duration), GFP-TUB6 was visualized in epidermal cells of the abaxial side of cotyledons of 7-day-old seedlings mounted in water, at 630x magnification (using a 63x glycerol lens). Videos were taken using Volocity™ software version 6.3, using a PerkinElmer UltraVIEW VoX spinning disc confocal system on a Leica DMI6000B inverted microscope, with a Hamamatsu 9100-02 electron multiplier CCD camera. GFP was excited using a 488 nm laser, and detected through a 525/36 nm emission filter. Images were acquired every 5 seconds. Sample images of microtubule organization in *mor1-11* are shown in Appendix 1.

4.4.5 Image processing, microtubule tracking, and statistical analysis for microtubule dynamics

Images were exported to ImageJ (Abràmoff *et al*., 2004). Microtubule plus-end dynamics were measured using the MTrackJ plugin (Meijering *et al*., 2012). For each genotype and each drug treatment, between 46 and 50 microtubules were tracked, for 35-65 seconds. Data were exported to Microsoft Excel, and the mean duration of each dynamic phase was calculated, based on recorded observations of growth/shrinkage/pausing between time points. Statistical significance was determined using a student's t-test.

4.4.6 *mor1-11* modifier screen

Approximately 15,000 *mor1-11* seeds were mutagenized with EMS (ethyl methanesulfonate), according to the protocol described by Kim *et al*. (2006). These M1 seeds were grown in large pots of soil

(Sunshine Mix #4), with approximately 200 seeds per pot. M2 seeds were harvested from mature M1 plants, and pooled according to the pot in which the M1 plant was grown. M2 seeds were screened for enhancer or suppressor phenotypes, by growing them for 5 days on modified Hoagland's growth medium containing 1.2% w/v agar (Baskin and Wilson, 1997) and 3 μM propyzamide. Plates were sealed with surgical tape and stored in the dark at 4 °C to promote germination, then placed vertically in a growth chamber (21 °C, continuous light at 80-100 μmol/m_2/second). After 5 days, plates were transferred to a 31 °C growth chamber for 2 days.

Putative mutants were allowed to self-fertilize, producing M3 plants. If plants with the mutant phenotype were observed in the M3 generation, these were allowed to self-fertilize, producing M4 plants. M4 plants were again checked for heritability of the mutant phenotype, and these were used for back-crossing to *mor1-11*. The segregation ratio of root skewing phenotypes from each *mor1-11* back-cross (in response to PPM treatment) was used to determine whether a modifier mutation was dominant, recessive, or semi-dominant. *som* mutants with recessive mutations were crossed to each other, to test for complementation (recovery of the *mor1-11* phenotype in the progeny), which indicates whether two mutations are allelic.

Images of root skewing were obtained from M4 plants grown for 7 days on plates containing 3 μM PPM (300 μL of a 10 mM stock solution in DMSO was added per L of medium), or DMSO (300 μL per L of medium).

Because EMS mutagenesis results in a high frequency of mutations (Page and Grossniklaus, 2002), *som* mutants were back-crossed twice to *mor1-11*, selecting for the homozygous *som* root skewing phenotype, in order to segregate the *som* mutations from additional background mutations. Map-based cloning in *Arabidopsis thaliana* relies on the use of genetic markers that vary between ecotypes (usually Columbia and Landsberg), so *mor1-11* was introgressed into the Landsberg *erecta* (L*er*) genetic

background by crossing *mor1-11* (originally in the Col background) to L*er* eight times. Primers used in genotyping the progeny of these successive crosses are shown in Table 4.3. Each back-crossed mutant was then back-crossed twice to *mor1-11*L*er*. The progeny of the second cross to *mor1-11*L*er* were allowed to self-fertilize, establishing an F2 mapping population for each of the *som* mutants.

Table 4.3 Primers used to genotype the *mor1-11* and *erecta* mutations

Mutation	Forward primer (5'→3')	Reverse primer (5' →3')
mor1^{WT} (for *mor1-11* SNP)	AGGATATGGAGAAAAGAAGAGAAG	TTCCAGTCTGTAGGGCCATT
mor1-11	AAGGATATGGAGAAAAGAAGAGAGA	As above
erecta	GATTGGGACACACGGCTTAATAA	GATCTGCCATTTCCATCACTTC

4.4.7 Identification of the causative mutation of *eom1*

The *PHS1* gene was amplified in overlapping fragments of 500-550 base pairs, using the primer sets listed in Table 4.4. The purified PCR products were sequenced at the NAPS DNA Sequencing Laboratory (UBC), and sequences were assessed using chromatograms posted to the NAPS website. The causative mutation was identified as CGT → TGT, causing the same R64C mutation as in *phs1-1* (Naoi and Hashimoto, 2004). Plants were genotyped for *mor1-11* (Table 4.3), to confirm that *eom1* had the *mor1-11* mutation and was not a *phs1-1* single mutant accidentally introduced into the M2 screening pool.

Table 4.4 Primers used to genotype the *eom1* (*phs1-1*) mutation

Primer set	Forward primer (5'→3')	Reverse primer (5' →3')
1	TGAGATTTCGCTATACAAGTTGG	AAGAGGAAAGTCTCAAGGTATC
2	AAATATCCGTCTTCTTTCTTCGTC	TCCAACCATTGAGTAAACCTATAAG
3	ATCTATACCTTGTTCACGACGAG	TCAGTGCTACTACTATGTTCAG
4	TGTGGATATTGATTCGAGCTG	ATGTCATTTCACCAACCTCG
5	ACAGGCTAGAGTAATTCACAG	TTGAAAGTGCCTACATGATCC
6	AATAGGATCATGTAGGCACTTTC	TCAGACATTGGACTCATTAAACC
7	AGTCACCTTCACATACTCATGG	TGGTTTCTCTGTATTAGCAGC
8	GCAACTGAACTCAAACATTGTC	AACCAGGATGAGATTGGAAAG

4.4.8 Map-based cloning of *som* mutants

Map-based cloning of the *som* mutants is currently underway, using the protocol and SSLP (simple sequence length polymorphism) PCR markers developed by Lukowitz *et al*. (2000).

Chapter 5: Conclusions and future directions

5.1 Main findings of this thesis

In this thesis, I studied the role of the MOR1 microtubule polymerase/depolymerase in the control of microtubule organization and dynamics, using *mor1* point mutants with conditional phenotypes to characterize domain-specific interactions with microtubules and with components of a stress-signalling pathway that promotes the phosphorylation of α-tubulin.

5.1.1 Analysis of *mor1*-tubulin double mutants provides insights into twisting growth

Helical (twisting) growth and radial swelling phenotypes are indicative of disruption to cortical microtubule arrays, and the severity and handedness of twisting are fixed for most tubulin and MAP mutants (Ishida *et al*., 2007b). It was previously suggested that twisting in a left-handed helix resulted from destabilization of microtubules, whereas twisting in a right-handed helix resulted from hyper-stabilization of microtubules (Ishida *et al*., 2007a). In an effort to characterize MOR1-microtubule interactions, and to understand the genetic basis of twisting, Zhang (2010) crossed tubulin mutants displaying right-handed twisting phenotypes to *mor1* mutants with left-handed twisting phenotypes. Genetic interactions were detected between the $tub4^{P220S}$ or $tub4^{G96D}$ mutations, lesions which affect the interdimer interface of β-tubulin, and the *mor1-1* and *rid5* mutations, which both affect the TOG1 domain of MOR1 (Zhang, 2010).

In the present study, analysis of microtubule organization and dynamics in these mutants and in *mor1*-tubulin double mutants indicated that the handedness of twisting does not always correlate with microtubule growth or shrinkage velocity. For example, microtubule growth and shrinkage velocity are statistically equivalent in $tub4^{P220S}$ and wild type at 31 ^{o}C, but $tub4^{P220S}$ roots grow with right-handed twisting, whereas those of wild type do not (Zhang, 2010; Appendix 1). Similarly, the *mor1-1* and *rid5*

mutants have similar parameters of dynamic instability, though *rid5* roots grow with left-handed twisting at 21 ^{o}C, whereas those of *mor1-1* do not.

A model for the handedness of twisting must therefore account for factors other than microtubule dynamicity or stability, perhaps including the angle of microtubule nucleation (Eren *et al*., 2010), as well as changes to microtubule-MAP interactions. Possible future experiments for directly characterizing microtubule-MOR1 interactions, through use of the tubulin purification method described in Chapter 2, are discussed in section 5.2.

5.1.2 The addition of a C-terminal tag to MOR1 increases propyzamide sensitivity, by promoting phosphorylation of α-tubulin

Because *MOR1* could not be cloned using traditional methods, MOR1^{WT}, MOR1$^{1\text{-}1}$, and MOR1$^{1\text{-}11}$ constructs were generated using recombineering (Zhou *et al*., 2011; Alonso and Stepanova, 2014), with the addition of a C-terminal YPet-6xHis tag to facilitate microscopy and affinity purification. Expression of MOR1^{WT}-3YPet in the *mor1-23* background was earlier demonstrated to rescue the lethal phenotype of *mor1-23*, and was thought to function in a manner similar to endogenous MOR1 (Eng, 2015).

In order to determine whether expressing MOR1$^{1\text{-}11}$-YPet in the *mor1-23* background phenocopied *mor1-11*, I tested the response of these plants to treatment with PPM. All of the MOR1^{X}-YPet variants were hypersensitive to PPM, in both the *mor1-23* and wild-type genetic backgrounds. Analysis of seedlings expressing MOR1^{WT}-3YPet or MOR1$^{1\text{-}11}$-YPet in the wild-type background indicated that addition of a C-terminal tag resulted in phosphorylation of α-tubulin, likely mediated by the tubulin kinase PHS1.

Affinity of MOR1^{WT}-3YPet for the microtubule plus end and lattice is dependent on the genetic background in which the recombineered construct is expressed: it localized primarily to the plus end in the *mor1-23* background, and to the plus end and lattice in the wild-type background, likely due to

competition for binding sites with endogenous MOR1 (Eng, 2015). MOR1$^{1\text{-}1}$-YPet localized primarily to the plus end in both genetic backgrounds, whereas MOR1$^{1\text{-}11}$-YPet localized to the plus end and lattice in the *mor1-23* background, and to the plus end in the wild-type background. Localization of MOR1^{X}-YPet did not vary with PPM treatment, or (in the case of MOR1$^{1\text{-}1}$-YPet) with temperature.

Microtubule disorganization was not observed in seedlings expressing MOR1$^{1\text{-}1}$-YPet at the restrictive temperature, in contrast to microtubules in the *mor1-1* mutant (Whittington *et al*., 2001). Lechner *et al*. (2012) had previously noted that the *mor1-1* mutation increased the binding affinity of a TOG12 construct (TOG12$^{mor1\text{-}1}$) for the microtubule lattice, and proposed that the mutation might impair plus-end tracking of MOR1. However, plus-end tracking of MOR1$^{1\text{-}1}$-YPet was not inhibited, potentially indicating that either the TOG345 domains contribute to plus-end tracking, or that addition of a C-terminal tag could counteract any increase in affinity for the microtubule lattice.

Because the addition of a C-terminal tag altered tubulin phosphorylation, microtubule organization, and sensitivity to PPM and temperature, caution is needed in interpreting the MOR1^{X}-YPet-microtubule co-localization results. However, the different microtubule-binding affinities of the MOR1^{WT}-3YPet and MOR1$^{1\text{-}11}$-YPet constructs suggests that localization of endogenous MOR1 is likely altered in the *mor1-11* mutant. N-terminal fluorescent tagging of a MOR1 TOG12 fragment inhibited microtubule localization (Lechner *et al*., 2012), so the use of a C-terminal tag is currently the best approach for live-cell imaging of MOR1. The finding that addition of a C-terminal tag to MOR1 results in increased phosphorylation of α-tubulin suggests that MOR1 may be involved in a signalling pathway for regulation of the tubulin kinase PHS1 in response to environmental stimuli. Phosphorylation of α-tubulin by PHS1 is promoted by various abiotic stressors, including cold, heat, salt, and osmotic stress, as well as by treatment with microtubule depolymerizing drugs such as PPM (Ban *et al*., 2013; Fujita *et al*., 2013).

5.1.3 Genetic interactions involving the *mor1-11* mutation

The finding that modification of the C-terminal region of MOR1 leads to phosphorylation of α-tubulin tied in with a project for analyzing genetic interactions involving the *mor1-11* mutation. *mor1-11* has a PPM-conditional phenotype similar to that of the *phs1-5* null mutant (Pytela *et al*., 2010), and because genetic interactions were previously detected between *mor1-1* and the *phs1-1* mutant, which has increased PHS1 activity (Naoi and Hashimoto, 2004; Walia, 2009). PHS1 binds to and dephosphorylates MPK18 (Walia *et al*., 2009), so I analyzed genetic interactions between *mor1-11* and *phs1-1*, *phs1-5*, or *mpk18-1* (null).

No genetic interaction was detected between *mor1-11* and *mpk18-1*, indicating that MPK18 is not involved in signalling events downstream of modification of the C-terminal region of MOR1. However, the *mor1-11phs1-1* mutant phenotype was equivalent to that of *phs1-1*, suggesting that PHS1 is activated downstream of modification of the C-terminal region of MOR1. The phenotype of the *mor1-11phs1-5* double mutant was additive, indicating that the *mor1-11* mutation might cause defects in microtubules by means other than by activation of PHS1. It is possible that moderate PHS1 activity offsets other effects of the *mor1-11* mutation. Analysis of microtubule dynamics in DMSO-treated seedlings showed that microtubules in *mor1-11* were more dynamic than those of wild type, spending less time in pause phase. In PPM-treated seedlings, this effect was lost.

In order to identify proteins that might interact with MOR1, or that might be involved in signalling pathways relating to MOR1, I also conducted a modifier mutant screen, using EMS mutagenesis in the *mor1-11* genetic background. I identified one enhancer of *mor1-11* (*eom1*), which was caused by the same mutation as in the *phs1-1* mutant, though the presence of background mutations abolished the constitutive left-handed skewing phenotype typical of *phs1-1*. I also isolated six suppressors of *mor1-11* (*som*), and have yet to identify the causative mutations via map-based cloning.

5.2 Future directions

5.2.1 *In vitro* microtubule polymerization and binding assays

The recovery of microtubule dynamics to wild type-like levels in the *tub4^{P220S}mor1-1* mutant at 31 ^{o}C, despite disruption of microtubule organization, raises questions about the effect of these mutations on MOR1-microtubule binding and of MOR1 polymerase/depolymerase activity. In addition, differences in microtubule dynamics and organization were observed with the tubulin-*mor1-1* and tubulin-*rid5* double mutants, likely indicating that the affected residues interact with different regions of the tubulin dimer, or may cause different changes to the conformation and binding affinity of MOR1 for the microtubule.

Through *in vitro* reconstitution of MOR1-microtubule interactions, binding affinity and (de)polymerase activity in *mor1* and tubulin mutants could be directly measured. Purification of MOR1^{X}-YPet-His, and of tubulin from wild-type and *tub4^{P220S}* and *tub4^{G96D}* mutant plants, is thus of interest. While purification of plant tubulin would yield a mix of different isoforms of α- and β-tubulin, these mutant tubulins have a dominant-negative effect on microtubule dynamics and organization *in vivo*, and potentially also *in vitro* (Breviario *et al*., 2013; Hashimoto, 2013). Purified tubulin could be used in *in vitro* polymerization assays, in order to determine the effects of mutated tubulin in the presence and absence of MOR1-YPet-His (or the MOR1$^{1-1}$ variant). Relative microtubule binding affinities of MOR1^{WT} and MOR1$^{1-1}$ could also be compared using co-sedimentation assays with taxol-stabilized microtubules (including mutant tubulins) and purified MOR1^{X}-YPet-His.

Previous attempts to reconstitute MOR1-microtubule interactions *in vitro* have used tubulin purified from animal brains, and TOG domain constructs rather than full-length MOR1 (Lechner *et al*., 2012). Although some aspects of microtubule function are similar in plants and neurons (Gardiner and Marc, 2011), plant tubulin has various properties that differ from animal tubulin. These include dynamicity (Moore *et al*., 1997), binding affinity for MAPs, sensitivity to temperature (Hugdahl *et al*., 1993), and

sensitivity to microtubule-targeted drugs, some of which are used commercially as herbicides due to their ability to bind to plant tubulin, but not animal tubulin (Morejohn *et al*., 1987; Akashi *et al*., 1988). Purification of tubulin from plant sources is thus a priority for *in vitro* analysis of microtubule interactions with MOR1 and/or other MAPs, particularly when studying plant MAP mutants.

For future *in vitro* studies of MOR1-microtubule interactions, I have begun to purify tubulin from *Arabidopsis*, using an affinity purification method, designed by Widlund *et al*., (2012). In this method, a column containing beads linked to a TOG12 construct from *S. cerevisiae* Stu2p (hereafter, Stu2p^{TOG12}), is used to purify tubulin dimers from an extract of *Arabidopsis* suspension cell cultures. I had previously attempted to purify *Arabidopsis* tubulin by other means, which are described in Appendix 2; however, it was reported by the Hashimoto lab at NAIST that the Stu2p^{TOG12} column could be used to purify tubulin from *Arabidopsis* seedlings (Fujita *et al*., 2013; Hotta *et al*., 2016), and they kindly taught me their method. I used this method to isolate highly pure tubulin from *Arabidopsis* T87 suspension cell cultures (Fig. 5.1 A). Multiple tubulin isoforms were purified, and appear on the SDS-PAGE gels and Western blot as distinct bands with slightly different molecular weights (Fig. 5.1). A tubulin polymerization and sedimentation assay was carried out, demonstrating that the purified tubulin was capable of assembling into microtubules, which form a pellet following ultracentrifugation (Fig. 5.1 B).

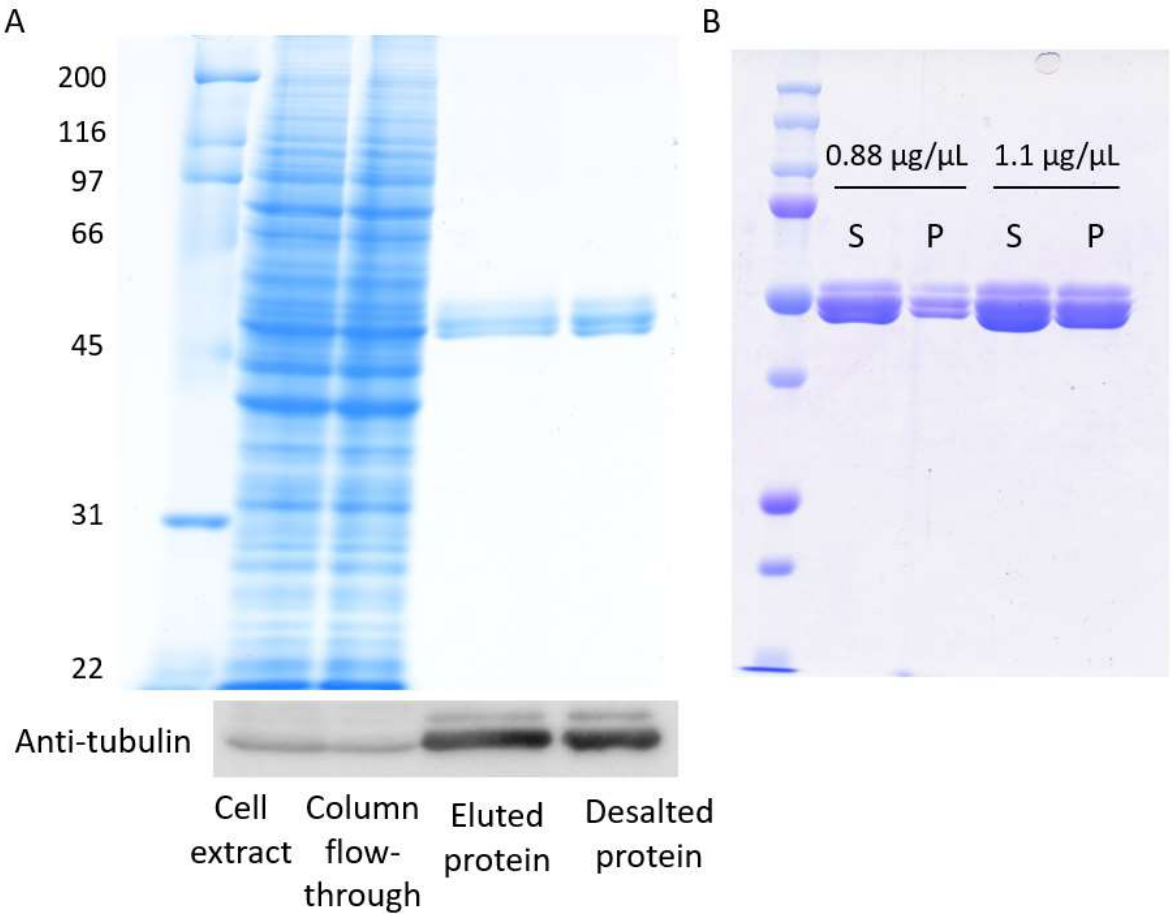

Figure 5.1 Plant tubulin purified using a Stu2p^{TOG12} affinity column was able to polymerize *in vitro*

(A) SDS-PAGE gel and corresponding Western blot, showing protein and tubulin content at different stages of the tubulin purification procedure.
(B) SDS-PAGE gel, showing that the purified tubulin is able to polymerize into microtubules. Tubulin (at two different concentrations) was allowed to polymerize, then samples were centrifuged, and protein content of the supernatant (S) and pellet (P) was analyzed separately. At both concentrations, tubulin is present as free dimers (S) and as microtubules (P).

5.2.2 Analysis of *mor1-11phs1* double mutants

Analysis of microtubule dynamics and organization determined that the plus-end growth rate of microtubules in PPM-treated *mor1-11* seedlings is lower than in wild type, and microtubules are shorter, though no major differences were observed in DMSO-treated seedlings (Zhang, 2010). Because the additive phenotype of the *mor1-11phs1-5* double mutant suggests that some PHS1 activity might offset

microtubule defects in *mor1-11*, I have generated *mor1-11phs1-1* and *mor1-11phs1-5* lines expressing *pro35S::GFP-TUB6*, for future analysis of how changes in PHS1 activity might affect microtubule dynamics and organization in *mor1-11*. Further experiments using Phos-tag™ and Western blotting could determine whether α-tubulin is phosphorylated in *mor1-11*, as my analysis of α-tubulin phosphorylation was limited to plants expressing MOR1$^{1-11}$-YPet. As MPK12 potentially interacts with PHS1 (Walia *et al*., 2009), analysis of a *mor1-11mpk12* mutant could be informative.

Purified MOR1$^{1-11}$-YPet-His could also be used to analyze MOR1-microtubule interactions *in vitro*, as discussed in section 5.2.1. Analysis of MOR1-microtubule co-localization suggests that the *mor1-11* mutation may alter the binding affinity of MOR1 for the microtubule plus end and lattice. Because the addition of a C-terminal YPet tag may alter the localization of MOR1, and because no full-length MOR1 construct without such a tag is currently available, it would also be useful to test the binding of C-terminal fragments of MOR1. For this purpose, I have introduced the *mor1-11* mutation into a TOG5-R4 construct via site-directed mutagenesis.

5.2.3 *mor1-11* modifier mutants

Map-based cloning of the *som* mutants is ongoing, using the approach detailed in Lukowitz *et al*. (2000). Currently, I plan to identify the causative mutations using a combination of PCR marker-based rough and fine mapping, next-generation sequencing, and informed guesses regarding gene products that are likely to affect microtubules. Next-generation mapping is becoming a more accessible approach (Austin *et al*., 2011), and the identification of the modifier mutation in *eom1* as *phs1-1* demonstrates that modifier mutations may be mapped to genes that are known to be involved in regulation of microtubules. Some suppressor mutations are likely to map to genes encoding tubulins: for instance, *tua6*^{C213Y} was previously identified as a suppressor of root skewing in *mor1-11* at 31 °C (Zhang, 2010). Other possible suppressor

mutations may include intragenic mutations in *MOR1*, and perhaps proteins that interact with MOR1 and/or PHS1.

5.3 Methods

5.3.1 Growth conditions for *Arabidopsis* T87 cell suspension cultures

Suspension-cultured T87 cells (Arabidopsis Biological Resource Center, Ohio State University) were grown in Murashige and Skoog liquid medium containing 18 μM 2,4-D and 1 μM kinetin, using a gyratory shaker at 110 rpm, and at 21 °C with a 16 hour light/8 hour dark cycle. Cells were sub-cultured every 7 days by adding 7.5 mL of cells to 42.5 mL of fresh medium in a 250 mL Erlenmeyer flask.

5.3.2 Purification of plant tubulin using the Stu2p^{TOG12} affinity column

This method has been published in Hotta *et al*. (2016). I performed the experiment under the direction of Drs. Takashi Hotta and Satoshi Fujita, who adapted the protocol for use in the purification of plant tubulin. I later made my own Stu2p^{TOG12} column, using the pGEX-6P-1 Stu2 1-590 plasmid, and following the protocol described by Widlund *et al*. (2012). The plasmid was kindly made available by Dr. Anthony Hyman (Addgene plasmid #38314).

5.3.3 Assessment of tubulin purity and ability to polymerize

For Western blot analysis, proteins were blotted onto a PVDF membrane, and α-tubulin was detected using a mouse anti-tubulin primary antibody (1: 4,000) and an anti-mouse horseradish peroxidase-conjugated secondary antibody (1: 10,000). Bands were visualized using Immobilon Western Chemiluminescent HRP Substrate (Merck Millipore; WBKLS0100).

The concentration of purified tubulin was measured using a Bradford assay (Bradford, 1976). To assess polymerization of tubulin, a solution of free tubulin dimers with no microtubules or tubulin aggregates was first obtained by ultracentrifugation of purified tubulin at 40,000 rpm and 4 °C, for 10 minutes. The

supernatant, containing tubulin dimers, was added to a solution of 1x BRB80 (80 mM PIPES-KOH, pH 6.8; 1 mM $MgCl_2$; 1 mM EGTA), 1 mM GTP, and 10% v/v glycerol, such that the concentration of tubulin was 0.88 μg/μL, or 1.1 μg/μL. These concentrations of tubulin were chosen as being sufficient for tubulin polymerization. Samples were incubated at 30 °C for 30 minutes, then the supernatant (containing tubulin dimers) and pellet (containing microtubules) were separated via ultracentrifugation, at 40,000 rpm and 30 °C, for 30 minutes. Samples were subsequently analyzed via SDS-PAGE.

Works cited

Abdrakhamanova, A., Wang, Q.Y., Khokhlova, L. and Nick, P. (2003) Is microtubule assembly a trigger for cold acclimation? Plant & Cell Physiology **44**: 676-686.

Abe, T. and Hashimoto, T. (2005) Altered microtubule dynamics by expression of modified alpha tubulin causes right-handed helical growth in transgenic *Arabidopsis* plants. Plant Journal **43 (2)**: 191-204.

Abràmoff, M.D., Magalhães, P.J., and Ram, S.J. (2004) Image processing with ImageJ. Biophotonics International **11 (7)**: 36-42.

Ahn, N.G., Weiel, J.E., Chan, C.P., and Krebs, E.G. (1990) Identification of multiple epidermal growth factor-stimulated protein serine/threonine kinases from Swiss 3T3 cells. The Journal of Biological Chemistry **265 (20)**: 11487-11494.

Akashi, T., Izumi, K., Nagano, E., Enomoto, M., Mizuno, K., and Shibaoka, H. (1988) Effects of propyzamide on tobacco cell microtubules in vivo and in vitro. Plant Cell Physiology **29 (6**): 1053-1062.

Akhmanova, A., and Steinmetz, M.O. (2008) Tracking the ends: a dynamic protein network controls the fate of microtubule tips. Nature Reviews Molecular Cell Biology **9**: 309-322.

Akhmanova, A., and Steinmetz, M.O. (2015) Control of microtubule organization and dynamics: two ends in the limelight. Nature Reviews Molecular Cell Biology **16**: 711-726.

Akita, K., Higaki, T., Kutsuna, N., and Hasezawa, S. (2015) Quantitative analysis of microtubule orientation in interdigitated leaf pavement cells. Plant Signaling & Behavior **10(5)**: e1024396

Al-Bassam, J., Larsen, N.A., Hyman, A.A., and Harrison, S.C. (2007) Crystal structure of a TOG domain: conserved features of XMAP215/Dis1-family TOG domains and implications for tubulin binding. Structure **15 (3)**: 355-362.

Al-Bassam, J. and Chang, F. (2011) Regulation of microtubule dynamics by TOG-domain proteins XMAP215/Dis1 and CLASP. Trends in Cell Biology **21** (10): 604-614.

Allard, J.F., Wasteneys, G.O., and Cytrynbaum, E.N. (2010) Mechanisms of self-organization of cortical microtubules in plants revealed by computation simulations. Molecular Biology of the Cell **21**: 278-286.

Alonso, J.M. and Stepanova, A.N. (2014) *Arabidopsis* transformation with large bacterial artificial chromosomes. Methods in Molecular Biology **1062**: 271-283.

Alushin, G.M., Lander, G.C., Kellogg, E.H., Zhang, R., Baker, D., and Nogales, E. (2014) High-resolution microtubule structures reveal the structural transitions in $\alpha\beta$-tubulin upon GTP hydrolysis. Cell **157 (5)**: 1117-1129.

Ambrose, J.C., Allard, J.F., Cytrynbaum, E.N., and Wasteneys, G.O. (2011) A CLASP-modulated cell edge barrier mechanism drives cell-wide cortical microtubule organization in *Arabidopsis*. Nature Communications **2**: 430.

Austin, R.S., Vidaurre, D., Stamatiou, G., Breit, R., Provart, N.J., Bonetta, D., Zhang, J., Fung, P., Gong, Y., Wang, P.W., McCourt, P., and Guttman, D.S. (2011) Next-generation mapping of *Arabidopsis* genes. The Plant Journal **67**: 715-725.

Ayaz, P., Ye, X., Huddleston, P., Brautigam, C.A., and Rice, L.M. (2012) A TOG:αβ-tubulin complex structure reveals conformation-based mechanisms for a microtubule polymerase. Science **337 (6096)**: 857-860.

Ayaz, P., Munyoki, S., Geyer, E.A., Piedra, F.A., Vu, E.S., Bromberg, R., Otwinowski, Z., Grishin, N.V., Brautigam, C.A., and Rice, L.M. (2014) A tethered delivery mechanism explains the catalytic action of a microtubule polymerase. eLife: 10.7554/eLife.0306

Ban, Y., Kobayashi, Y., Hara, T., Hamada, T., Hashimoto, T., Takeda, S., and Hattori, T. (2013) α-tubulin is rapidly phosphorylated in response to hyperosmotic stress in rice and *Arabidopsis*. Plant & Cell Physiology **54 (6)**: 848-858.

Baskin, T.I., and Wilson, J.E. (1997) Inhibitors of protein kinases and phosphatases alter root morphology and disorganize cortical microtubules. Plant Physiology **113**: 493-502.

Baum, G., Long, J.C., Jenkins, G.I., and Trewavas, A.J. (1999) Stimulation of the blue light phototropic receptor NPH1 causes a transient increase in cytosolic Ca^{2+}. PNAS **96 (23)**: 13554-13559.

Beck, M., Komis, G. Müller, J., Menzel, D., and Šamaj, J. (2010) *Arabidopsis* homologs of nucleus- and phragmoplast-localized kinase 2 and 3 and mitogen-activated protein kinase 4 are essential for microtubule organization. The Plant Cell **22**: 755-771.

Beck, M., Komis, G., Ziemann, A., Menzel, D. and Šamaj, J. (2011) Mitogen-activated protein kinase 4 is involved in the regulation of mitotic and cytokinetic microtubule transitions in *Arabidopsis thaliana*. New Phytologist **189**: 1069-1083.

Bisgrove, S.R., Hable, W.E, and Kropf, D.L. (2004) +TIPs and microtubule regulation: the beginning of the plus end in plants. Plant Physiology **136**: 3855-3863.

Bisgrove, S.R. (2008) The roles of microtubules in tropisms. Plant Science **175**: 747-755.

Blume, Y.B., Krasylenko, Y.A., Demchuk, O.M., and Yemets, A.I. (2013) Tubulin tyrosine nitration regulates microtubule organization in plant cells. Frontiers in Plant Science **4**: 530.

Bögre, L., Calderini, O., Binarová, P., Mattauch, M., Till, S., Kiegerl, S., Jonak, C., Pollaschek, C., Barker, P., Huskission, N.S., Hirt, H., and Heberle-Bors, E. (1999) A MAP kinase is activated late in plant mitosis and becomes localized to the plane of cell division. The Plant Cell **11**: 101-113.

Bokros, C.L., Hugdahl, J.D., Blumenthal, S.S.D., and Morejohn, L.C. (1996) Proteolytic analysis of polymerized maize tubulin: regulation of microtubule stability to low temperature and Ca^{2+} by the carboxyl terminus of β-tubulin. Plant, Cell and Environment **19**: 539-548.

Borisy, G.G., Marcum, J.M., Olmsted, J.B., Murphy, D.B., and Johnson, K.A. (1975) Purification of tubulin and associated high molecular weight proteins from porcine brain and characterization of microtubule assembly *in vitro*. Annals of the New York Academy of Sciences **253**: 107-132.

Boulton, T.G., Yancopoulos, G.D., Gregory, J.S., Slaughter, C., Moomaw, C., Hsu, J., Cobb, M.H. (1990) An insulin-stimulated protein kinase similar to yeast kinases involved in cell cycle control. Science **249 (4964)**: 64-67.

Bradford, M.M. (1976) A rapid and sensitive method for the quantitation of microgram quantities of protein utilizing the principle of protein-dye binding. Analytical Biochemistry **72**: 248-254.

Breviario, D., Gianì, S., and Morello, L. (2013) Multiple tubulins: evolutionary aspects and biological implications. The Plant Journal **75**: 202-218.

Brouhard, G.J., Stear, J.H., Noetzel, T.L., Al-Bassam, J., Kinoshita, K., Harrison, S.C., Howard, J., and Hyman, A.A. (2008) XMAP215 is a processive microtubule polymerase. Cell **132**: 79-88.

Buschmann, H. and Lloyd, C.W. (2008) *Arabidopsis* mutants and the network of microtubule-associated function. Molecular Plant **1 (6)**: 888-898.

Cao, L., Wang, L., Zhen, M., Cao, H., Ding, L., Zhang, X. and Fu, Y. (2013) *Arabidopsis* AUGMIN subunit8 is a microtubule plus-end binding protein that promotes microtubule reorientation in hypocotyls. The Plant Cell **25**: 2187-2201.

Cassimeris, L., Gard, D., Tran, P.T., and Erickson, H.P. (2001) XMAP215 is a long thin molecule that does not increase microtubule stiffness. Journal of Cell Science **114 (16)**: 3205-3233.

Chuong, S.D.X., Good, A.G., Taylor, G.J., Freeman, M.C., Moorhead, G.B.G., and Muench, D.G. (2004) Large-scale identification of tubulin-binding proteins provides insight on subcellular trafficking, metabolic channeling, and signaling in plant cells. Molecular & Cell Proteomics **3 (10)**: 970-983.

Collings, D.A., Lill, A.W., Himmelspach, R., and Wasteneys, G.O. (2006) Hypersensitivity to cytoskeletal antagonists demonstrates microtubule-microfilament cross-talk in the control of root elongation in *Arabidopsis thaliana*. New Phytologist **170**: 275-290.

Crowell, E.F., Bischoff, V., Desprez, T., Rolland, A., Stierhof, Y.D., Schumacher, K., Gonneau, M., Höfte, H., Vernhettes, S. (2009) Pausing of Golgi bodies on microtubules regulates secretion of cellulose synthase complexes in *Arabidopsis*. Plant Cell **21**: 1141-1154.

Currie, J.D., Stewman, S., Schimizzi, G., Slep, K.C., Ma, A., and Rogers, S.L. (2011) The microtubule lattice and plus-end association of *Drosophila* Mini spindles is spatially regulated to fine-tune microtubule dynamics. Molecular Biology of the Cell **22**: 4343-4361.

Derbyshire, P., Ménard, D., Green, P., Saalbach, G., Buschmann, H., Lloyd, C.W., and Pesquet, E. (2015) Proteomic analysis of microtubule-interacting proteins over the course of xylem tracheary element formation in *Arabidopsis*. The Plant Cell **27**: 2709-2726.

Dhonukshe, P., Laxalt, A.M., Goedhart, J., Gadella, T.W.J., and Munnik, T. (2003) Phospholipase D activation correlates with microtubule reorganization in living plant cells. The Plant Cell **15**: 2666-2679.

Dixit, R., and Cyr, R. (2004) The cortical microtubule array: from dynamics to organization. The Plant Cell **16**: 2546-2552.

Durek, P., Schmidt, R., Heazlewood, J.L., Jones, A., MacLean, D., Nagel, A., Kersten, B., and Schulze, W.X. (2010) PhosPhAt: the *Arabidopsis thaliana* phosphorylation site database. An update. Nucleic Acids Research **38**: D828-834.

Ehrhardt, D.W., and Shaw, S.L. (2006) Microtubule dynamics and organization in the plant cortical array. Annual Review of Plant Biology **56**: 859-875.

Eleftheriou, E.P., Baskin, T.I., and Hepler, P.K. (2005) Aberrant cell plate formation in the *Arabidopsis thaliana microtubule organization 1* mutant. Plant & Cell Physiology **46 (4)**: 671-675.

Endler, A., Kesten, C., Schneider, R., Zhang, Y., Ivakov, A., Froehlich, A., Funke, N., and Persson, S. A mechanism for sustained cellulose synthesis during salt stress. Cell **162 (6)**: 1353-1364.

Endler, A., Schneider, R., Kesten, C., Lampugnani, E.R., and Persson, S. (2016) The cellulose synthase companion proteins act non-redundantly with CELLULOSE SYNTHASE INTERACTING1/POM2 and CELLULOSE SYNTHASE 6. Plant Signaling & Behavior **11 (4)**: e1135281

Eng, R.C. (2015) Characterizing the role of proteins in modulating microtubule dynamics and cell morphogenesis in *Arabidopsis thaliana*. Doctoral dissertation, University of British Columbia.

Eren, E.C., Dixit, R., and Gautam, N. (2010) A three-dimensional computer simulation model reveals the mechanisms for self-organization of plant cortical microtubules into oblique arrays. Molecular Biology of the Cell **21**: 2674-2684.

Fiil, B.K., Petersen, K., Petersen, M., and Mundy, J. (2009) Gene regulation by MAP kinase cascades. Current Opinion in Plant Biology **12**: 615-621.

Fox, J.C., Howard, A.E., Currie, J.D., Rogers, S.L., and Slep, K.C. (2014) The XMAP215 family drives microtubule polymerization using a structurally diverse TOG array. Molecular Biology of the Cell **25**: 2375-2392.

Fujita, M., Himmelspach, R., Hocart, C.H., Williamson, R.E., Mansfield S.D., and Wasteneys, G.O. (2011) Cortical microtubules optimize cell wall crystallinity to drive unidirectional growth in *Arabidopsis*. The Plant Journal **66**: 915-928.

Fujita, M., Lechner, B., Barton, D.A., Overall, R.L., and Wasteneys, G.O. (2012) The missing link: do cortical microtubules define plasma membrane nanodomains that modulate cellulose biosynthesis? Protoplasma **249**: S59-S67.

Fujita, S., Pytela, J., Hotta, T., Kato, T., Hamada, T., Akamatsu, R., Ishida, Y., Kutsuna, N., Hasezawa, S., Nomura, Y., Nakagami, H., and Hashimoto, T. (2013) An atypical tubulin kinase mediates stress-induced microtubule depolymerization in *Arabidopsis*. Current Biology **23**: 1969-1978.

Furutani, I., Watanabe, Y., Prieto, R., Masukawa, M., Suzuki, K., Naoi, K., Thitamadee, S., Shikanai, T., and Hashimoto, T. (2000) The *SPIRAL* genes are required for directional control of cell elongation in *Arabidopsis thaliana*. Development **127**: 4443-4453.

Galva, C., Kirik, V., Lindeboom, J.J., Kaloriti, D., Rancour, D.M., Hussey, P.J., Bednarek, S.Y., Ehrhardt, D.W., and Sedbrook, J.C. (2014) The microtubule plus-end tracking proteins SPR1 and EB1b interact to maintain polar cell elongation and directional organ growth in *Arabidopsis*. The Plant Cell **26**: 4409-4425.

Gard, D.L., Becker, B.E., and Romney, S.J. (2004) Mapping the eukaryotic tree of life: structure, function, and evolution of the MAP215/Dis1 family of microtubule-associated proteins. International Review of Cytology **239**: 179-272.

Gardiner, J., and Marc, J. (2011) *Arabidopsis thaliana*, a plant model organism for the neuronal microtubule cytoskeleton? Journal of Experimental Botany **62 (1)**: 89-97.

Gardiner, J. (2013) The evolution and diversification of plant microtubule-associated proteins. The Plant Journal **75**: 219-229.

Gutierrez, R., Lindeboom, J.L., Paredez, A.R., Emons, A.M.C, and Ehrhardt, D.W. (2009) *Arabidopsis* cortical microtubules position cellulose synthase delivery to the plasma membrane and interact with cellulose synthase trafficking compartments. Nature Cell Biology **11**: 797-806.

Hamada, T. Itoh, T.J., Hashimoto, T., Shimmen, T., and Sonobe, S. (2009) GTP is required for the microtubule catastrophe-inducing activity of MAP200, a tobacco homolog of XMAP215. Plant Physiology **151**: 1823-1830.

Hamada, T., Nagasaki-Takeuchi, N., Kato, T., Fujiwara, M., Sonobe, S., Fukao, Y., and Hashimoto, T. (2013) Purification and characterization of novel microtubule-associated proteins from *Arabidopsis* cell suspension cultures. Plant Physiology **163 (4)**: 1804-1816.

Hamada, T. (2014) Microtubule organization and microtubule-associated proteins in plant cells. International Review of Cell and Molecular Biology **312**: 1-52.

Hamel, L.P., Nicole, M.C., Sritubtim, S., Morency, M.J., Ellis, M., Ehlting, J., Beaudoin, N., Barbazuk, B., Klessig, D., Lee, J., Martin, G., Mundy, J., Ohashi, Y., Scheel, D., Sheen, J., Xing, T., Zhang, S.Q., Seguin, A., and Ellis, B.E. (2006) Ancient signals: comparative genomics of plant MAPK and MAPKK gene families. Trends in Plant Science **11 (4)**: 192-198.

Hardham, A.R. (2013) Microtubules and biotic interactions. The Plant Journal **75**: 278-289.

Hashimoto, T. (2013) Dissecting the cellular functions of plant microtubules using mutant tubulins. Cytoskeleton **70**: 191-200.

Hashimoto, T. (2015) Microtubules in Plants. The *Arabidopsis* Book **13**: e0179.

Henikoff, S., Till, B.J., and Comai, L. (2004) TILLING: traditional mutagenesis meets functional genomics. Plant Physiology **135**: 630-636.

Hotta, T., Fujita, S., Uchimura, S., Noguchi, M. Demura, T., Muto, E., and Hashimoto, T. (2016) Affinity purification and characterization of functional tubulin from cell suspension cultures of *Arabidopsis* and tobacco. Plant Physiology **170 (3)**: 1189-1205.

Howard, A.E., Fox, J.C., and Slep, K.C. (2015) *Drosophila melanogaster* Msps TOG3 utilizes unique structural elements to promote domain stability and maintain a TOG1- and TOG2-like tubulin-binding surface. Journal of Biological Chemistry **290** (16): 10149-10162.

Hua, Z.M., Yang, X.C., and Fromm, M.E. (2006) Activation of the NaCl- and drought-induced RD29A and RD29B promoters by constitutively active Arabidopsis MAPKK or MAPK proteins. Plant, Cell and Environment **29**: 1761-1770.

Huang, R.F., and Lloyd, C.W. (1999) Gibberellic acid stabilises microtubules in maize suspension cells to cold and stimulates acetylation of α-tubulin. FEBS Letters **443**: 317-320.

Hugdahl, J.D., Bokros, C.L., Hanesworth, V.R., Aalund, G.R., and Morejohn, L.C. (1993) Unique functional characteristics of the polymerization and MAP binding regulatory domains of plant tubulin. The Plant Cell **5**: 1063-1080.

Hyman, A.A., Salser, S., Drechsel, D.N., Unwin, N., and Mitchison, T.J. (1992) Role of GTP hydrolysis in microtubule dynamics: information from a slowly hydrolyzable analogue, GMPCPP. Molecular Biology of the Cell **3**: 1155-1167.

Ishida, T. and Hashimoto, T. (2007) An *Arabidopsis* thaliana tubulin mutant with conditional root-skewing phenotype. Journal of Plant Research **120**: 635-640.

Ishida, T., Kaneko, Y., Iwano, M., and Hashimoto, T. (2007a) Helical microtubule arrays in a collection of twisting tubulin mutants of *Arabidopsis thaliana*. PNAS **104 (20)**: 8544-8549.

Ishida, T., Thitamadee, S., and Hashimoto, T. (2007b) Twisted growth and organization of cortical microtubules. Journal of Plant Research **120**: 61-70.

Jiang, C.J., and Sonobe, S. (1993) Identification and preliminary characterization of a 65 kDa higher-plant microtubule-associated protein. Journal of Cell Science **105**: 891-901.

Kato, M., Nagasaki-Takeuchi, N., Ide, Y., Tomioka, R., and Maeshima, M. (2010) PCaPs, possible regulators of PtdInsP signals on plasma membrane. Plant Signaling & Behavior **5** (7): 848-850.

Kawamura, E., Himmelspach, R., Rashbrooke, M.C., Whittington, A.T., Gale, K.R., Collings, D.A., and Wasteneys, G.O. (2006) MICROTUBULE ORGANIZATION 1 regulates structure and function of microtubule arrays during mitosis and cytokinesis in the *Arabidopsis* root. Plant Physiology **140**: 102-114.

Kawamura, E. (2007) Mechanisms of microtubule dynamics regulation by the Microtubule Organization 1 protein. Doctoral dissertation, University of British Columbia.

Kawamura, E. and Wasteneys, G.O. (2008) MOR1, the *Arabidopsis thaliana* homologue of *Xenopus* MAP215, promotes rapid growth and shrinkage, and suppresses the pausing of microtubules *in vivo*. Journal of Cell Science **121 (24)**: 4114-4123.

Kerssemakers, J.W.J., Munteanu, E.L., Laan, L., Noetzel, T.L., Janson, M.E., and Dogterom, M. (2006) Assembly dynamics of microtubules at molecular resolution. Nature **442**: 709-712.

Kilian, J., Whitehead, D., Horak, J., Wanke, D., Weinl, S., Batistic, O., D'Angelo, C., Bornberg-Bauer, E., Kudla, J., and Harter, K. (2007) The AtGenExpress global stress expression data set: protocols, evaluation and model data analysis of UV-B light, drought and cold stress responses. The Plant Journal **50 (2)**: 347-363.

Kim, Y.S., Schumaker, K.S., and Zhu, J.K. (2006) EMS mutagenesis of *Arabidopsis*. Methods in Molecular Biology 323: *Arabidopsis* Protocols, 2nd ed. Ed. J. Salinas and J.J. Sanchez- Serrano. Humana Press Inc., Totowa, N.J.

Kinoshita, E., Kinoshita-Kikuta, E., Takiyama, K., and Koike, T. (2006) Phosphate-binding tag, a new tool to visualize phosphorylated proteins. Molecular & Cellular Proteomics **5 (4)**: 749-757.

Kirik, A., Ehrhardt, D.W., and Kirik, V. (2012) *TONNEAU2/FASS* regulates the geometry of microtubule nucleation and cortical array organization in interphase *Arabidopsis* cells. The Plant Cell **24**: 1158-1170.

Kohoutová, L., Kourová, H., Nagy, S.K., Volc, J., Halada, P., Mészáros, T., Meskiene, I., Bögre, L., and Binarová, P. (2015) The *Arabidopsis* mitogen-activated protein kinase 6 is associated with γ-tubulin on

microtubules, phosphorylates EB1c and maintains spindle orientation under nitrosative stress. New Phytologist **207** (4): 1061-1074.

Konishi, M., and Sugiyama, M. (2003) Genetic analysis of adventitious root formation with a novel series of temperature-sensitive mutants of *Arabidopsis thaliana*. Development **130 (23)**: 5637-5647.

Korolev, A.V., Chan, J., Naldrett, M.J., Doonan, J.H., and Lloyd, C.W. (2005) Identification of a novel family of 70 kDa microtubule-associated proteins in *Arabidopsis* cells. The Plant Journal **42**: 547-555.

Krtková, J., Zimmermann, A., Schwarzerová, K., and Nick, P. (2012) Hsp90 binds microtubules and is involved in the reorganization of the microtubular network and in angiosperms. Journal of Plant Physiology **169**: 1329-1339.

Krtková, J., Benáková, M., and Schwarzerová, K. (2016) Multifunctional microtubule-associated proteins in plants. Frontiers in Plant Science **7**: 474

Landrein, B., Lathe, R., Bringmann, M., Vouillot, C. Ivakov, A., Boudaoud, A., Persson, S., and Hamant, O. (2013) Impaired cellulose synthase guidance leads to stem torsion and twists phyllotactic patterns in *Arabidopsis*. Current Biology **23**: 895-900.

Lechner, B., Rashbrooke, M.C., Collings, D.A., Eng, R.C., Kawamura, E., Whittington, A.T., and Wasteneys, G.O. (2012) The N-terminal TOG domain of *Arabidopsis* MOR1 modulates affinity for microtubule polymers. Journal of Cell Science **125**: 4812-4821

Lei, L., Li, S., Du, J., Bashline, L., and Gu, Y. (2013) CELLULOSE SYNTHASE INTERACTIVE3 regulates cellulose biosynthesis in both a microtubule-dependent and microtubule-independent manner in *Arabidopsis*. Plant Cell **25**: 4912-4923.

Li, H., Zeng, X., Liu, Z.Q., Meng, Q.T., Yuan, M., Mao, T.L. (2009) *Arabidopsis* microtubule-associated AtMAP65-2 acts as a microtubule stabilizer. Plant Molecular Biology **69 (3)**: 313-324.

Li, J., Wang, X., Qin, T., Zhang, Y., Liu, X., Sun, J., Zhou, Y., Zhu, L.., Zhang, Z., Yuan, M., and Mao, T. (2011) MDP25, a novel calcium regulatory protein, mediates hypocotyl cell elongation by destabilizing cortical microtubules in *Arabidopsis*. The Plant Cell **23 (2)**: 4411-4427.

Li, S., Lei, L., Somerville, C.R., and Gu, Y. (2012) Cellulose synthase interactive protein 1 (CSI1) links microtubules and cellulose synthase complexes. PNAS **109 (1)**: 185-190.

Lindeboom, J.J., Nakamura, M., Hibbel, A., Shundyak, K., Gutierrez, R., Ketelaar, T., Emons, A.M.C., Mulder, B.M., Kirik, V., and Ehrhardt, D.W. (2013) A mechanism for reorientation of cortical microtubule arrays driven by microtubule severing. Science **342 (6163)**: 1245533.

Littlejohn, G.R., Mansfield, J.C., Christmas, J.T., Witterick, E., Fricker, M.D., Grant, M.R., Smirnoff, N., Everson, R.M., Moger, J., and Love, J. (2014) An update: improvements in imaging perfluorocarbon-mounted plant leaves with implications for studies of plant pathology, physiology, development and cell biology. Frontiers in Plant Science **5** (140): 1-8.

Liu, X., Qin, T., Ma, Q., Sun, J., Liu, Z., Yuan, M., and Mao, T. (2013) Light-regulated hypocotyl elongation involves proteasome-dependent degradation of the microtubule regulatory protein WDL3 in *Arabidopsis*. The Plant Cell **25**: 1740-1755.

Lucas, J.R., Courtney, S., Hassfurder, M., Dhingra, S., Bryant, A., and Shaw, S.L. (2011) Microtubule-associated proteins MAP65-1 and MAP65-2 positively regulate axial cell growth in etiolated *Arabidopsis* hypocotyls. The Plant Cell **23**: 1889-1903.

Lukowitz, W., Gillmor, C.S., and Scheible, W.R. (2000) Positional cloning in *Arabidopsis*. Why it feels good to have a genome initiative working for you. Plant Physiology **123**: 795-805.

Mao, T., Jin, L., Li, H., Liu, B., and Yuan, M. (2005) Two microtubule-associated proteins of the *Arabidopsis* MAP65 family function differently on microtubules. Plant Physiology **138**: 654-662.

McCourt, P., and Desveaux, D. (2009) Plant chemical genetics. New Phytologist **185**: 15-26.

Meijering, E., Jacob, M., Sarria, J.C.F., Steiner, P., Hirling, H., Unser, M. (2004) Design and validation of a tool for neurite tracing and analysis in fluorescence microscopy images. Cytometry **58A (2)**: 167-176.

Meijering, E., Dzyubachyk, O., and Smal, I. (2012) Methods for cell and particle tracking. Methods in Enzymology Volume 504: Imaging and Spectroscopic Analysis of Living Cells. Ed. P.M. Conn. Elsevier Inc.

Menéndez, M., Rivas, G., Díaz, J.F., and Andreu, J.M. (1998) Control of the structural stability of the tubulin dimer by one high affinity bound magnesium ion at nucleotide N-site. Journal of Biological Chemistry **273**: 167-176.

Mitchison, T., and Kirschner, M. (1984) Dynamic instability of microtubule growth. Nature **312**: 237-242.

Moore, R.C., Zhang, M., Cassimeris, L., and Cyr, R.J. (1997) *In vitro* assembled plant microtubules exhibit a high state of dynamic instability. Cell Motility and the Cytoskeleton **38**: 278-286.

Morejohn, L.C., and Fosket, D.E. (1982) Higher plant tubulin identified by self-assembly into microtubules *in vitro*. Nature **297**: 426-

Morejohn, L.C., Bureau, T.E., Molè-Bajer, J., Bajer, A.S., and Fosket, D.E. (1987) Oryzalin, a dinitroaniline herbicide, binds to plant tubulin and inhibits microtubule polymerization *in vitro*. Planta **172**: 252-264.

Morishima-Kawashima, M., and Kosik, K.S. (1996) The pool of MAP kinase associated with microtubules is small but constitutively active. Molecular Biology of the Cell **7**: 893-905.

Moustafa, K., Lefebvre-De Vos, D., Leprince, A.S., Savouré, A., and Laurière, C. (2008) Analysis of the *Arabidopsis* mitogen-activated protein kinase families: organ specificity and transcriptional regulation upon water stresses. Scholarly Research Exchange **2008**: 1-12.

Müller, J., Beck, M., Mettbach, U., Komis, G., Hause, G., Menzel, D., and Šamaj, J. (2010) *Arabidopsis* MPK6 is involved in cell division plane control during early root development, and localizes to the pre-prophase band, phragmoplast, trans-Golgi network and plasma membrane. The Plant Journal **61**: 234-248.

Nakajima, K., Kawamura, T., and Hashimoto, T. (2006) Role of the *SPIRAL1* gene family in anisotropic growth of *Arabidopsis thaliana*. Plant & Cell Physiology **47 (4)**: 513-522.

Nakamura, M., Naoi, K., Shoji, T., and Hashimoto, T. (2004) Low concentrations of propyzamide and oryzalin alter microtubule dynamics in *Arabidopsis* epidermal cells. Plant & Cell Physiology **45 (9)**: 1330-1334.

Naoi, K., and Hashimoto, T. (2004) A semidominant mutation in an *Arabidopsis* mitogen-activated protein kinase phosphatase-like gene compromises cortical microtubule organization. The Plant Cell **16**: 1841-1853.

Nick, P. (2013) Microtubules, signalling and abiotic stress. The Plant Journal **75**: 309-323.

Nogales, E., Whittaker, M., Milligan, R.A., and Downing, K.H. (1999) High-resolution model of the microtubule. Cell **96**: 79-88.

Oda, Y. (2015) Cortical microtubule rearrangements and cell wall patterning. Frontiers in Plant Science **6**: 236.

Oh, S.A., Pal, M.D., Park, S.K., Johnson, J.A., Twell, D. (2010) The tobacco MAP215/Dis1-family protein TMBP200 is required for the functional organization of microtubule arrays during male germline establishment. Journal of Experimental Botany **61**: 969-981.

Oliva, M. and Dunand, C. (2007) Waving and skewing: how gravity and the surface of growth media affect root development in Arabidopsis. New Phytologist **176**: 37-43.

Page, D.R. and Grossniklaus, U. (2002) The art and design of genetic screens: *Arabidopsis thaliana*. Nature Reviews Genetics **3**: 124-136.

Parrotta, L., Cresti, M., and Cai, G. (2014) Accumulation and post-translational modifications of plant tubulins. Plant Biology **16 (3)**: 521-527.

Paschal, B.M., Obar, R.A., and Vallee, R.B. (1989) Interaction of brain cytoplasmic dynein and MAP2 with a common sequence at the C terminus of tubulin. Nature **342**: 569-572.

Popov, A.V., Pozniakovsky, A., Arnal, I., Antony, C., Ashford, A.J., Kinoshita, K., Tournebize, R., Hyman, A.A., and Karsenti, E. (2001) XMAP215 regulates microtubule dynamics through two distinct domains. The EMBO Journal **20 (3)**: 397-410.

Pytela, J., Kato, T., and Hashimoto, T. (2010) Mitogen-activated protein kinase phosphatase PHS1 is retained in the cytoplasm by nuclear extrusion signal-dependent and independent mechanisms. Planta **231**: 1311-1322.

Qiu, Q.S., Guo, Y., Dietrich, M.A., Schumaker, K.S., and Zhu, J.K. (2002) Regulation of SOS1, a plasma membrane Na^+/H^+ exchanger in *Arabidopsis thaliana*, by SOS2 and SOS3. PNAS **99 (12)**: 8436-8441.

Quettier, A.L., Bertrand, C., Habricot, Y., Miginiac, E., Agnes, C., Jeannette, E., and Maldiney, R. (2006) The *phs1-3* mutation in a putative dual-specificity protein tyrosine phosphatase gene provokes hypersensitive responses to abscisic acid in *Arabidopsis thaliana*. The Plant Journal **47**: 711-179.

Rashbrooke, M.C. (2005) Molecular and genetic analysis of MOR1, a microtubule-associated protein in the model plant *Arabidopsis thaliana*. Doctoral dissertation, Australia National University.

Roitinger, E., Hofer, M., Köcher, T., Pichler, P., Novatchkova, M., Yang, J., Schlögelhofer, P., and Mechtler, K. (2015) Quantitative phosphoproteomics of the Ataxia Telangiectasia-Mutated (ATM) and Ataxia Telangiectasia-Mutated and Rad3-related (ATR) dependent DNA damage response in *Arabidopsis thaliana*. Molecular & Cellular Proteomics **14 (3)**: 556-571.

Roux, K.J., Kim, D.I., Raida, M., and Burke, B. (2012) A promiscuous biotin ligase fusion protein identifies proximal and interacting proteins in mammalian cells. Journal of Cell Biology **196 (6)**: 801-810.

Sambade, A., Pratap, A., Buschmann, H., Morris, R.J., and Lloyd, C. (2012) The influence of light on microtubule dynamics and alignment in the *Arabidopsis* hypocotyl. Plant Cell **24**: 192-201.

Sasabe, M., Soyano, T., Takahashi, Y., Sonobe, S., Igarashi, H., Itoh, T.J., Hidaka, M., and Machida, Y. (2006) Phosphorylation of NtMAP65-1 by a MAP kinase down-regulates its activity of microtubule bundling and stimulates progression of cytokinesis of tobacco cells. Genes & Development **20**: 1004-1014.

Sasabe, M., Kosetsu, K., Hidaka, M., Murase, A., and Machida, Y. (2011) *Arabidopsis thaliana* MAP65-1 and MAP65-2 function redundantly with MAP65-3/PLEIADE in cytokinesis downstream of MPK4. Plant Signaling & Behavior **6 (5)**: 743-747.

Sasabe, M., and Machida, Y. (2012) Regulation of organization and function of microtubules by the mitogen-activated protein kinase cascade during plant cytokinesis. Cytoskeleton **69**: 913-918.

Sedbrook, J.C. (2004) MAPs in plant cells: delineating microtubule growth dynamics and organization. Current Opinion in Plant Biology **7**: 632-640.

Sedbrook, J.C., and Kaloriti, D. (2008) Microtubules, MAPs and plant directional cell expansion. Trends in Plant Science **13 (6)**: 303-310.

Shoji, T., Suzuki, K., Abe, T., Kaneko, Y., Shi, H., Zhu, J.K., Rus, A., Hasegawa, P.M., and Hashimoto, T. (2006) Salt stress affects cortical microtubule organization and helical growth in *Arabidopsis*. Plant Cell Physiology **47 (8)**: 1158-1168.

Stecker, K., Minkoff, B.B., and Sussman, M.R. (2014) Phosphoproteomic analysis of early osmosignalling. Plant Physiology **165 (3)**: 1171-1187.

Slep, K.C., and Vale, R.D. (2007) Structural basis of microtubule plus end tracking by XMAP215, CLIP-170 and EB1. Molecular Cell **27 (6)**: 976-991.

Smertenko, A., Dráber, P., Viklický, V., and Opatrný, Z. (1997) Heat stress affects the organization of microtubules and cell division in *Nicotiana tabacum* cells. Plant, Cell and Environment **20**: 1534-1542.

Soyano, T., Nishihama, R., Morikiyo, K., Ishikawa, M., and Machida, Y. (2003) NQK1/NtMEK1 is a MAPKK that acts in the NPK1 MAPKKK-mediated MAPK cascade and is required for plant cytokinesis. Genes & Development **17**: 1055-1067.

Suarez Rodriguez, M.C., Petersen, M., and Mundy, J. (2010) Mitogen-activated protein kinase signaling in plants. Annual Review of Plant Biology **61**: 621-649.

Sugimoto, K., Himmelspach, R., Williamson, R.E., and Wasteneys, G.O. (2003) Mutation or drug-dependent microtubule disruption causes radial swelling without altering parallel cellulose microfibril deposition in *Arabidopsis* root cells. The Plant Cell **15**: 1414-1429.

Sui, H., and Downing, K.H. (2010) Structural basis of interprotofilament interaction and lateral deformation of microtubules. Structure **18 (8)**: 1022-1031.

Sun, J., Ma, Q., and Mao, T. (2015) Ethylene regulates the *Arabidopsis* microtubule-associated protein WAVE-DAMPENED2-LIKE5 in etiolated hypocotyl elongation. Plant Physiology **169**: 325-337.

Tang, Q., Guittard-Crilat, E., Maldiney, R., Habricot, Y., Miginiac, E., Bouly, J.P., and Lebreton, S. (2016) The mitogen-activated protein kinase phosphatase PHS1 regulates flowering in *Arabidopsis thaliana*. Planta **243**: 909-923.

Teige, M., Scheikl, E., Eulgem, T., Dóczi, R., Ichimura, K., Shinozaki, K., Dangl, J.L., and Hirt, H. (2004) The MKK2 pathway mediates cold and salt stress signaling in *Arabidopsis*. Molecular Cell **15 (1)**: 141-152.

Thitamadee, S., Tuchihara, K., and Hashimoto, T. (2002) Microtubule basis for left-handed helical growth in *Arabidopsis*. Nature **417**: 193-196.

Twell, D., Park, S.K., Hawkins, T.J., Schubert, D., Schmidt, R., Smertenko, A., and Hussey, P.J. (2002) MOR1/GEM1 has an essential role in the plant-specific cytokinetic phragmoplast. Nature Cell Biology **4**: 711-714.

Uyttewaal, M., Burian, A., Alim, K., Landrein, B., Borowska-Wykręt, Dedieu, A., Peaucelle, A., Ludynia, M., Traas, J., Boudaoud, A., Kwiatkowska, D., and Hamant, O. (2012) Mechanical stress acts via katanin to amplify differences in growth rate between adjacent cells in *Arabidopsis*. Cell **149 (2)**: 439-451.

van der Vaart, B., Manatschal, C., Grigoriev, I., Olieric, V., Montenegro Gouveia, S., Bjelić, S., Demmers, J., Vorobjev, I. Hoogenraad, C.C., Steinmetz, M.O., and Akhmanova, A. (2011) SLAIN2 links microtubule plus end-tracking proteins and controls microtubule growth in interphase. The Journal of Cell Biology **193 (6)**: 1083-1099.

van Damme, D., van Poucke, K., Boutant, E., Ritzenthaler, C., Inzé, D., and Geelen, D. (2004) *In vivo* dynamics and differential microtubule-binding activities of MAP65 proteins. Plant Physiology **136**: 3956-3967.

Walia, A. (2009) Involvement of mitogen-activated protein kinase signalling in plant microtubule function. Doctoral dissertation, University of British Columbia.

Walia, A., Lee, J.S., Wasteneys, G., and Ellis, B. (2009) *Arabidopsis* mitogen-activated protein kinase MPK18 mediates cortical microtubule functions in plant cells. The Plant Journal **59**: 565-575.

Wang, C., Li, J., and Yuan, M. (2007) Salt tolerance requires cortical microtubule reorganization in *Arabidopsis*. Plant & Cell Physiology **48**: 1534-1547.

Wang, X., Zhu, L., Liu, B., Wang, C., Jin, L., Zhao, Q., and Yuan, M. (2007) *Arabidopsis* MICROTUBULE-ASSOCIATED PROTEIN18 functions in directional cell growth by destabilizing cortical microtubules. The Plant Cell **19 (3)**: 877-889.

Wang, C., Zhang, L., and Chen, W. (2011) Plant cortical microtubules are putative sensors under abiotic stresses. Biochemistry (Moscow) **76**: 320-326.

Wang, S., Kurepa, J., Hashimoto, T., and Smalle, J.A. (2011) Salt stress-induced disassembly of *Arabidopsis* cortical microtubule arrays involves 26S proteasome-dependent degradation of SPIRAL1. The Plant Cell **23**: 3412-3427.

Wang, T., McFarlane, H.E., and Persson, S. (2016) The impact of abiotic factors on cellulose synthesis. Journal of Experimental Botany **67 (2)**: 543-552.

Wasteneys, G.O. (2003) Microtubules show their sensitive nature. Plant & Cell Physiology **44 (7)**: 653-654.

Wasteneys, G.O. (2004) Progress in understanding the role of microtubules in plant cells. Current Opinion in Plant Biology **7**: 651-660.

Wasteneys, G.O. and Ambrose, J.C. (2009) Spatial organization of plant cortical microtubules: close encounters of the 2D kind. Trends in Cell Biology **19 (2)**: 62-71.

Weizbauer, R., Peters, W.S., and Schulz, B. (2011) Geometric constraints and the anatomical interpretation of twisted plant organ phenotypes. Frontiers in Plant Science **2 (62)**: 1-8.

Whittington, A.T., Vugrek, O., Wei, K.J., Hasenbein, N.G., Sugimoto, K., Rashbrooke, M.C., and Wasteneys, G.O. (2001) MOR1 is essential for organizing cortical microtubules in plants. Nature **411**: 610-613.

Widlund, P.O, Stear, J.H., Pozniakovsky, A., Zanic, M., Reber, S., Brouhard, G.J., Hyman, A.A., and Howard, J. (2011) XMAP215 polymerase activity is built by combining multiple tubulin-binding TOG domains and a basic lattice-binding region. PNAS **108 (7)**: 2741-2746.

Widlund, P.O., Podolski, M., Reber, S., Alper, J., Storch, M., Hyman, A.A., Howard, J., and Drechsel, D.N. (2012) One-step purification of assembly-competent tubulin from diverse eukaryotic sources. Molecular Biology of the Cell **23**: 4393-4401.

Winter, D., Vinegar, B., Nahal, H., Ammar, R., Wilson, G.V., and Provart, N.J. (2007) An "electronic fluorescent pictograph" browser for exploring and analyzing large-scale biological data sets. PLOS One **2 (8)**: e718.

Wong, J.H., and Hashimoto, T. (2017) Novel *Arabidopsis* microtubule-associated proteins track growing microtubule plus ends. BMC Plant Biology **17 (33)**: DOI 10.1186/s12870-017-0987.

Xiong, X., Xu, D., Yang, Z., Huang, H., and Cui, X. (2013) A single amino acid substitution at lysine 40 of an *Arabidopsis thaliana* α-tubulin causes extensive cell proliferation and expansion defects. Journal of Integrative Plant Biology **55 (3)**: 209-220.

Yao, M., Wakamatsu, Y., Itoh, T.J., Shoji, T., and Hashimoto, T. (2008) *Arabidopsis* SPIRAL2 promotes uninterrupted microtubule growth by suppressing the pause state of microtubule dynamics. Journal of Cell Science **121 (14)**: 2372-2381.

Yu, J., Qiu, H., Liu, X., Wang, M., Gao, Y., Chory, J., and Tao, Y. (2015) Characterization of *tub4*^{P287L}, a β-tubulin mutant, revealed new aspects of microtubule regulation in shade. Journal of Integrative Plant Biology **57 (9)**: 757-769.

Yu, J., Dong, K., He, Q., Li, Y., Wang, M., and Tao, Y. (2017) Studies on suppressors of *sav2/shade avoidance 2* revealed altered interaction at the interface of αβ-tubulin intradimer affects microtubule dynamics. Plant Growth Regulation **81**: 71-79.

Zanic, M., Widlund, P.O., Hyman, A.A., and Howard, J. (2013) Synergy between XMAP215 and EB1 increases microtubule growth rates to physiological levels. Nature Cell Biology **15**: 688-693.

Zhang, Y. (2010) TOG domain-tubulin interactions and the function of the *Arabidopsis* MICROTUBULE ORGANIZATION 1 protein. Master's thesis, University of British Columbia.

Zhang, Q., Lin, F., Mao, T., Nie, J., Yan, M., Yuan, M., Zhang, W. (2012) Phosphatidic acid regulates microtubule organization by interacting with MAP65-1 in response to salt stress in *Arabidopsis*. Plant Cell **24 (11)**: 4555-4576.

Zhou, R., Benavente, L.M., Stepanova, A.N., and Alonso, J.M. (2011) A recombineering-based gene tagging system for *Arabidopsis*. The Plant Journal **66**: 712-723.

Zhu, J.K. (2016) Abiotic stress signaling and responses in plants. Cell **167 (2)**: 313-324.

Appendix 1: Root skewing and microtubule organization phenotypes

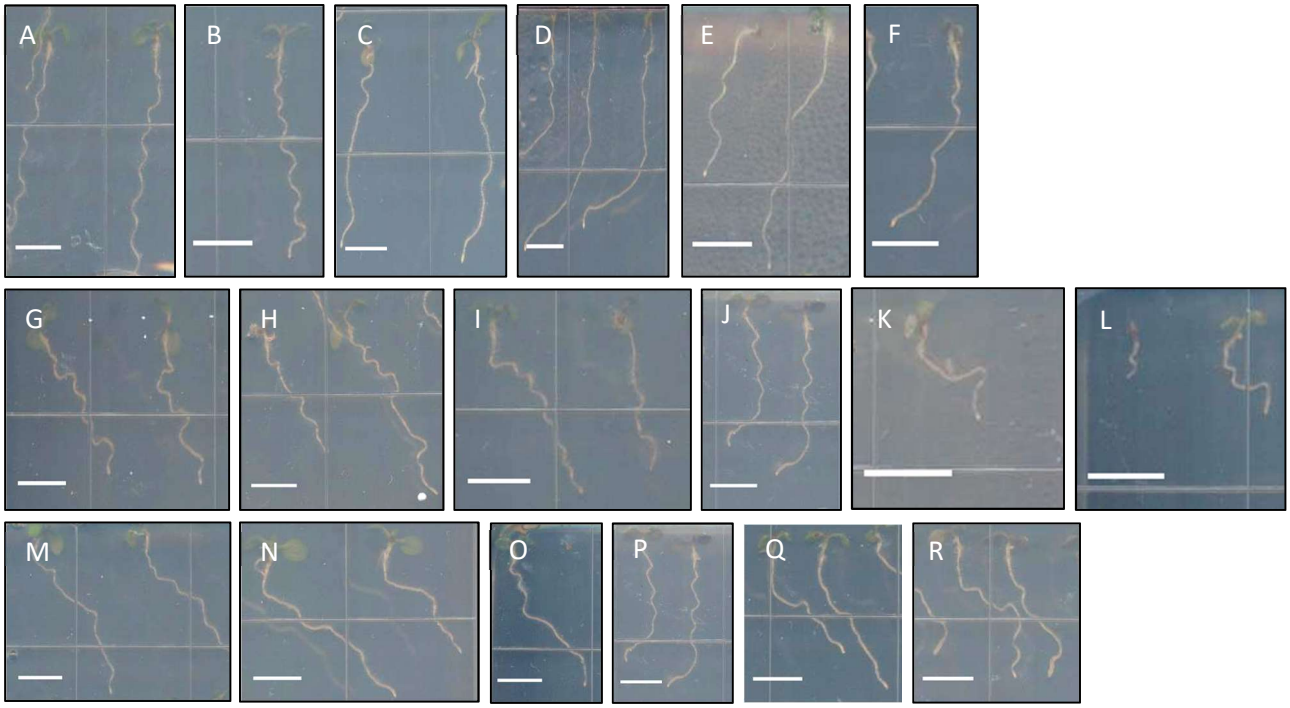

Figure A1.1 Root growth phenotypes for tubulin and *mor1* mutants (expressing *pro35S::GFP-TUB6*) studied in Chapter 2

Root growth phenotypes for these mutants were previously published in Zhang (2010). I acquired these images to confirm that root growth phenotypes are not altered with expression of *pro35S::GFP-TUB6*. These are shown here for reference. Images were adjusted to enhance contrast and brightness. Scale bars = 5 mm.

(A, B) Wild type at 21 °C (A) and 31 °C (B)

(C, D) *mor1-1* at 21 °C (C) and 31 °C (D)

(E, F) *rid5* at 21 °C (E) and 31 °C (F)

(G, H) *tub4*^{P220S}

(I, J) *tub4*^{P220S}*mor1-1*

(K, L) *tub4*^{P220S}*rid5*. These plants are stunted. This was not the case for *tub4*^{P220S}*rid5* without *pro35S::GFP-TUB6*, which have mild right-handed twisting, with radial swelling at 31 °C (Zhang, 2010).

(M, N) *tub4*^{G96D}

(O, P) *tub4*^{G96D}*mor1-1*

(Q, R) *tub4*^{G96D}*rid5*

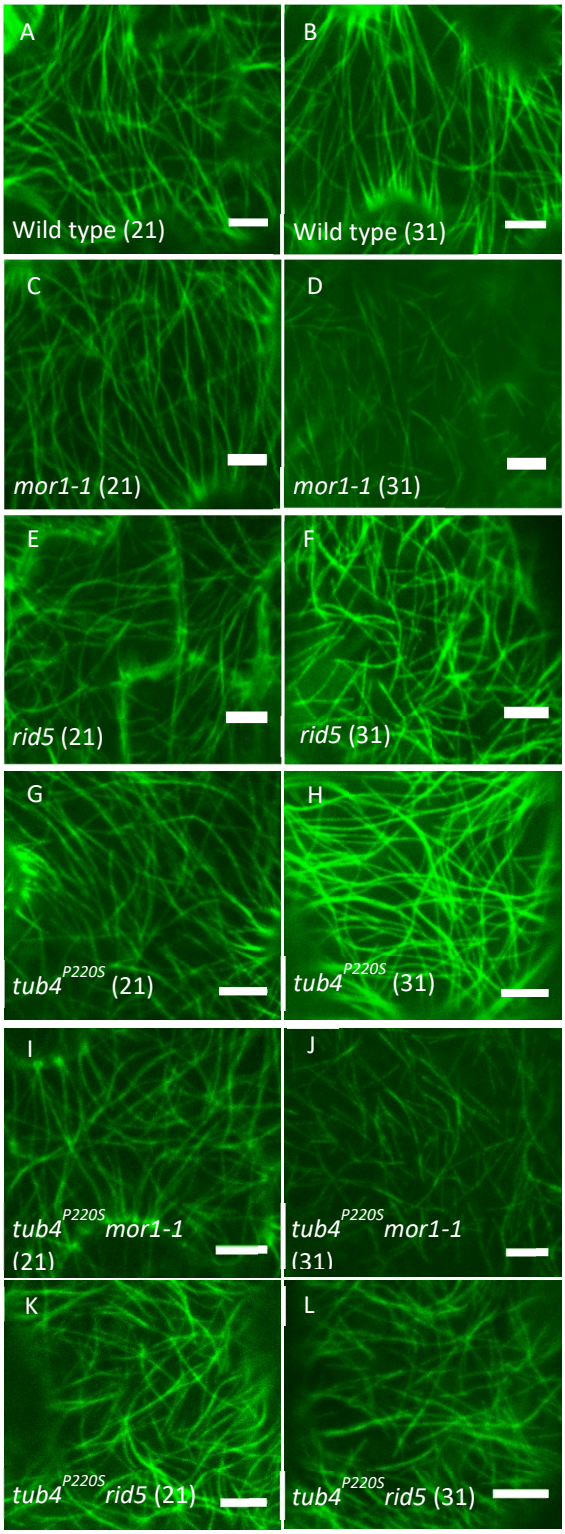

Figure A1.2 Microtubule organization phenotypes in *tub4*^{P220S} and *tub4*^{P220S}*mor1* double mutants

Confocal micrographs of *35S::GFP-TUB6* labelling cortical microtubule arrays in cotyledon epidermal cells of 7-day-old seedlings grown and imaged at 21 °C (left column) or 31 °C (right column).

Microtubule organization phenotypes in these mutants were previously published in Zhang (2010). I acquired these images, which are shown here for reference. Representative images are shown from a selection of 15-20 images acquired for each genotype and at each temperature.
(A,B) Microtubule organization in wild type (Col) is similar at 21 °C and 31 °C.
(C-F) Microtubule organization in *mor1-1* and *rid5* is similar to wild type at 21 °C, but microtubules are short and disorganized at 31 °C.
(G, H) Microtubule organization in $tub4^{P220S}$ is similar to wild type at 21 °C, but microtubules are hyper-parallel at 31 °C, with increased bundling.
(I-L) Microtubule organization in $tub4^{P220S}$*mor1-1* and $tub4^{P220S}$*rid5* is similar to wild type at 21 °C, but microtubules are short and disorganized at 31 °C.
Scale bars = 5 μm.

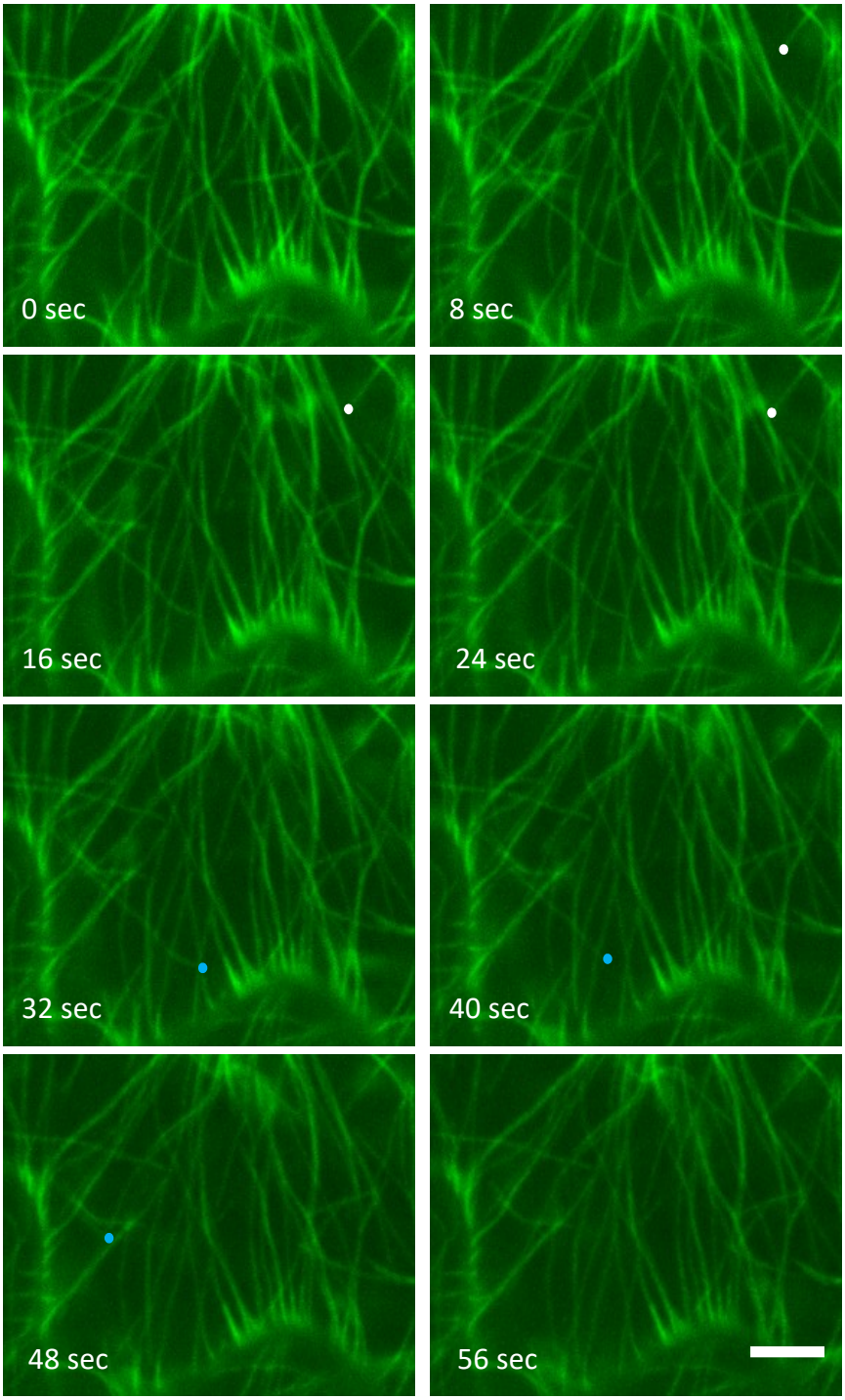

Figure A1.3 Sample time series used for tracking microtubule plus-end dynamics

Confocal micrographs of *35S::GFP-TUB6* labelling cortical microtubule arrays in cotyledon epidermal cells of 7 day-old wild-type seedlings at 31 ^{o}C. The white dot marks the plus end of a growing microtubule, and the blue dot marks the plus end of a shrinking microtubule. Scale bar = 5 μm.

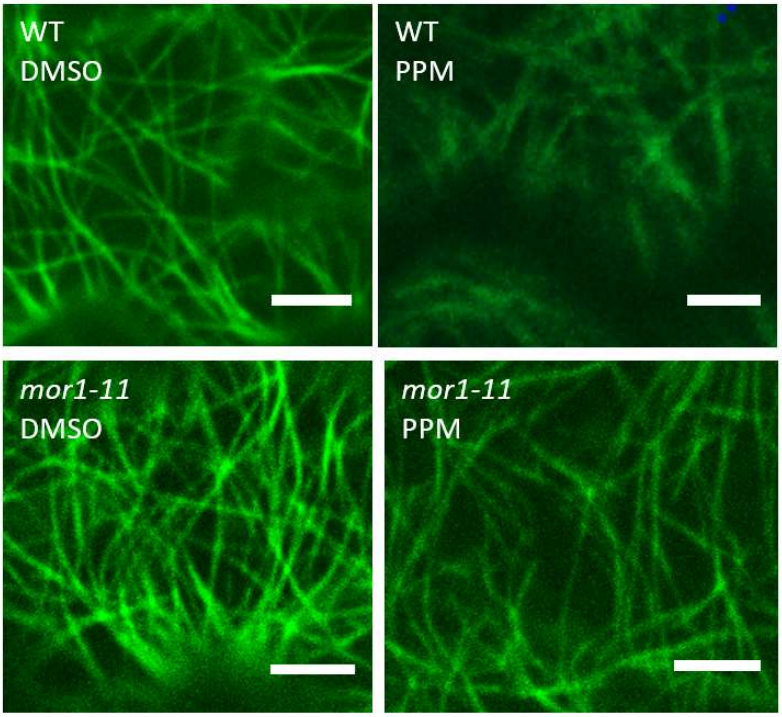

Figure A1.4 Microtubule organization in wild type and *mor1-11*

Confocal micrographs of *35S::GFP-TUB6* labelling cortical microtubule arrays in cotyledon epidermal cells of 7 day-old wild-type seedlings at 21 ^{o}C. Wild type (WT) and *mor1-11* seedlings were grown on solid Hoagland's medium containing DMSO (300 μL/L) or 3 μM PPM (300 μL of a 10 mM stock). Scale bar = 5 μm.

Appendix 2: Tubulin purification

In this appendix, I describe alternative approaches to purifying plant tubulin, which I attempted before purifying tubulin by the method described in Chapter 5.

A2.1 Purification of *Arabidopsis* tubulin using anion exchange chromatography and polymerization/depolymerization cycling

Purification of taxol-stabilized microtubules from plant cell suspension cultures and protoplasts has been achieved with various species, including rose, carrot, maize, and *Arabidopsis* (Morejohn and Fosket, 1982; Moore *et al*., 1987; Bokros *et al*., 1996; Hamada *et al*., 2013). While taxol-stabilized microtubules are of use in microtubule-MAP binding (co-sedimentation) assays, MOR1 is a microtubule polymerase/depolymerase, and the study of microtubule-MOR1 interactions *in vitro* necessitates the purification of tubulin dimers (rather than microtubules) for use in polymerization assays. Tubulin dimers are commonly purified from animal brains, using temperature-dependent polymerization and depolymerization cycling in combination with ultracentrifugation (Borisy *et al*., 1975).

I designed a polymerization/depolymerization cycling-based protocol for purification of tubulin from *Arabidopsis* cell suspension cultures, with modifications to account for the properties of plant tubulin (Fig. A2.1 A). Because tubulin in plant suspension cell cultures is less abundant than in animal brains (Hotta *et al*., 2016), and since the C-terminal tail regions of tubulin are negatively charged, tubulin from plant cell lysate was first concentrated using anion exchange chromatography. One cycle of polymerization and depolymerization was used, with polymerization at 25 ^{o}C rather than the usual 32-37 ^{o}C, since plant tubulin can polymerize more efficiently than animal tubulin at lower temperatures (Hugdahl *et al*., 1993).

This method yielded relatively pure tubulin (Fig. A2.1 B); however, this tubulin was unable to re-polymerize *in vitro*, even when treated with the microtubule-stabilizing drug taxol (Fig. A2.1 C).

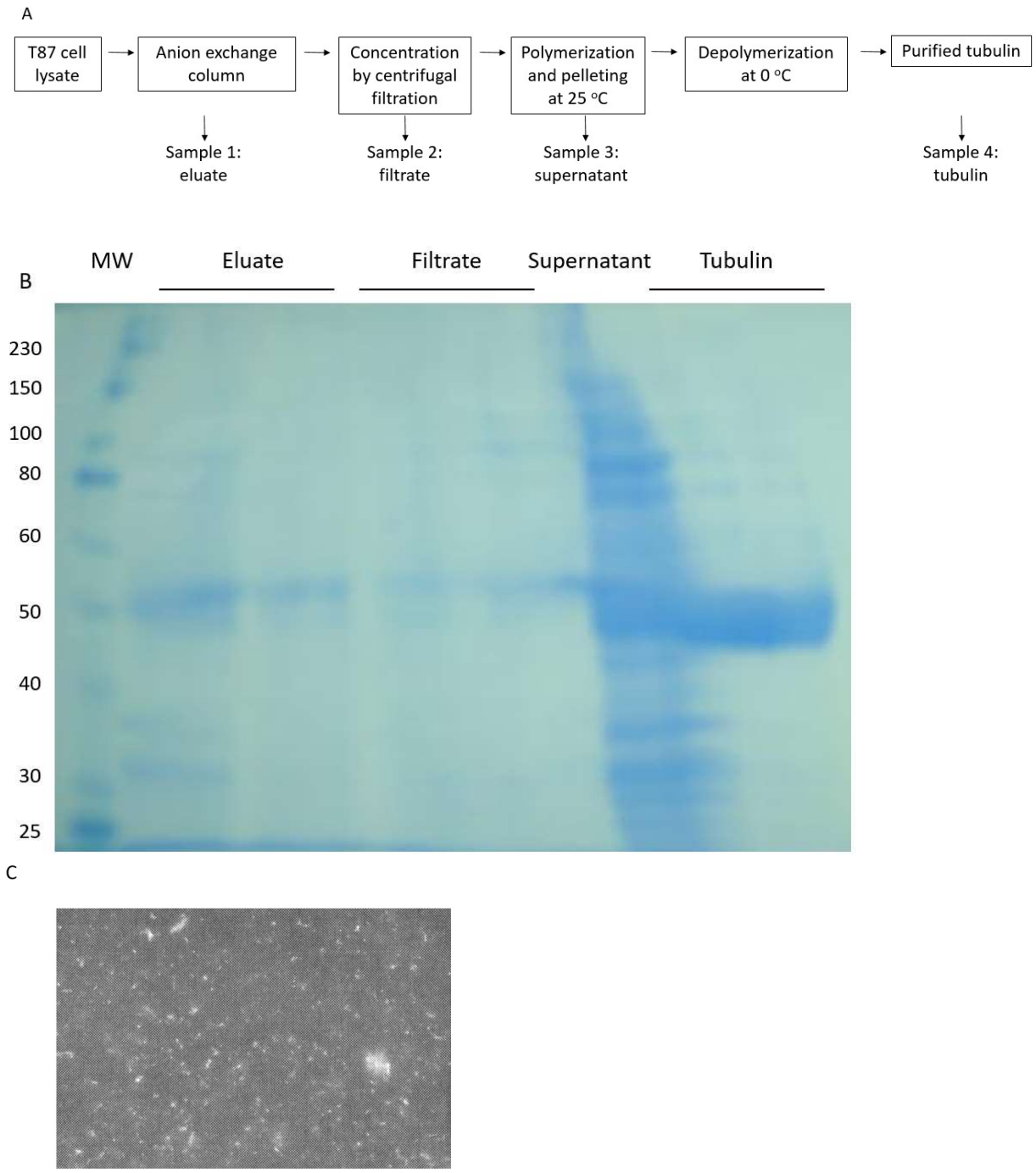

Figure A2.1 Plant tubulin purified using polymerization and depolymerization cycling was not able to polymerize *in vitro*

A. Experimental flow chart, indicating steps at which samples were taken for the gel in Fig. A2.1 B.
B. SDS-PAGE gel, showing protein content at different stages of the tubulin purification procedure. MW, molecular weight standards. 20 μL were loaded for each sample. Eluate from the anion exchange column (sample 1) had a prominent band corresponding to the molecular weight of a tubulin monomer (55 kDa). Concentration of tubulin and other proteins via centrifugal filtration was efficient, as only a

small amount of lost protein was detected in the centrifugal filtrate (sample 2). Polymerization and pelleting of microtubules at 25 °C was also efficient, as various proteins are seen in the supernatant from the pelleting step (sample 3), but not in the final sample of purified tubulin (sample 4).
C. When mixed with rhodamine-labelled sheep brain tubulin (5 μM plant tubulin: 0.24 μM labelled tubulin) and 0.2 mM taxol, only very short microtubules were able to form.

A2.2 Purification of *Arabidopsis* tubulin using MOR1^{TOG1234} affinity purification

A method for purifying tubulin dimers without the use of temperature-driven polymerization and depolymerization cycling was published by Widlund *et al*. (2012). This method uses a construct with the TOG1 and TOG2 domains from *S. cerevisiae* Stu2p, fused to a glutathione *S*-transferase (GST) tag; the GST-TOG12 construct is coupled to N-hydroxysuccinimide ester-activated Sepharose beads, creating an affinity column. This affinity purification method was shown to yield highly pure tubulin from animal and fungal sources (Widlund *et al*., 2012).

As plant tubulin has various characteristics that are distinct from animal tubulin (discussed in Chapter 5), I hypothesized that plant tubulin might be more easily purified using a MOR1-based affinity column, and instead used a TOG1234-His construct to create an affinity column. This column was not effective when used to purify tubulin from *Arabidopsis* T87 cells: no protein was detected in the eluate, even when filter-centrifuged to concentrate any eluted protein (Figure A2.2 A). In order to determine whether the MOR1^{TOG1234} column could bind tubulin at all, I loaded purified sheep brain tubulin onto the column. Interestingly, the column was able to bind sheep tubulin: no tubulin was detected in the column flow-through, though some was washed out, and enough remained bound to the column during the multiple wash stages (which used a total of 22 column volumes of two different wash buffers) that some tubulin was detected in the eluate (Figure A2.2 B).

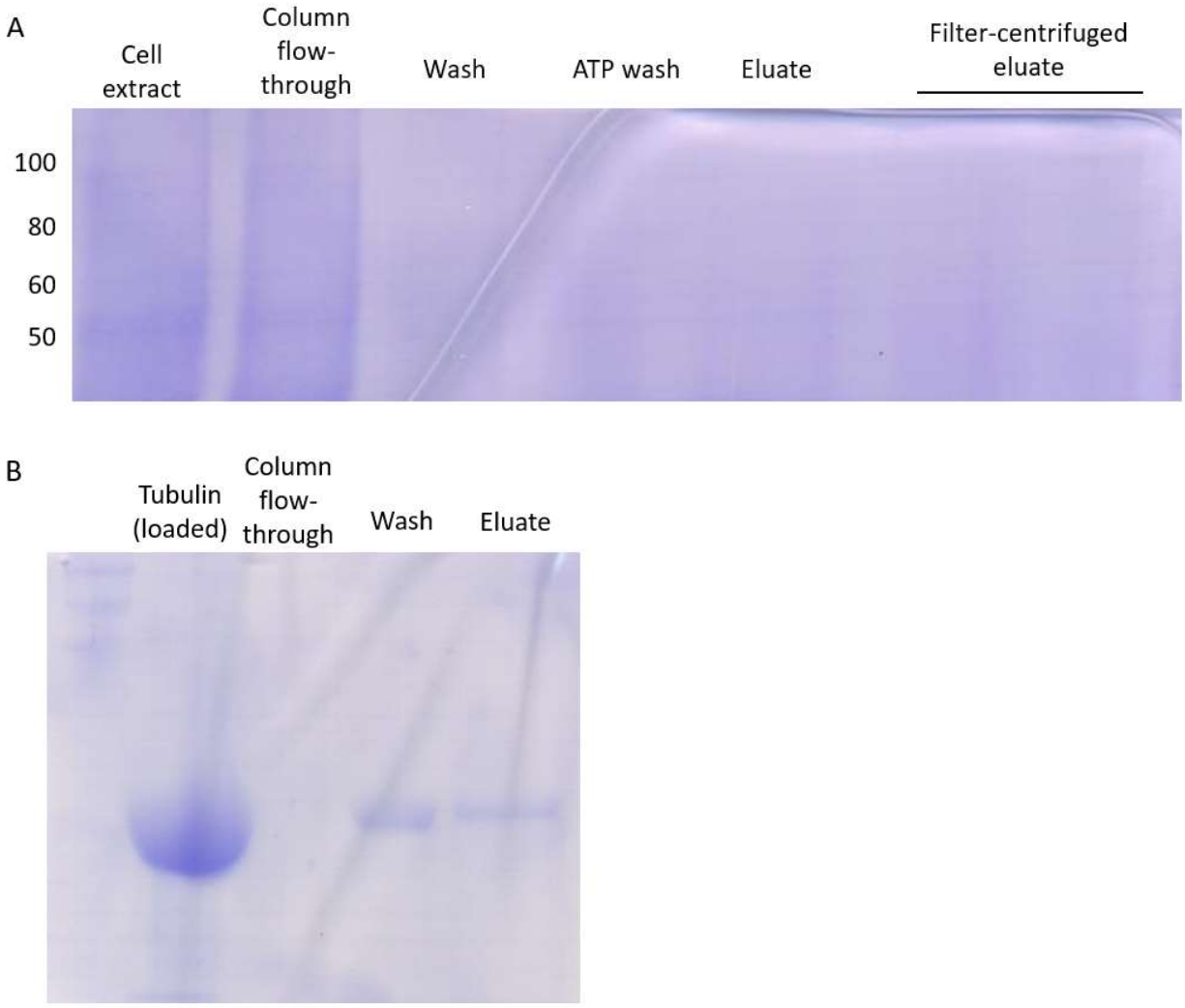

Figure A2.2 A MOR1^{TOG1234} affinity column did not efficiently bind plant tubulin

(A) SDS-PAGE gel, showing protein content at different stages of the *Arabidopsis* tubulin purification procedure. 20 μL were loaded for each sample, except the last (10 μL). No protein bands were observed in the filter-centrifuged (concentrated) eluate, indicating that any tubulin present in the cell extract failed to bind to the MOR1^{TOG1234} column.
(B) SDS-PAGE gel, showing protein content at different stages of an experiment designed to determine whether sheep brain tubulin could bind to the MOR1^{TOG1234} column. 20 μL were loaded for each sample. Sample 1 shows the purified sheep brain tubulin that was loaded onto the column (approx. 100 μM); sample 2 shows that none of the tubulin was lost in the column flow-through; sample 3 was taken from the first wash step (which used 4 column volumes of wash buffer), showing some loss of tubulin; sample 4 shows the presence of tubulin in the eluate, indicating that some of the tubulin did bind to the MOR1^{TOG1234} column.

A2.3 Considerations for the use of plant tubulin and MOR1 in *in vitro* work

Although I was able to purify plant tubulin using a combination of anion exchange chromatography and polymerization/depolymerization cycling, the purified tubulin was unable to re-polymerize (Fig. A2.1). I hypothesize that plant tubulin is more temperature-sensitive than animal tubulin; this effect may be especially pronounced due to the lower abundance of plant tubulin (Morejohn and Fosket, 1982). Microtubule reassembly following cold-induced depolymerization was shown to be impaired *in vivo* following inhibition of the Hsp90 chaperone by geldanamycin (Krtková *et al*., 2012); removal of Hsp90 or other chaperones during the purification process may therefore prevent microtubule re-assembly, perhaps more so in plants than in animals.

I created a MOR1^{TOG1234} affinity column, using the longest MOR1 construct available at the time, and hypothesized that TOG domains from MOR1 would be able to bind plant tubulin more efficiently than the Stu2p^{TOG12} construct used by Widlund *et al*. (2012). MOR1^{TOG12} had been previously shown to bind weakly to sheep brain tubulin (Lechner *et al*., 2012), and the MOR1^{TOG1234} column was indeed able to bind concentrated sheep brain tubulin (Fig. A2.2 B). Binding of plant tubulin, however, was ineffective (Fig. A2.2 A), and a similar attempt to make a MOR1^{TOG12} affinity column also failed (Hotta *et al*., 2016).

On the other hand, the Stu2p^{TOG12} column described in Chapter 5 proved to be effective for purifying plant tubulin (Fig. 5.1). In addition to its usefulness for future experiments using plant tubulin, this result demonstrates the importance of studying the mechanism of action of MOR1. As MOR1 TOG domains bind tubulin with lower affinity than the TOG domains of other orthologues, and as plant and animal tubulin differ in their ability to bind to TOG domains, caution should be used when extrapolating from information derived from studies of MOR1 orthologues or animal tubulin.

A2.4 Methods

A2.4.1 Growth conditions for *Arabidopsis* T87 cell suspension cultures

Suspension-cultured T87 cells (Arabidopsis Biological Resource Center, Ohio State University) were grown in Murashige and Skoog liquid medium containing 18 μM 2,4-D and 1 μM kinetin, using a gyratory shaker at 110 rpm, and at 21 °C with a 16 hour light/8 hour dark cycle. Cells were sub-cultured every 7 days by adding 7.5 mL of cells to 42.5 mL of fresh medium in a 250 mL Erlenmeyer flask.

A2.4.2 Purification of plant tubulin using anion exchange chromatography followed by polymerization and depolymerization cycling

Filtered T87 cells (about 40 g) were resuspended in 200 mL PME buffer (100 mM PIPES, pH 6.9; 2 mM EGTA; 1 mM $MgSO_4$; 1 mM DTT; 100 μM GTP) containing plant protease inhibitor cocktail (Sigma-Aldrich). This suspension was divided into 25 mL aliquots, which were kept on ice. Each aliquot of cells was homogenized using a glass tissue homogenizer, then by a probe sonicator (each aliquot was subjected to 1 minute of sonication, followed by 6 minutes of incubation on ice, repeated 7 times). Cell intactness was assessed using a light microscope at 100x magnification, with the goal of disrupting the cell walls in approx. 90% of cells. The cell lysate was cooled on ice for 30 minutes, then centrifuged at 40,000xg and 4 °C for 40 minutes. The supernatant was decanted into a new tube, and GTP was added to 100 μM.

An anion exchange column was prepared, using 5 mL DEAE Sepharose bead suspension (Sigma-Aldrich). All steps relating to anion exchange chromatography were carried out at 4 °C, and all solutions were pre-cooled. The column was pre-equilibrated using 10 mL PME buffer, then the supernatant from the centrifuged lysate was run through the column. The column was washed with 35 mL wash buffer (100 mM PIPES, pH 6.9; 1 mM $MgCl_2$; 1 mM EGTA; 250 mM KCl; 1 mM DTT; 100 μM GTP; plant protease inhibitor cocktail). The concentrated tubulin was eluted with two column volumes of elution buffer (100

mM PIPES, pH 6.9; 1 mM $MgCl_2$; 1 mM EGTA; 300 mM KCl; 750 mM glutamate; pH adjusted to 6.6; 1 mM DTT; 100 μM GTP; plant protease inhibitor cocktail). Proteins in the eluate were concentrated via filter centrifugation (Amicon Ultra-15 centrifugal filter units, Millipore) at 4,000xg for 15 minutes, at 4 °C. The concentrated protein sample was then washed by adding 15 mL PME buffer, and centrifuged again at 4,000xg for 15 minutes, at 4 °C.

Microtubule assembly was induced by adding 2 mM GTP, 8% v/v DMSO, and 10 mM $MgCl_2$ to the concentrated protein sample, and incubating for 30 minutes at 25 °C. Polymerized microtubules were recovered by centrifugation at 70,000xg for 30 minutes, at 25 °C. The microtubule pellet was resuspended with careful pipetting in chilled PME buffer containing 100 μM GTP, to a concentration of approximately 10 mg tubulin/mL, based on the estimated mass of the pellet. Microtubule disassembly was then induced by incubating the solution on ice for 30 minutes. The depolymerized tubulin sample was centrifuged at 70,000xg for 30 minutes, at 4 °C, to remove insoluble contaminants. Protein concentration in the resulting supernatant was determined using a Bradford assay (Bradford, 1976), and 50 μL aliquots of tubulin were frozen in liquid nitrogen and stored at -80 °C.

A2.4.3 *In vitro* tubulin polymerization assay with fluorescent animal tubulin

50 μL 7 μM *Arabidopsis* tubulin was mixed with 0.2 μL 85 μM rhodamine-labelled sheep brain tubulin, 19 μL glycerol, 1 μL 100 μM GTP, and 0.35 μL 4 mM taxol. The sheep brain tubulin was labelled with rhodamine by Dr. Bettina Lechner. This solution was incubated at 37 °C for 20 minutes, then pipetted onto a microscope slide and covered with a coverslip. Microtubules were visualized using a Zeiss Observer Z1 microscope.

A2.4.4 Assessing tubulin binding using the MOR1^{TOG1234} affinity column

Dr. Bettina Lechner created a TOG1234-His construct, by amplifying *MOR1* cDNA and cloning the sequence into the pET21b vector (Novagen, Merck KGaA, Germany), which added a C-terminal 6xHis

fusion tag. I carried out all of the procedures described subsequently. Terrific Broth (1.2% w/v tryptone, 2.4% w/v yeast extract, 0.4% v/v glycerol, 17 mM KH_2PO_4, 72 mM K_2HPO_4) containing 50 μg/mL ampicillin was inoculated with *E. coli* BL21 cells expressing TOG1234-His, and this batch culture was grown on a temperature-controlled gyratory shaker at 37 °C and 225 rpm. Optical density at λ = 600 nm (OD_{600}) was measured using a spectrophotometer. When OD_{600} reached 0.5, the temperature was shifted to 18 °C for 1 hour. Protein expression was induced by adding isopropyl β-D-1-thiogalactopyranoside (IPTG) to a concentration of 0.2 mM, and the culture was grown at 18 °C for a further 18 hours. Cells were harvested via centrifugation at 3,500xg and 4 °C.

To purify TOG1234-His, cells were lysed in lysis buffer (3.4 mM NaH_2PO_4, 46.6 mM Na_2HPO_4, 250 mM NaCl, 2 mM $MgCl_2$, 40 mM imidazole, pH 8.0; with 1 mM DTT and plant protease inhibitor cocktail (Sigma-Aldrich); 5 mL of buffer per 1 g of cells) using a probe sonicator for 5 minutes, and cell lysate was cleared via centrifugation for 30-40 minutes at 14,000 rpm and at 4 °C. Cleared cell lysate was mixed with Ni-NTA agarose (Qiagen) and gently shaken at 4 °C for 1 hour. The beads were loaded onto a column, washed with 10 column volumes lysis buffer, and eluted with 2 column volumes elution buffer (15.8 mM NaH_2PO_4, 34.2 mM Na_2HPO_4, 250 mM NaCl, 2 mM $MgCl_2$, 250 mM imidazole, pH 7.2). The eluate was desalted using PD MidiTrap columns (GE Healthcare) that had been pre-equilibrated with BRB80+ buffer (80 mM PIPES-KOH, pH 6.8; 5 mM $MgCl_2$; 1 mM EGTA). Protein concentration was measured using a Bradford assay (Bradford, 1976). Purified TOG1234-His was then conjugated to NHS-activated Sepharose 4 Fast Flow resin (GE Healthcare), as described in the protocol published by Widlund *et al*. (2012).

When attempting to purify plant tubulin, I prepared plant cell extracts using the same protocol I had used when purifying tubulin via anion exchange chromatography and polymerization/depolymerization cycling, substituting a bead homogenizer (Glen Mills Inc.) for the glass homogenizer. Subsequent wash,

elution, and desalting steps followed the protocol published by Widlund *et al*. (2012). When assessing binding of purified sheep brain tubulin, I pre-equilibrated the MOR1^{TOG1234} column with BRB80+ buffer, then loaded 240 μL tubulin (approx. 100 μM) that I had previously helped Dr. Bettina Lechner to purify. Subsequent steps followed the protocol published by Widlund *et al*. (2012).